**POLYTECHNIQUE MONTRÉAL**

Affiliée à l'Université de Montréal

# Development of a Procedure to Optimize the Geometric and Dynamic Designs of Assistive Upper Limb Exoskeletons

**LAURENT BLANCHET**

Département de génie mécanique

Mémoire présenté en vue de l'obtention du diplôme de *Maîtrise ès sciences appliquées*

Génie mécanique

Février 2020

**POLYTECHNIQUE MONTRÉAL**

Affiliée à l'Université de Montréal

Ce mémoire intitulé :

**Development of a Procedure to Optimize the Geometric and Dynamic Designs of Assistive Upper Limb Exoskeletons**

présenté par **Laurent BLANCHET**

en vue de l'obtention du diplôme de *Maîtrise ès sciences appliquées*

a été dûment acceptée par le jury d'examen constitué de :

**Alain BATAILLY**, président

**Maxime RAISON**, membre et directeur de recherche

**Sofiane ACHICHE**, membre et codirecteur de recherche

**Jozsef KÖVECSES**, membre

# ACKNOWLEDGEMENTS

First of all, I would like to thank the members of the jury for taking the time to read and evaluate this thesis. As leaders of their respective fields, it is an honor for me.

Then, I especially want to thank my director and co-director, Maxime Raison and Sofiane Achiche for their continuous support throughout my masters, but also since 2015, when I first started as a research intern in their lab. I found my passion in the biomechanics and mechatronics field and without them, this project would not have been possible. The devotion and the trust they give to their team inspired me to work harder. Their dynamism creates a positive work environment where fun and rigor go well together.

Thanks to all the students and interns from the COSIM lab at Polytechnique and all the members of the Technopole de Réadaptation that worked with me. These last years allowed me to meet great people and my project would not have been the same without you.

Again, I want to thank my director Maxime Raison and Paul Fisette, Professor at the Institute of Mechanics, Materials and Civil Engineering from the Université Catholique de Louvain, where they gave me the chance to realize an internship to work with the ROBOTRAN software. This pushed my project way further than anticipated and I am grateful for this experience. I would also like to thank Quentin Docquier who greatly helped with the understanding of Optimal Control Problems and their application to the multibody dynamics field.

I am also grateful to the Natural Sciences and Engineering Research Council of Canada, to Fonds de recherche du Québec – Nature et technologies (FRQNT), to Canada First Research Excellence Fund (Institut TransMedTech) and to Polytechnique Montréal for funding during my research project.

Finally, I would like to thank my family for their continuous support in all my projects. You allowed me to keep my motivation and to enjoy all my academic years and I am deeply grateful for that. A special thanks to my girlfriend who supported me in the toughest parts of this project.

Thank you all and onto the next project!

# RÉSUMÉ

La faiblesse musculaire chez les patients atteints de maladies neuromusculaires peut réduire leur capacité à réaliser des activités quotidiennes primordiales telles que manger ou se laver. Les dispositifs d'assistance disponibles offrent des fonctionnalités limitées et ne permettent pas de restaurer l'autonomie des patients. D'autre part, la fatigue musculaire chez les travailleurs œuvrant dans un environnement éprouvant peut provoquer des blessures et une mauvaise qualité de vie. Bien qu'il existe de nombreux outils pour les aider, l'effort requis peut tout de même être hautement exigeant.

Les exosquelettes d'assistance sont bien adaptés pour aider ces deux populations, car ils visent à supporter l'utilisateur en diminuant l'effort nécessaire pour accomplir ses tâches quotidiennes. Le développement de tels dispositifs est une tâche fastidieuse, car les interactions en 3D entre le corps humain et l'exosquelette ainsi que le choix des caractéristiques du système de transmission de puissance, c'est-à-dire les moteurs ou les éléments passifs, sont très complexes et interdépendants. Pour ajouter à cette difficulté, il existe très peu de lignes directrices ou de procédures claires pour soutenir la synthèse géométrique et dynamique d'exosquelettes d'assistance et portable des membres supérieurs. Les paramètres géométriques sont les dimensions de l'exosquelette tandis que les paramètres dynamiques sont les caractéristiques des moteurs et des éléments passifs, tels que des ressorts.

L'objectif de ce mémoire de maîtrise est de développer une procédure de synthèse géométrique et dynamique pour soutenir la conception d'un exosquelette de membre supérieur. Tout d'abord, une optimisation géométrique des dimensions de l'exosquelette a permis de maximiser la fermeture de la boucle cinématique et d'éviter les collisions avec les segments du corps tout en réalisant des tâches fonctionnelles spécifiques. Ensuite, grâce à un problème de contrôle optimal, les caractéristiques dynamiques de l'exosquelette ont été obtenues en minimisant les couples articulaires de l'utilisateur pour les mêmes tâches fonctionnelles.

Les dimensions optimisées de l'exosquelette ont permis de réussir la fermeture de boucles pour toutes les tâches, soit 10,8 % de plus qu'avec une identification visuelle des dimensions. Quant à eux, les paramètres dynamiques ont pu réduire le couple articulaire de l'utilisateur à moins de 10,6 % des simulations sans exosquelettes pour presque toutes les articulations et les tâches.

En conclusion, ces résultats ont montré que la procédure de synthèse était réussie. Cela pourra permettre le développement d'exosquelettes plus légers et plus petits ayant le potentiel d'être commercialisés à court terme. Les perspectives de cette recherche sont de développer une procédure d'optimisation où les paramètres géométriques et dynamiques sont optimisés simultanément et de minimiser les forces musculaires plutôt que les couples articulaires de l'utilisateur pour soutenir des objectifs de design et des objectifs cliniques.

# ABSTRACT

Muscular weakness for patients affected by neuromuscular diseases can reduce their ability to realize primordial daily activities such as eating or washing themselves. The available assistance devices offer limited functionalities and do not restore autonomy for the patients. On the other hand, muscular fatigue for workers in tough physical environments can cause injuries and poor quality of life. While there are a lot of tools to help them, the required effort can still be very demanding.

Assistive exoskeletons are well suited to help both these populations as they aim to assist the user by lowering the effort necessary to accomplish his everyday tasks. The development of such devices is a tedious task as the 3D human-exoskeleton interactions and the selection of the power transmission system characteristics, i.e. motors or passive elements, are highly complex and interdependent. To add to this complexity, there are very little to no guidelines or clear procedures for supporting the geometric and dynamic synthesis of wearable and assistive upper limb exoskeletons. The geometric parameters are the dimensions of the exoskeleton while the dynamic parameters are the characteristics of motors and passive elements such as springs.

The objective of this master thesis was to develop a geometric and dynamic synthesis procedure to support the design of an upper limb exoskeleton. First, a geometric optimization of the exoskeleton dimensions enabled to maximize the kinematic loops closure and to avoid collisions with the body segments while carrying out specific functional tasks. Then, through an optimal control problem, the exoskeleton dynamic characteristics were obtained by minimizing the user joint torques for the same functional tasks.

The optimized exoskeleton dimensions could reach loop closure for all tasks, 10.8% more than with a visual identification of the dimensions. The resulting dynamic parameters could reduce the user’s joint torque to less than 10.6% of the human-only simulations for nearly all joints and tasks.

To conclude, these results showed that the synthesis procedure was successful. This is important as it can enable the development of lighter and smaller exoskeletons that have the potential to reach commercialization. The future perspectives are to build an optimization framework where the geometric and dynamic parameters are optimized together and to minimize the muscle force instead of the user’s joint torques to support clinical and design purposes.

# TABLE OF CONTENTS

# LIST OF TABLES

# LIST OF FIGURES

# LIST OF SYMBOLS AND ABBREVIATIONS

| | |
|---|---|
| AC | Acromioclavicular joint |
| AoR | Axis of rotation |
| AR | Arm frontal reach functional task |
| CH | Comb hair functional task |
| CoR | Center of rotation |
| DAE | Differential algebraic equation |
| DOF | Degree of freedom |
| E. FE | Elbow Flexion/Extension |
| ES | Eat with a spoon functional task |
| F. PS | Forearm Pronation/Supination |
| GH | Glenohumeral joint |
| HO | Human only |
| HR | Humeroradial joint |
| HU | Humeroulnar joint |
| MBS | Multibody systems |
| NLP | Non-linear Problem |
| OCP | Optimal Control Problem |
| OD | Open a door functional task |
| ODE | Ordinary differential equation |
| RC | Radiocarpal joint |
| RL | Arm frontal reach right to left functional task |
| RMS | Root Mean Square |
| RU | Radioulnar joint |

| | |
|---|---|
| S. AA | Shoulder Abduction/Adduction |
| SC | Sternoclavicular joint |
| S. FE | Shoulder Flexion/Extension |
| ZC | Zip Coat functional task |

# LIST OF APPENDICES

# CHAPTER 1 INTRODUCTION

The human body is a complex articulate system that is able to perform a great number of movements and tasks. This is especially true for the upper limb which is primordial in many basic need activities such as eating or washing yourself. However, for people affected by physical disabilities such as neuromuscular pathologies, these simple tasks can be difficult and tiring. Indeed, those conditions generally result in a lack of muscle force [1] which reduces the autonomy of the person. The upper limb is also crucial for most workplace environments as it allows to accomplish a majority of practical tasks like lifting objects and using tools. Workers in manufacture, construction, mines, and other tough environments often spend a lot of effort in their everyday tasks [2]. This can result in injuries and poor quality of life as the workers age.

Fortunately, there exist numerous devices that can help for both populations. For the neuromuscular population, mechanical and robotic aids exist, such as the JACO from Kinova Robotics [3] or self-feeding devices such as the one from the Sant'Anna School of Advanced Studies [4]. However, these systems are only suited for a number of tasks and restore limited autonomy to the patient. For the workers, there are plenty of tools to help them accomplish their tasks more easily, but the required effort can still be very demanding.

Recently, exoskeleton devices have been emerging for those populations [5]. Exoskeletons are articulated systems, whose joints are generally aligned with the user's joints. The main purpose of the exoskeleton is to provide force in order to compensate or augment the capabilities of the user. Three main categories exist:

1. Rehabilitation exoskeletons: Aim to recover, train or develop motricity for post-surgery patients and neuromuscular pathology patients in the course of their rehabilitation program.
2. Augmentation exoskeletons: Aim to give more capacity to healthy users such as great strength.
3. Assistive exoskeletons: Aim to assist the user in his everyday tasks by lowering the effort necessary to accomplish those tasks.

Hence, to give autonomy to the neuromuscular affected patients and to reduce the effort of workers, assistive exoskeletons are well suited. Within current technology and research, there are no commercially available upper limb assistive and wearable exoskeletons that can help users for

a broad range of tasks. In the medical field, the WREX exoskeleton can help to balance the weight of the arm for simple gravity affected movements, such as lifting the arm in front of a person [6]. Devices with similar technologies are also emerging in the industrial field such as the Levitate exoskeleton [7] or the Ekso Vest system [8]. However, these devices are not suitable for a wide range of tasks and can quickly reach their limits as they are solely based on spring elements that act in a single direction and possess very precise characteristics.

To overcome this problem, motorized upper limb assistive and wearable exoskeletons are a solution [5]. However, the complexity of the upper limb with its high number of degrees of freedom (DOF), the size and cost of the available motors and the high variability of human size, shape and capacity, increase the difficulty of developing those devices.

The literature shows that there is a lack of procedures to determine the right geometric parameters such as the dimensions of the device and the right dynamic parameters such as motors and springs characteristics.

Consequently, the objective of this project is to develop a geometric and dynamic synthesis procedure to design and personalize an upper limb assistive and wearable exoskeleton for specific functional tasks.

This thesis presents the globality of the work done to achieve the development of such a synthesis tool and is built around the article submitted to the Journal of Multibody System Dynamics in Chapter 4. Chapter 2 contains the theoretical background and a critical review of the literature. Chapter 3 defines the research objectives and the position of the article in the work. Chapter 4 presents the full article: *Development of a procedure to optimize the geometric and dynamic designs of assistive upper limb exoskeletons*. Chapter 5 adds complementary methods and results. A general discussion of these results, a critical review of the article and the limits of the work are presented in Chapter 6. Finally, Chapter 7 concludes the work.

# CHAPTER 2 THEORETICAL BACKGROUND AND CRITICAL REVIEW OF LITTERATURE

This chapter combines the theoretical background and literature to grasps the essential concepts behind the research project. Section 2.1 resumes the biomechanics of the upper limb, going through the main articular groups. Section 2.2 briefly reviews the developments in upper limb exoskeletons. Section 2.3 sets the background for optimal control theory and non-linear programming. Section 2.4 resumes the multibody system dynamics and their use in biomechanics. Finally, Section 2.5 combines all the previous ones to describe the human-exoskeleton interactions and to summarizes the trends in exoskeleton optimal synthesis.

## 2.1 Biomechanics of the upper limb [9]

The upper limb is essential for a multitude of activities in daily living such as eating, writing, working and many more. Another important purpose of the upper limb is carrying objects and transferring the load to the thorax and the legs.

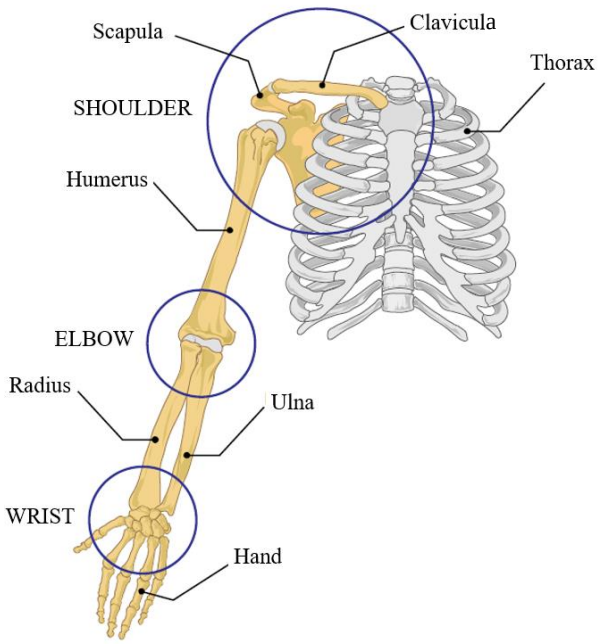


Figure 2-1. Osteoarticular system of the upper limb (*Figure adapted from* [10])

The upper limb is composed of a series of bone segments and articulations. The thorax, the clavicula, the scapula, and the humerus are joined together by the shoulder complex. Then, the

humerus, radius, and ulna are joined together by the elbow joint and finally, the ulna, radius and hand are joined by the wrist joint (Figure 2-1).

The bones are held together by ligaments and linked to muscles by tendons. Muscles are the actuators of the human body, moving the bones by pulling on them at the muscle insertion points. However, the general motion of the bones is influenced by the interface between them which are called the articulations. Diarthrosis or synovial joints are the most movable articulations in the human body and can have a great range of motion. Figure 2-2 summarizes the diarthrosis type of articulations found in the human body. For each joint shown in Figure 2-2, its number of translational, i.e., prismatic, and rotational degrees of freedom (DOF) are defined in Table 2-1.

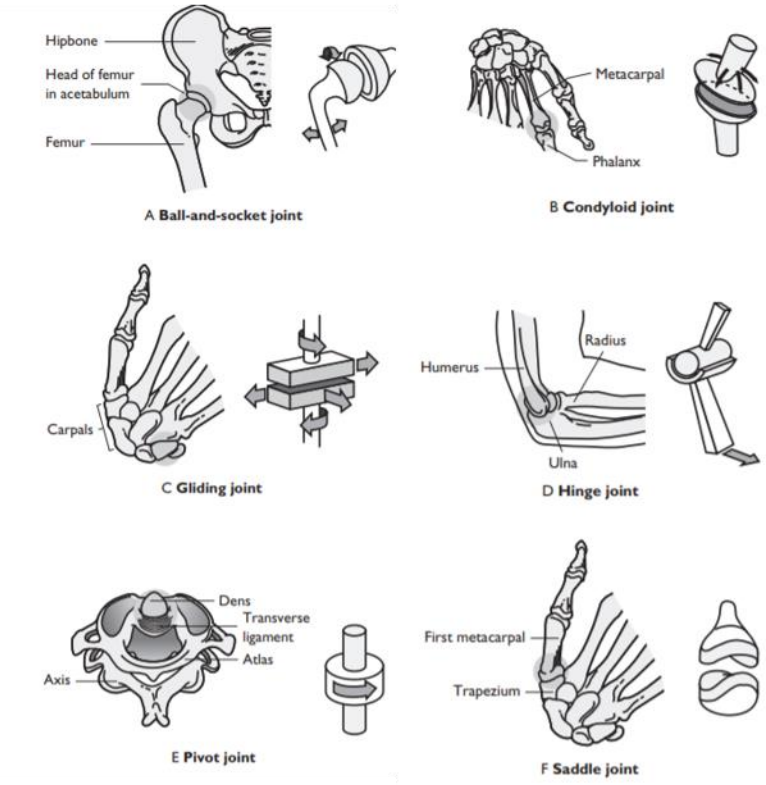


Figure 2-2. Definition of the different types of diarthrosis articulations in biomechanics [11]. A. Ball-and-socket joint. B. Condyloid joint. C. Gliding joint. D. Hinge joint. E. Pivot joint. F. Saddle joint.

Table 2-1. Biomechanics joint types and the number of prismatic (translation) or rotation DOF

| Articulation | Prismatic DOF | Rotation DOF |
|---|---|---|
| Ball-and-socket | 0 | 3 |
| Condyloid | 0 | 3 |
| Gliding | 2 | 1 |
| Hinge | 0 | 1 |
| Pivot | 0 | 1 |
| Saddle | 0 | 2 |

### 2.1.1 The shoulder

Considering bones by pairs of two, the articulations that compose the shoulder complex are:

- The sternoclavicular (SC) joint, between the thorax and the clavicula, which can be considered as a ball-and-socket joint [12], [13] or a saddle joint [9];
- The acromioclavicular (AC) joint, between the scapula and clavicula, which can be considered as a ball-and-socket joint [12], [13] or a gliding joint [9];
- The glenohumeral (GH) joint, between the scapula and the humerus, which can be considered as a ball-and-socket joint [9], [12], [13]
- The scapulothoracic (ST) joint, between the thorax and the scapula which allows the scapula to slide on the thorax [14].

A final joint is also included in the shoulder complex, the subdeltoid (SD) joint, however, this joint is mostly important to reduce friction in the shoulder girdle movements and is mechanically linked to the GH joint. These fives joints allow three main DOF at the shoulder as presented in Figure 2-3. They are the flexion-extension, the abduction-adduction and internal-external rotation of the shoulder. The SC, AC and ST joints significantly contribute to the three previous DOF [13]. They are also responsible for the displacement of the center of rotation (CoR) of the shoulder girdle which is why it is important to consider them in the biomechanical models of the shoulder [14].

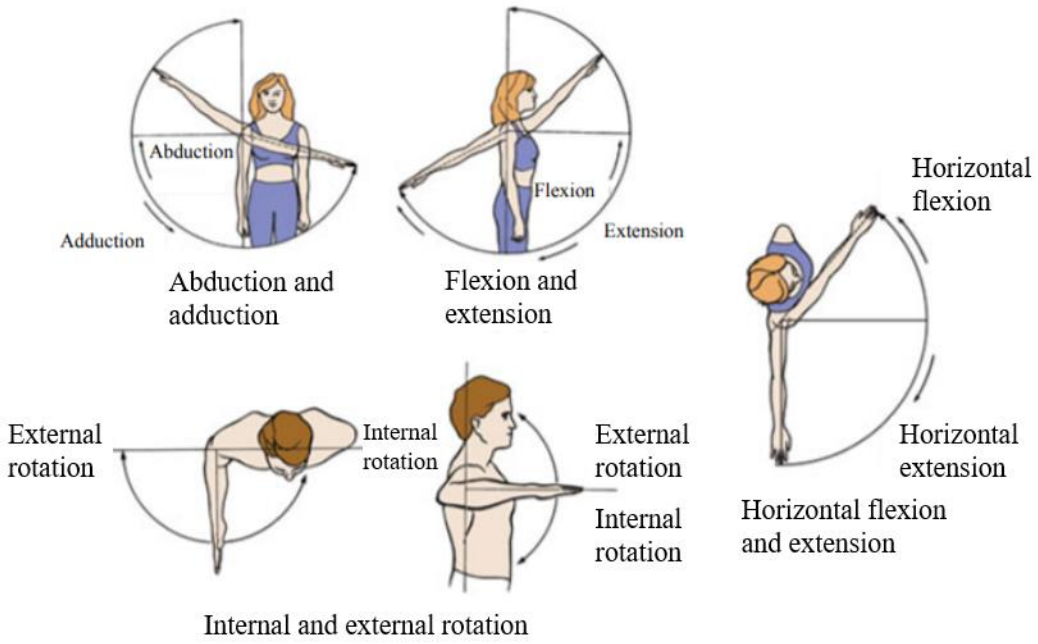


Figure 2-3. Shoulder movements (*Figure adapted from* [15])

### 2.1.2 The elbow and forearm

The following articulations compose the elbow and forearm joint. Four joints are important to understand the movements of the elbow [9]:

- The humeroulnar (HU) joint, between the humerus and the ulna, which can be considered as a hinge joint;
- The humeroradial (HR) joint, between the humerus and the radius, which can be considered as a ball-and-socket joint [10];
- The radioulnar (RU) proximal joint, between the sigmoid cavity of the ulna and the radius head, which can be considered as a pivot joint;
- The RU distal joint, which is located at the wrist, but greatly affects the elbow joint, between the distal points of the ulna and the radius, which can be considered as a pivot joint;

These joints allow two global DOF at the elbow, the flexion-extension movement shown in Figure 2-4 and the pronation-supination movement shown in Figure 2-5. The flexion-extension (FE)

movement follows a single hinge type joint. In contrast, the pronation-supination movement follows complex articular interfaces and its axis of rotation (AoR) is not perpendicular to the FE joint [16]. This carrying angle varies among different subject, thus, it is important to take it into consideration in the biomechanical models [10], [17].

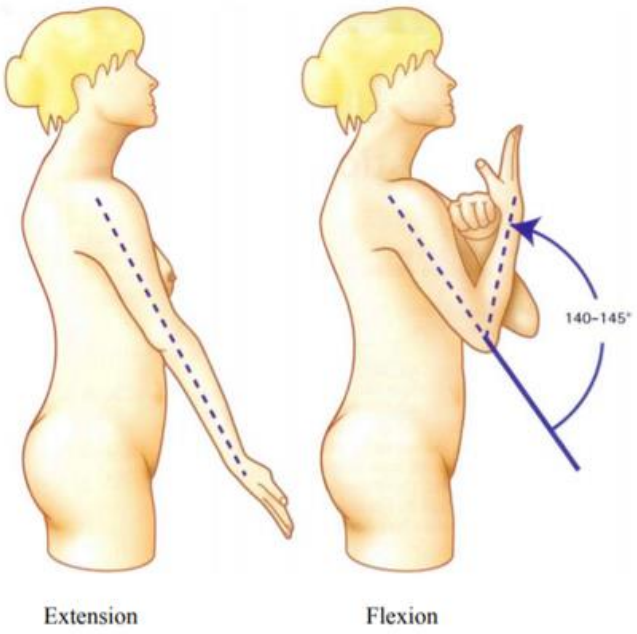


Figure 2-4. Flexion-extension movement of the elbow (*Figure from* [9])

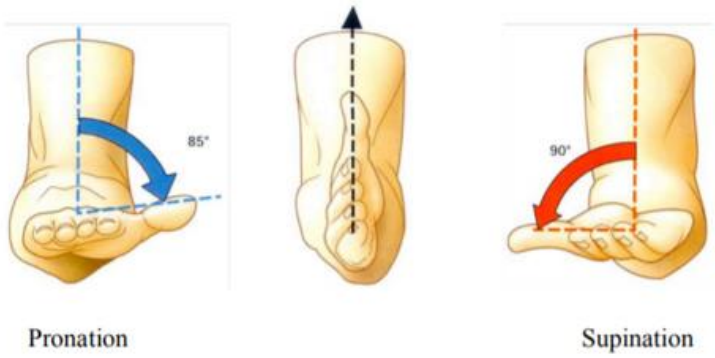


Figure 2-5. Pronation-supination movement of the forearm (*Figure from* [9])

### 2.1.3 The wrist

Considering the hand as a rigid body, the only joint between the forearm and the hand is the radiocarpal (RC) joint that links the distal head of the radius to the carpals. It can be considered as

a condyloid joint with 3 DOF, however, only 2 DOF are practically used in the literature [9]. These two movements, the flexion-extension and abduction-adduction, are shown in Figure 2-6.

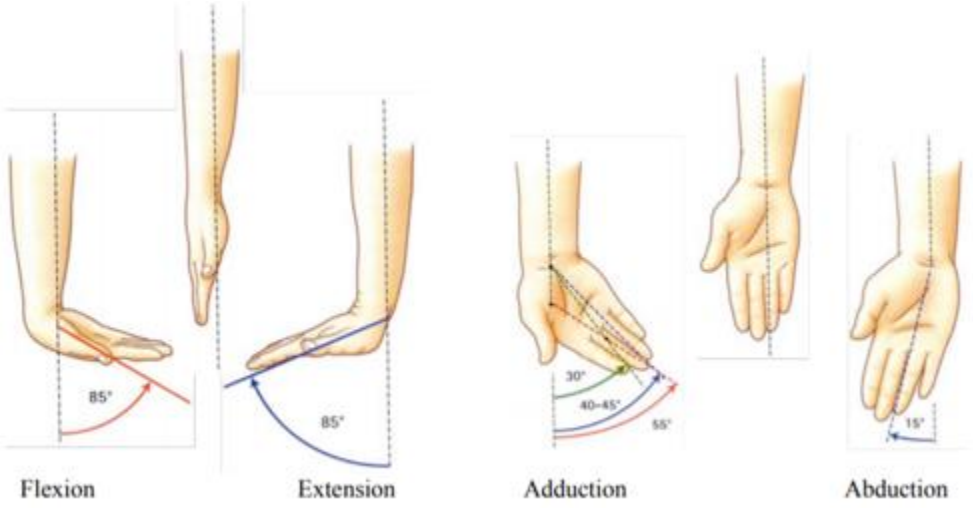


Figure 2-6. Wrist movements (*Figure from* [9])

This project is built on the biomechanical model developed by Laitenberger et al. [10] from Pr. Raison's and Pr. Achiche's research teams. It considers the shoulder as a series of ball joints, the elbow as a hinge joint, the forearm as a complex closed-loop and the wrist as a universal joint. See Section 4.3.1 for more details. This model was chosen as it is one of the most precise models of the forearm in the literature and can represent the movement of the shoulder for all the DOF shown in section 2.1.1. Sections 2.3, 2.4 and 2.5 describe the fundamental theory and literature to help understand the biomechanical model of the upper limb and its interaction with the exoskeleton model.

## 2.2 Review of upper limb exoskeletons

This section will first describe exoskeletons in a general way, then, a review on the development of upper limb exoskeletons in research and in the industry will be presented.

Exoskeletons are devices that work with the user through an interaction which can be passive, i.e. the exoskeleton mechanically answers to the movement of the user through springs or flexible beams [18], or active, i.e., the exoskeleton answers to user's movement through a control law with active actuators such as motors. However, this statement could also define end-effector robotic devices as shown in Figure 2-7A. The difference between end-effector devices and exoskeletons is

that the exoskeleton joint axes are generally aligned with the user's joint axes as seen in Figure 2-7B. While end-effector robots are used in the medical field [19], [20] and in the work environment [21] they are generally not wearable systems. Moreover, as they control the hand of the user, they are less intuitive than exoskeletons which control the user's joints [22]. Therefore, to restore autonomy for patients with muscular weakness or to reduce the effort for workers, exoskeleton devices are well suited.

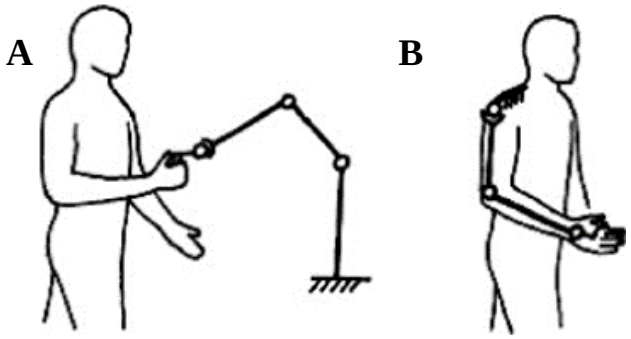


Figure 2-7. A. End-effector robotic device and B. Exoskeleton device. (*Figure from* [23])

There are three main groups of exoskeletons: 1. Rehabilitation devices, Figure 2-8A, 2. Augmentation devices, Figure 2-8B, 3. Assistive devices, Figure 2-8C.

Rehabilitation devices are mostly used for therapy sessions for patients accompanied by medical personnel. The patients follow a program of exercises that aim at the recovery, training or development of their motor skills. They are mostly used for post-surgery, stroke and neuromuscular pathology patients. These devices are generally only available at the clinic or hospital as they are expensive, heavy and voluminous. Moreover, because of the size of the motors and mechanisms, they need to be fixed to a solid base attached to the ground [5].

Augmentation devices aim to augment one's motor capabilities by giving extra strength to the user's joints. They generally target healthy adults in a work environment or in the military and are used to carry or lift heavy loads that would be impossible without the device. In order to achieve this purpose, the devices are equipped with powerful motors and solid mechanisms that are often heavy and bulky while still being wearable. However, the use of these systems is tiring for the user and the devices need to be precisely controlled and secure to avoid user injuries [24].


Figure 2-8. Main types of exoskeletons. A. Rehabilition device [25]. B. Augmentation device [24]. C. Assistive device [26].

Assistive devices can be considered as a weaker version of the augmentation systems. They aim at reducing the effort required to accomplish daily tasks by supporting the upper limb. For the neuromuscular weakness population, the exoskeleton allows the patient to do activities that are considered normal in a healthy population [6]. For the workers, the exoskeleton should reduce fatigue and effort of the user's tasks with the objective of reducing long term work injuries [27]. An important feature of this type of exoskeletons is that they should be worn by users for long periods of time, such as a full school or workday. This is a crucial design constraint as the exoskeleton should not be too heavy or too bulky to efficiently help the user without causing fatigue due to the weight of the device.

As the problem targeted by this research project is to help the neuromuscular patients and workers in their everyday tasks, assistive exoskeletons are best suited to the task. Table 2-2 presents a review of upper limb exoskeletons in the last 10 years and is based on the review made by Gopura et al. [5] and Lecours et al. [28]. Commercial availability considers if the exoskeleton can be bought by companies, hospitals or individuals or if it is only at a research-level. Table 2-2 shows that upper limb exoskeletons were mostly developed for rehabilitation while assistive systems are barely emerging. Indeed, for the assistive systems, commercial solutions are almost only available as passive devices. However, these passive devices can only support simple gravity affected movements and cannot help the user for complex tasks [26], [27]. Therefore, there is still a need to develop and design active assistive exoskeletons or active and passive exoskeletons.

Table 2-2. Review of upper limb exoskeletons from the last ten years [5], [28]

| Name | Active/ Passive | Targeted population | Availability | Type of exoskeleton |
|---|---|---|---|---|
| IntelliArm [29] | Active | Medical | Research | Rehabilitation |
| CADEN-7 [30] | Active | Medical | Research | Rehabilitation |
| ExoRob [31] | Active | Medical | Research | Rehabilitation |
| ARMin III [32] | Active | Medical | Research | Rehabilitation |
| MEDARM [33] | Active | Medical | Research | Rehabilitation |
| MGA [34] | Active | Medical | Research | Rehabilitation |
| ABLE [35] | Active | Workers and Medical | Research | Rehabilitation |
| RehabExos [36] | Active | Medical | Research | Rehabilitation |
| WOTAS [37] | Active | Medical | Research | Rehabilitation |
| RUPERT [38] | Active | Medical | Research | Rehabilitation, Wearable |
| Hand Mentor [39] | Active | Medical | Research | Rehabilitation |
| BONES [40] | Active | Medical | Research | Rehabilitation |
| ASSISTON-SE [41] | Active | Medical | Research | Rehabilitation |
| CAREX [42] | Active | Medical | Research | Rehabilitation |
| SAM [43] | Active | Medical | Research | Rehabilitation |
| SHOULDER-RO [44] | Active | Medical | Research | Rehabilitation |
| WREX [6] | Passive | Medical | Research and commercial | Assistive |
| P-WREX [26] | Passive | Medical | Research and commercial | Assistive |
| MYOPRO [45] | Active | Medical | Commercial | Assistive and Rehabilitation |
| SPEXO [46] | Active | Medical | Research | Assistive |
| Body Extender [24] | Active | Workers | Research | Augmentation |
| ArmeoSpring [25] | Passive | Medical | Commercial | Rehabilitation |
| Ekso Vest [8] | Passive | Workers | Commercial | Assistive |
| Airframe [7] | Passive | Workers | Commercial | Assistive |
| MATE [47] | Passive | Workers | Commercial | Assistive |
| Paexo [48] | Passive | Workers | Commercial | Assistive |
| Shoulder X [49] | Passive | Workers | Commercial | Assistive |
| SkelEx [50] | Passive | Workers | Commercial | Assistive |
| Guardian XO [51] | Active | Workers | Research | Assistive |
| x-Ar [52] | Passive | Workers | Commercial | Assistive |
| Vex [53] | Passive | Workers | Commercial | Assistive |
| Lecours et al. [28] | Active | Medical and workers | Research | Assistive |

This project is built on the exoskeleton model from Lecours et al. [28] from Pr. Raison's and Pr. Achiche's research teams. See Section 4.3.2 for more details. This model was chosen as it is one of the first active, assistive and wearable exoskeleton models to compensate the shoulder abduction-adduction, shoulder flexion-extension, elbow flexion-extension, and forearm pronation supination movements. Sections 2.3, 2.4 and 2.5 describe the fundamental theory and literature to help understand the interaction between the upper limb model and the exoskeleton model.

## 2.3 Optimal control: Fundamentals

The objective of optimal control theory is to find a control law for a dynamic system over a certain amount of time. This is done by separating control variables $\boldsymbol{u}$ and state variables $\boldsymbol{x}$ and by describing the state by dynamic equations. These dynamic equations are influenced by the control variables thus influencing the state variables. For instance, steering the wheel or pushing on the accelerator pedal of a car controls the position and speed of the car. Generally, controls and states are subject to constraints such as the limit of rotation of the steering wheel for a car. Finally, to complete this optimal control problem (OCP), the state and control variable should minimize or maximize an objective function while respecting their respective constraints. In the car example, the objective could be to follow a given trajectory by minimizing the difference between the state variables and the trajectory at each point in time [54].

The use of optimal control is spread around many fields of research such as chemical engineering [55], economics [56] and multibody system dynamics [57].

### 2.3.1 The optimal control problem

An optimal control problem with cost functional $C$ can be formulated as,

$$\min_{x(t),u(t)} C = \Phi\big(\boldsymbol{x}(t_f), t_f\big) + \int_{t_0}^{t_f} L(\boldsymbol{x}(t), \boldsymbol{u}(t), t)dt \tag{2.1}$$

where $\boldsymbol{x}(t)$ is the state vector, $\boldsymbol{u}(t)$ is the control vector, $t_0$ is the initial time, $t_f$ the final time, $\Phi$ is the scalar terminal weighting function and $L$ the scalar function.

Eq. 2.1 is subject to,

$$\boldsymbol{x}_0 = \boldsymbol{x}(t_0) \tag{2.2}$$

$$F(\dot{\boldsymbol{x}}(t), \boldsymbol{x}(t), \boldsymbol{u}(t), t) = 0 \tag{2.3}$$

$$g(\boldsymbol{x}(t), \boldsymbol{u}(t), t) \geq 0 \tag{2.4}$$

$$\varphi\left(\boldsymbol{x}(t_f)\right) = 0 \tag{2.5}$$

Where, $\boldsymbol{x}_0$ is the fixed initial state, $F$ are the dynamic equations of the system, $g$ are the inequality constraints on the control and state variables and finally $\varphi$ denotes the terminal state constraints [58], [59]. $F$ can be a set of ordinary differential equations (ODE) or a set of differential algebraic equations (DAE).

### 2.3.2 Solving the OCP: A summary

Literature shows that in order to solve an OCP, there are three categories of solutions: dynamic programming, indirect methods and direct methods [59]–[61].

Dynamic programming, defined by Bellman [62], considers the principle of optimality that any sub-arc of an optimal trajectory is also optimal. The method uses a backward cost-to-go minimization function starting from the end of the trajectory and recursively finds the complete solution [60] for all times and all initial values. It can also be stated in continuous time which leads to the Hamilton-Jacobi-Bellman equation, a partial differential equation. Numeric methods such as [63] can compute solution approximations but as it is a recursive method, dynamic programming is limited to small state spaces [64].

Indirect methods are based on the calculus of variations, the Euler-Lagrange differential equations and Pontryagin's maximum (or minimum) principle [65]. In this principle, it is stated that the control variables must optimize the Hamiltonian at every instant in time, thus optimizing the problem in a continuous form [61]. States and controls can be subject to path constraints. Globally, the necessary conditions must satisfy the dynamic system of equations (Eq. 2.3) and partial derivatives of the Hamiltonian with respect to the state and control variables. This implies that these derivatives must be computed. Finally, with boundary conditions at the initial and final time, the problem becomes a two-point boundary value problem that can be solved by gradient, shooting

or collocation methods [59]. The shooting and collocation methods are defined hereafter. Indirect methods are difficult to implement as, on the one hand, the derivatives of the Hamiltonian need to be computed and, on the other hand, they are sensitive to the initial values provided to the system [61]. Another drawback is the difficulty in treating inequality constraints such as Eq. 2.4 [66]. Generally, this approach can be depicted as *first optimize then discretize*.

With the emergence of powerful non-linear programming solvers in the 1980's the focus on methods to solve OCPs changed to direct methods [64]. The basis of these techniques is the discretization of the OCP stated by Eqs. 2.1 to 2.5 and reducing it to a non-linear problem (NLP). All direct methods parametrize the control variables, $\boldsymbol{u}(t)$ but treat the state trajectories $\boldsymbol{x}(t)$ differently.

With the direct methods being the most widespread techniques to solve OCPs and as they can be solved by state-of-the-art non-linear programming solvers such as IPOPT [67], this research project will focus on them to solve the optimal control problems.

### 2.3.3 Solving the OCP: Direct methods [66]

The direct methods rewrite the OCP in Eqs. 2.1 to 2.5 by formulating a NLP problem such as Eq. 2.6:

$$\min_{\boldsymbol{w}} a(\boldsymbol{w}) \qquad \text{subject to} \qquad b(\boldsymbol{w}) = 0, \qquad c(\boldsymbol{w}) \geq 0, \tag{2.6}$$

where $\boldsymbol{w}$ is a discrete vector representing the optimization variables and $a$, the cost function, $b$, the equality constraints, and $c$, the inequality constraints, are differentiable functions.

#### 2.3.3.1 Direct single shooting

Direct methods can again be divided into two segments, the sequential and simultaneous approaches. In the sequential approach, called direct single shooting [68], the state variables $\boldsymbol{x}(t)$ are considered as an implicit function of the controls $\boldsymbol{u}(t)$. Therefore, the state variables are not variables of the NLP. The controls are discretized as piecewise constant $\boldsymbol{v}$. In sequence: 1. By a forward simulation through an ODE solver, the states are calculated from their value at the initial time and from the controls $\boldsymbol{v}$, 2. The solver verifies if the states and controls respect constraints $b$ and $c$ in Eq. 2.6 and compares the value to the previous evaluation of the cost function, 3. Repeat

until the constraints are met and the optimization conditions are met. Figure 2-9 shows step 1 of the sequence. A major drawback of this method is that there is no initial guess for the state trajectories $\boldsymbol{x}(t)$, hence, it is not well suited for trajectory tracking problems.

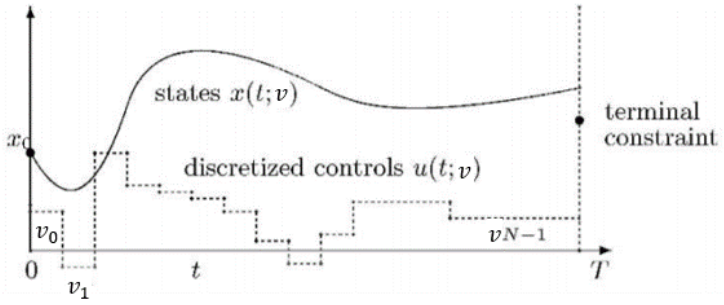


Figure 2-9. Illustration of direct single shooting *(Image adapted from* [66]*)*

In the simultaneous approaches, the states are considered as variables of the NLP which is validated by adding the equality constraints representing the ODE model. The simulation and optimization can then be done at the same time and the states will only represent a valid ODE model in respect to the controls at the solution of the NLP. The most widespread methods for simultaneous approaches are the multiple shooting [69] and collocation [70] techniques.

#### 2.3.3.2 Direct multiple shooting

In the multiple shooting technique, from Bock and Plitt [69] and shown in Figure 2-10, the controls, $\boldsymbol{u}(t)$ are discretized as piecewise constant controls $\boldsymbol{v}_i$ on a grid, the same way it is done for direct single shooting. For each of these intervals between $t_i$ and $t_{i+1}$, the ODE model is solved independently

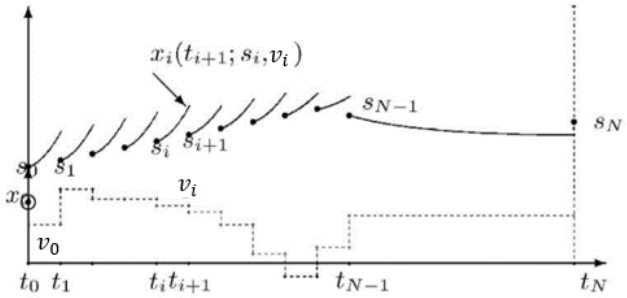


Figure 2-10. Illustration of direct multiple shooting *(Image adapted from* [66]*)*

with an initial value $\boldsymbol{s}_i$ for the state trajectory such as $\boldsymbol{x}_i(t_i) = \boldsymbol{s}_i$ and $\dot{\boldsymbol{x}}_i(t_i) = f(\boldsymbol{x}_i(t_i), \boldsymbol{v}_i)$. With the numerical solution of the ODE, the trajectory $\boldsymbol{x}_i$ is obtained for each interval as shown in Figure 2-10. To constrain the trajectory to feasible and meaningful values, conditions for continuity are added such as $\boldsymbol{s}_{i+1} = \boldsymbol{x}_i(t_i, \boldsymbol{s}_i, \boldsymbol{v}_i)$. The integrals from Eq. 2.1 are numerically computed by Eq. 2.7 for each interval:

$$\boldsymbol{l}_i(\boldsymbol{s}_i, \boldsymbol{v}_i) = \int_{t_i}^{t_{i+1}} L(\boldsymbol{x}_i(t_i, \boldsymbol{s}_i, \boldsymbol{v}_i), \boldsymbol{v}_i) dt \tag{2.7}$$

Finally, the NLP problem can be written as [66],:

$$\min_{\boldsymbol{s},\boldsymbol{v}} \Phi(\boldsymbol{s}_N) + \sum_{i=0}^{N} \boldsymbol{l}_i(\boldsymbol{s}_i, \boldsymbol{v}_i) \tag{2.8}$$

where $N$ is the number of intervals and $\Phi$ is the scalar terminal weighting function. Eq. 2.8 is subject to Eqs. 2.9 to 2.12:

$$\boldsymbol{s}_0 - \boldsymbol{x}(t_0) = 0 \tag{2.9}$$

$$\boldsymbol{s}_{i+1} - \boldsymbol{x}_i(t_i, \boldsymbol{s}_i, \boldsymbol{v}_i) = 0 \tag{2.10}$$

$$g(\boldsymbol{s}_i, \boldsymbol{v}_i) \geq 0 \tag{2.11}$$

$$\varphi(\boldsymbol{s}_N) = 0 \tag{2.12}$$

Where Eq. 2.9 are the initial values of the OCP, Eq. 2.10 are the continuity constraints, Eq. 2.11 are the constraints on the controls and states and Eq. 2.12 are the terminal constraints on the state variables. The NLP can then be solved by well known non-linear programming solvers or sequential quadratic programming solvers. The direct multiple shooting method has been widely used for practical engineering problem such as vehicle dynamics [71], robotics [66] and aircrafts [72].

#### 2.3.3.3 Direct collocation

The second simultaneous approach the direct collocation. Again, the controls $\boldsymbol{u}(t)$ can be considered as piecewise constant, $\boldsymbol{v}_i$, for each interval from $t_i$ to $t_{i+1}$. The states $\boldsymbol{x}(t)$, rather than being defined by the ODE in the same way than single or multiple shooting, are defined by

piecewise polynomials such as Lagrange Polynomials [73]–[75]. Each collocation interval $i$ is divided by a number of collocation points $K$. The grid time for the collocation points inside time interval $t_i$ to $t_{i+1}$ can be defined by *Radau* collocation points [75].

For Lagrange polynomial of degree $K$, same as the number of collocation points, and $k = 0, \dots, K$, their formula is stated in Eq. 2.13:

$$P_{i,k}(t) = \prod_{j=0, j \neq k}^{K} \frac{t - t_{i,j}}{t_{i,k} - t_{i,j}} \tag{2.13}$$

Then, for each interval from $t_i$ to $t_{i+1}$ the state trajectories are approximated by Eq. 2.14:

$$\boldsymbol{x}(\boldsymbol{s}_i, t) = \sum_{k=0}^{K} \boldsymbol{s}_{i,k} \cdot P_{i,k}(t) \tag{2.14}$$

With property that $\boldsymbol{x}(\boldsymbol{s}_i, t_{i,j}) = \boldsymbol{s}_{i,j}$. Then to find the semi-explicit formulation of the dynamics, $\dot{\boldsymbol{x}}(t) = F(\boldsymbol{x}(t), u(t))$, on $t_i$ to $t_{i+1}$, one can derivate Eq. 2.14 with respect to time and obtain Eq 2.15:

$$\sum_{k=0}^{K} \boldsymbol{s}_{i,k} \cdot \dot{P}_{i,k}(t_{i,j}) = F(\boldsymbol{s}_{i,j}, \boldsymbol{v}_i), \quad j = 1, \dots, K \tag{2.15}$$

Eq. 2.15 is the first element of the collocation constraints which enforces the state dynamics. The second collocation constraint is shown in Eq. 2.16:

$$\boldsymbol{s}_{i,0} = \boldsymbol{x}(\boldsymbol{s}_i, t_i) \tag{2.16}$$

This last constraint requires the state approximation at the start of the interval to be equal to the state. The combination of Eq. 2.15 and 2.16 are the complete collocation constraints for interval $t_i$ to $t_{i+1}$. A matrix of constraints can be built:

$$c_i(\boldsymbol{s}_i, \boldsymbol{v}_i) = \begin{bmatrix} \boldsymbol{s}_{i,0} = \boldsymbol{x}(\boldsymbol{s}_i, t_i) \\ F(\boldsymbol{s}_{i,1}, \boldsymbol{v}_i) \\ \dots \\ F(\boldsymbol{s}_{i,K}, \boldsymbol{v}_i) \end{bmatrix} = 0$$

Then to ensure continuity between the intervals, continuity constraints can be stated as Eq. 2.17:

$$\sum_{k=0}^{K} \boldsymbol{s}_{i,k} \cdot P_{i,k}(t_{i+1}) = \boldsymbol{x}(\boldsymbol{s}_{i+1}, t_{i+1}) \tag{2.17}$$

Finally, to approximate the integrals from Eq. 2.1 $\int_{t_i}^{t_{i+1}} L(\boldsymbol{x}(t), \boldsymbol{u}(t), t)dt$ for each interval, a quadrature formula can be used on the collocation points $k$ [76]. The result will be noted as $\boldsymbol{l}_i(\boldsymbol{s}_i, \boldsymbol{v}_i)$. Moreover, path constraints can also be added to state and controls at each time point $i$.

The NLP can then be written as [76]:

$$\min_{\boldsymbol{s},\boldsymbol{v}} \Phi(\boldsymbol{s}_N) + \sum_{i=0}^{N} \boldsymbol{l}_i(\boldsymbol{s}_i, \boldsymbol{v}_i) \tag{2.18}$$

where $N$ is the number of intervals and $\Phi$ is the scalar terminal weighting function. Eq. 2.18 is subject to Eqs. 2.19 to 2.23:

$$\boldsymbol{s}_0 - \boldsymbol{x}(t_0) = 0 \tag{2.19}$$

$$c_i(\boldsymbol{s}_i, \boldsymbol{v}_i) = 0 \tag{2.20}$$

$$\sum_{k=0}^{K} \boldsymbol{s}_{i,k} \cdot P_{i,k}(t_{i+1}) - \boldsymbol{x}(\boldsymbol{s}_{i+1}, t_{i+1}) = 0 \tag{2.21}$$

$$g(\boldsymbol{s}_i, \boldsymbol{v}_i) \geq 0 \tag{2.22}$$

$$\varphi(\boldsymbol{s}_N) = 0 \tag{2.23}$$

where Eq. 2.19 are the initial values of the OCP, Eq. 2.20 are the collocation constraints, Eq. 2.21 are the continuity constraints, Eq. 2.22 are the path constraints on the controls and states and Eq. 2.23 are the terminal constraints on the state variables. As with the other direct methods, the NLP can then be solved by well known non-linear programming solvers or sequential quadratic programming solvers.

The main advantages of the collocation method are that it can treat unstable systems well and can handle path and terminal constraints robustly [66]. As this research project is based on a model of the human arm that has a high number of DOF (see Section 4.3.1) and as constraints on the movement of the arm will be necessary, the direct collocation method was preferred. The collocation algorithms and optimization framework from the CasADi symbolic software [64] were used for this project.

Note: In the three direct methods presented above, the controls $\boldsymbol{u}(t)$ were discretized as piecewise constant as it is a common choice in literature [66], [77]. This method was chosen for this project. However, the controls can be discretized by different approximations such as Lagrange interpolation polynomials [60], [75] or linear interpolating functions [74]. These approximations generally result in faster optimization time and better accuracy [78]. As the results of this project were satisfactory in the author's view, these were not implemented.

## 2.4 Modeling and simulation of multibody systems in biomechanics

The most commonly used methods to model biomechanical systems are the multibody dynamics or finite element analysis.

Multibody system (MBS) dynamics represent the human body by a series of articulated rigid bodies, i.e. non-elastic and of constant mass. This method allows to study complex articular movements and the associated internal efforts. Various fields and applications use this type of model such as ergonomics [79], rehabilitation [80] and sports [81].

On the other side, finite element analysis in biomechanics is mostly used to evaluate the deformation and constraints undergone by the human body in static or quasi-static situations. One of most common applications of these analyses is the study of the spine for scoliosis assessment and treatment [82].

These methods can also be combined to study both highly dynamic movements and body deformation such as prediction of spine treatments [83]. Flexible MBS often use this approach to account for the flexibility of the articulated bodies [84], [85]. Finite element analysis and flexible MBS are generally numerically expensive and tedious to implement.

Different software are used to model biomechanical systems depending on the application: Adams [86], Anybody Modeling System [87], OpenSim [88], Simpack [89], MOBILE [90], ROBOTRAN [91] and others. Extensive lists are presented in [92], [93].

In this project, the hypothesis of rigid bodies and the multibody dynamics method were chosen to model the biomechanical system. This choice simplifies the study of the human body as classical laws of mechanics can be applied. The choice is also adequate as the deformations of the bodies are not significant in this project. ROBOTRAN symbolic equation generator was used as it is easy to use and well interfaced with Matlab software.

To model the human body with multibody system dynamics, a first step is to build the kinematic chains which are the succession of rigid bodies linked by joints which describe the DOF between each body. The joints can be prismatic, i.e. translation, or revolute, and possess a maximum of 6 DOF, 3 rotations and 3 translations. They are considered ideal, i.e. force and torque are transmitted without loss between each body. In biomechanics, the bodies are generally limb segments such as the arm and forearm for the upper limb and joints are the articular complex such as the elbow joint between the arm and forearm.

### 2.4.1 Open-loop and closed-loop systems

The kinematic chains can be tree-like systems that are either open-loops or closed-loops systems as presented in Figure 2-11. For instance, an open-loop system can be a serial manipulator robot such as the JACO assistive device [3] and a closed-loop system parallel manipulator robot such as the delta robot [94].

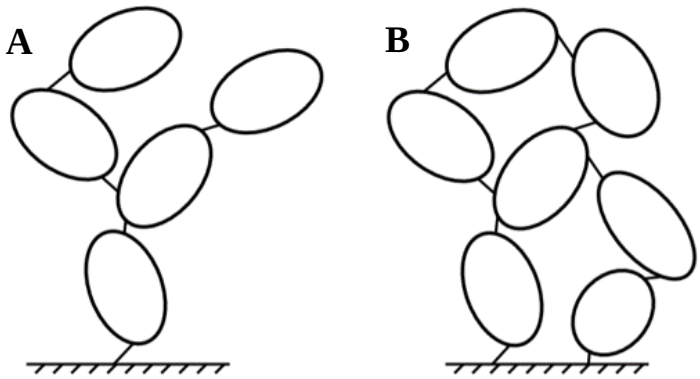


Figure 2-11. Multibody kinematic chains [92]. A. Tree-like system. B. Closed-loop system.

In biomechanics, osteoarticular systems, i.e. bones and articulations, are often considered as open loops model [10], [95]. However, for the shoulder joint and the forearm pronation and supination movement, some studies, respectively [96], [97] and [10], [17], use closed-loop systems as it increased the biofidelity of the model and produced more accurate internal efforts. Moreover, musculoskeletal models use closed-loop to attach the muscle around the osteoarticular models [98].

### 2.4.2 Dynamics [91], [92]

To obtain the equation of motion of MBS, different formalisms can be used such as the Lagrange equations or the Newton/Euler laws formulated recursively. The latter is used by ROBOTRAN.

For a tree-like system, in terms of the generalized acceleration, the semi-explicit or direct dynamics form the equation of motion is presented by Eq. 2.24:

$$\boldsymbol{M}(\boldsymbol{q},\boldsymbol{\delta})\ddot{\boldsymbol{q}} + \boldsymbol{c}(\boldsymbol{q},\dot{\boldsymbol{q}}) = \boldsymbol{Q}(\boldsymbol{q},\dot{\boldsymbol{q}}) \tag{2.24}$$

where $\boldsymbol{q}$ [rad] or [m], $\dot{\boldsymbol{q}}$ $[\frac{\text{rad}}{\text{s}}]$ or $[\frac{\text{m}}{\text{s}}]$ and $\ddot{\boldsymbol{q}}$ $[\frac{\text{rad}}{\text{s}^2}]$ or $[\frac{\text{m}}{\text{s}^2}]$ are, respectively, the generalized positions, velocities, and accelerations, $\boldsymbol{\delta}$ corresponds to the dynamic parameters of the system (body masses [kg], centers of mass [m], inertias [$\text{kgm}^2$]), $\boldsymbol{M}$ is the generalized mass matrix, $\boldsymbol{c}$ is the non-linear vector containing the external, gravity, centrifugal and gyroscopic forces and $\boldsymbol{Q}$, [Nm] or [N], is the generalized forces or torques vector. The implicit or inverse dynamic formulation (Eq. 2.25) expresses the generalized joint forces (or torques) as a function of the kinematics $\boldsymbol{q},\dot{\boldsymbol{q}},\ddot{\boldsymbol{q}}$ and the MBS dynamic parameters:

$$\boldsymbol{Q}(\boldsymbol{q},\dot{\boldsymbol{q}}) = \Phi(\boldsymbol{q},\dot{\boldsymbol{q}},\ddot{\boldsymbol{q}},\boldsymbol{\delta}) \tag{2.25}$$

For a closed-loop system, the generalized joint position, $\boldsymbol{q}$ must satisfy geometric loop constraints written as $\boldsymbol{h}_l(\boldsymbol{q}) = 0$. Then, to complete the system, the first- and second-time derivatives of those constraints are required to be able to "close the loop" at the velocity and acceleration level. Moreover, to introduce the force created by the constraints, the Lagrange multipliers technique can be used. The system can then be described by the following set of DAEs (Eqs. 2.26-2.30):

Semi-implicit form or direct dynamics:

$$\boldsymbol{M}(\boldsymbol{q},\boldsymbol{\delta})\ddot{\boldsymbol{q}} + \boldsymbol{c}(\boldsymbol{q},\dot{\boldsymbol{q}}) = \boldsymbol{Q}(\boldsymbol{q},\dot{\boldsymbol{q}}) + \boldsymbol{J}^T\boldsymbol{\lambda} \tag{2.26}$$

Implicit form or inverse dynamics:

$$\Phi(\boldsymbol{q},\dot{\boldsymbol{q}},\ddot{\boldsymbol{q}},\boldsymbol{\delta}) = \boldsymbol{Q}(\boldsymbol{q},\dot{\boldsymbol{q}}) + \boldsymbol{J}^T\boldsymbol{\lambda} \tag{2.27}$$

And the constraints with time derivatives:

$$\boldsymbol{h}_l(\boldsymbol{q}) = 0 \tag{2.28}$$

$$\dot{\boldsymbol{h}}_l = \boldsymbol{J}(\boldsymbol{q})\dot{\boldsymbol{q}} = 0 \tag{2.39}$$

$$\ddot{\boldsymbol{h}}_l = \boldsymbol{J}(\boldsymbol{q})\ddot{\boldsymbol{q}} + \dot{\boldsymbol{J}}\dot{\boldsymbol{q}}(\boldsymbol{q}, \dot{\boldsymbol{q}}) = 0 \tag{2.30}$$

where $\boldsymbol{h}_l$ are the loop closure geometrical constraints, $\boldsymbol{J}$ is the Jacobian matrix of the system, $\dot{\boldsymbol{J}}\dot{\boldsymbol{q}}$ is the quadratic term of the constraints at acceleration level and $\boldsymbol{\lambda}$ represents the Lagrange multipliers associated with the constraints. To solve this DAE system, the Coordinate Partitioning Method [99], an index reduction method, can be used, transforming this index-3 system to an index-0 system. Globally, the method consists in creating a partition of independent and dependent generalized coordinates and separate the constraint Jacobian accordingly:

$$\boldsymbol{q} = \begin{pmatrix} \boldsymbol{q}_u \\ \boldsymbol{q}_v \end{pmatrix}; J = \begin{pmatrix} J_u & J_v \end{pmatrix} \tag{2.31}$$

Then, the index reduction is performed, relying on matrix permutations and operations. See [91] for more details. Finally, to solve the algebraic constraints $\boldsymbol{h}_l(\boldsymbol{q})$, which are generally non-linear, an iterative method like the Newton-Raphson algorithm can be used, expressing $\boldsymbol{q}_v$, the dependent coordinates, for given $\boldsymbol{q}_u$, the independent coordinates, through successive iterations of $\boldsymbol{q}_v$.

For the optimal control part of this project, the DAE system is not solved by this index reduction method. It is solved inside the direct collocation NLP. However, the concept of independent and dependant variables will be important for the interaction of the human-exoskeleton system presented in 2.5.1.

### 2.4.3 Loop constraints [91], [92]

The geometric constraints $\boldsymbol{h}_l$ must be expressed to deal with a closed MBS. A so-called *cutting* method can be used to identify the constraints that will re-create a tree-like MBS (Figure 2-11A). The ROBOTRAN software proposes 3 types of *cuts*:

- Body cut: cut inside a body (Figure 2-12A);
- Ball cut: cut a joint (Figure 2-12B);
- Rod cut: used to replace a connecting rod with negligible mass and inertia;

As body cuts and ball cuts are the most commonly used loop constraints in biomechanics, these two are detailed hereafter.

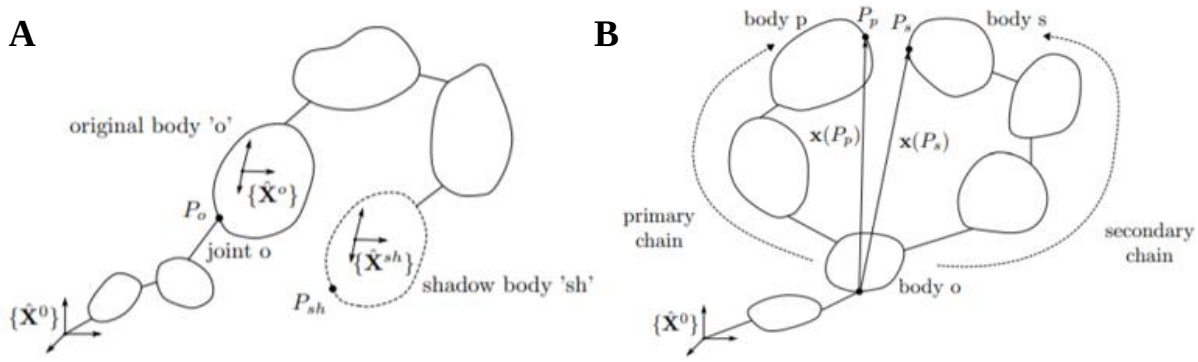


Figure 2-12. Kinematics constraints for multibody system loop-closure [91]. A. Body cut. B. Ball cut.

The body cut, shown in Figure 2-12A, is the procedure of cutting a body into an original body and a shadow copy of this body. The mass and inertia properties are distributed between both bodies. The first 3 imposed constraints require points $P_o$ and $P_{sh}$ to have the same position in the global frame $\{\hat{X}^0\}$. Then 3 more constraints impose that the original and shadow body frame, $\{\hat{X}^o\}$ and $\{\hat{X}^{sh}\}$ coincide at any time. This is the most general type of cut and allow torques and forces to be transmitted between the original and shadow body. Practical examples of such constraints are solder between two metal parts, a solid brace to attach an exoskeleton to an arm or a shoe to a foot.

The ball cut, shown in Figure 2-12B, is the equivalent of a ball joint and is ideal, i.e. no torque is transmitted through. In this case, points $P_p$and $P_s$ of bodies $p$ and $s$, which are part of the kinematic chain, are imposed to coincide at any time, thus creating 3 constraints. Practical examples of such constraints are any ball joint in mechanical systems, a muscle attachment to a bone or a joystick on a game controller.

## 2.5 Multibody system dynamics applied to exoskeleton synthesis

This last section of the literature:

1. Briefly covers the human-exoskeleton interactions theory and literature as the research article in Chapter 4 is extensive on the subject.
2. Summarizes the optimal exoskeleton synthesis in the literature.

To help with the clarity of these following sections, Figure 2-13 presents a simplified model of the upper limb and of an exoskeleton with the variables $\boldsymbol{q}_H$, the user's joint generalized positions, $\boldsymbol{Q}_H$, the user's joint generalized torques, $\boldsymbol{q}_E$, the exoskeleton joint generalized positions, $\boldsymbol{Q}_E$, the exoskeleton joint generalized positions, and, $\boldsymbol{l}_E$, the exoskeleton dimensions.

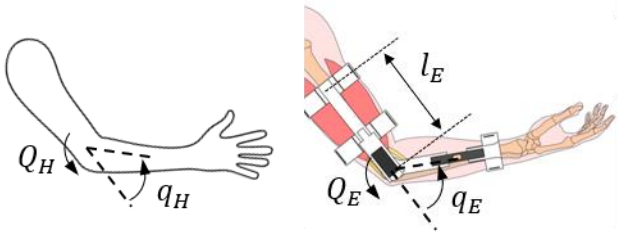


Figure 2-13. A simplified version of the upper limb and an exoskeleton to illustrate the main variables of the human-exoskeleton interaction, $\boldsymbol{q}_H$, the user's joint generalized positions, $\boldsymbol{Q}_H$, the user's joint generalized torques, $\boldsymbol{q}_E$, the exoskeleton joint generalized positions, $\boldsymbol{Q}_E$, the exoskeleton joint generalized positions, and, $\boldsymbol{l}_E$, the exoskeleton dimensions. *(Image adapted from* [100]*)*

### 2.5.1 Human-exoskeleton interaction

For the kinematic interaction between the limb and the exoskeleton, the most common modeling method is to use algebraic constraints that ensure the connected exoskeleton and limb segment are solidly attached to one another [44], [101], [102]. This is the equivalent of the body cuts presented in Section 2.4.3. A body cut creates 3 orientation constraints and 3 positions constraints, which are defined in the vector of kinematic loop constraints $\boldsymbol{h}_l$ (Section 2.4.2). In practical terms, the body cut between the exoskeleton and the limb is represented by a solid brace wrapped around the user's arm. This implies that the brace does not move in respect to the arm. However, this is not the case in real-life situations. Indeed, with the skin movements of user's limb and the imperfections in the

brace system, the brace will move in respect to the arm. The exoskeleton model used in this study possesses a prismatic joint (see Section 4.3.2) at the forearm segment. While this joint was not added to compensate for the skin displacement problems, it can act as such. The same method was used by [103]

**The inverse dynamics problem**

The inverse dynamics of a model provides the necessary generalized forces and torques to accomplish a certain trajectory as written in Eq. 2.27 for closed loop-systems. To design an exoskeleton, one can desire to find the exoskeleton torques $\boldsymbol{Q}_E$ that globally reduce the user's joint torque $\boldsymbol{Q}_H$ (or other costs as presented in the next section) for a trajectory of the user's joint $\boldsymbol{q}_H(t)$ by simulation. As the exoskeleton must follow the user's limb, the exoskeleton trajectory is dependent of the user's trajectory, hence, $\boldsymbol{q}_E = f\big(\boldsymbol{q}_H(t)\big)$. This is the partitioning of the generalized coordinates (Section 2.4.2), $\boldsymbol{q}_H = \boldsymbol{q}_u$, the independent variables and $\boldsymbol{q}_E = \boldsymbol{q}_v$ the dependent variables.

The effect of the previously stated kinematic loop constraints is presented in Eqs. 2.26 and 2.27 (Section 2.4.2), where the last term of the equations $\boldsymbol{J}^T\boldsymbol{\lambda}$ introduces the constraints forces to the DAE system. Then, with the partitioning (Section 2.4.2), it is possible to write the following version of the inverse dynamics of the problem (see details in [104]), Eq. 2.32:

$$\boldsymbol{Q}_u = \Phi_u + B^T{}_{vu}(\boldsymbol{Q}_v - \Phi_v) \tag{2.32}$$

where $\boldsymbol{Q}_u$ and $\boldsymbol{Q}_v$ are the generalized independent and dependant forces and torques, $\Phi_u$ and $\Phi_v$ are the implicit functions of the kinematics and dynamics parameters (mass, CoM, Inertia) and $B_{vu} = -(J_v)^{-1}J_u$. In this case the $\boldsymbol{Q}_u = \boldsymbol{Q}_H$ and $\boldsymbol{Q}_v = \boldsymbol{Q}_E$. However, to find the need actuation of the joints, i.e. motorization, the generalized forces and torques must be separated in two, their active and their passive components. The passive components come from friction, external forces, spring elements, etc. The active component is the motorization of the joint. Therefore, one can write, Eq. 2.33:

$$\boldsymbol{Q}_{u,a} = \Phi_u - \boldsymbol{Q}_{u,p} + B^T{}_{vu}(\boldsymbol{Q}_{v,p} - \Phi_v) \tag{2.33}$$

where $\boldsymbol{Q}_{u,a}$ is the active component of the independent generalized joint forces and torques, and $\boldsymbol{Q}_{u,p}$is the passive component and $\boldsymbol{Q}_{v,p}$ is the passive component of the dependent joints. Two

things are important here, (i) the active component of the dependent joint is not included in the equation because (ii) this system has a single solution if the number of independent joints is equal to the number of active joints. By adding, the active component of the dependent joints $\boldsymbol{Q}_{v,p}$, the problem becomes *over-actuated*. This is the case of the human-exoskeleton interaction, as both the user's joints and the exoskeleton joints will produce torque to move the arm. The over-actuation problem has an infinite number of solutions; therefore, it needs to be solved.

To solve it, one can use the Moore-Penrose pseudo-inverse method [95] or a non-linear optimization problem. The inverse dynamics problem is one of the most common methods for the design of exoskeletons as is it simple and efficient. This is covered in the following Section 2.5.2.

**Adding the trajectories to the problem**

The main drawback of the inverse dynamics problem is that the user's trajectories $\boldsymbol{q}_H$ are known, generally from a motion capture analysis, and are not part of the optimization variables. However, the exoskeleton does not follow the human limb exactly as it will be controlled by embedded control systems different strategies that will affect the user's joint trajectory [28], [105], [106].

To add the trajectories to the problem, one can use a constrained optimal control problem such as the one depicted in Section 2.3. The control vector can be defined by $\boldsymbol{u}(t) = [\boldsymbol{Q}_H \quad \boldsymbol{Q}_E]$ and the state vector can be defined as $\boldsymbol{x}(t) = [\dot{\boldsymbol{q}}_H \quad \boldsymbol{q}_H]$. Then, the NLP variables include the user's joint torques, the exoskeleton joint torques and the user's joint positions and velocities, therefore, the full kinematic-dynamic interaction between the exoskeleton and the limb is considered.

### 2.5.2 Optimal synthesis of exoskeletons

This section presents a short summary of the main trends in optimal synthesis of exoskeletons. It is not indented as an extensive review, but as to find the most interesting methods or gaps in the optimization of upper limb exoskeleton parameters. Therefore, the summary is not limited to upper limb exoskeleton devices as methods from other types of devices can be of interest.

**Rehabilitation devices**

Section 2.2 showed that exoskeleton devices for rehabilitation purposes are proliferating. The constraints on their development are less restrictive as the weight and size of their actuators and mechanism is not critical. However, with their powerful motors, these devices can produce high

levels of forces and torques on the user's joint. When the exoskeleton joints are misaligned with those of the user, parasitic forces and torques can occur. These can be defined as efforts that act in a different axis than the user's joint main axis [41]. This can cause injuries or pain to the user. Therefore, extensive studies have been done on the subject [44], [107]–[109]. Most of these studies focus on the mechanism design and topology and then evaluate the parasitic forces by experimentation. Nonetheless, they all conclude that parasitic forces should be assessed when designing an exoskeleton. Although this was not the case in this thesis, it is an important problem and should be taken into account in future work.

**Device centered optimizations**

Some emerging exoskeleton devices tend to be designed for complex purposes such as spasm control in the spasticity affected population [110] or for complex body parts such as the hand [111]. The optimization procedures or objective are therefore specific to the task. For instance a kinematic and dynamic optimization of an underactuated finger exoskeleton to maximize the force transmission [112]. While those studies are not complete procedures for the optimization of an exoskeleton, the underlying mechanisms and optimizations methods can be of interest.

**Passive and active power transmission system**

Most studies and devices found in the literature either had a passive or active power system transmission (see Table 2-2). However, some studies [113]–[115] used both systems with success, generally showing that the passive elements could reduce the required motor torque and size, therefore reducing the weight of the exoskeleton.

**Inverse dynamics**

The over-actuated inverse dynamics problem depicted in Section 2.5.1 is common in the literature for exoskeleton design. The variants are generally the optimization problem cost functions such as minimizing user joint torques [116], parasitic forces and torques [103], user joint power [117] or user muscle force [118]. The seems to be no agreement in the literature as to which of these cost functions is best for the design of exoskeletons. Therefore, in this study, the user's joint torque was selected as is it the most direct evaluation of the user's joint effort.

The variables of the optimization can be geometric [18], [119], i.e. the dimensions of the exoskeleton, or dynamic such as the motor torques [120] and/or passive elements characteristics [121].

**Interference and collision avoidance**

To obtain a good kinematic fit between the exoskeleton and the user, the most important element is the loop closure as seen in Section 2.4 and 2.5.1. However, this can be compromised if the exoskeleton touches or interferes with the user. Some studies tend to build optimization frameworks that optimize the loop closure, generally by maximizing the number of closed-loop configurations [122], and add collision avoidance constraints [103] or algorithms [123].

**Optimal control problems**

To add the user's joint trajectories in the design and optimization process, studies use variants of the optimal control problem described in Sections 2.3 and 2.5.1. In general, this provides a more physiologically meaningful human-exoskeleton interaction simulation [124] that can lead to user centered designs [125], [126] and to insights for potential control laws [105], [127] that could be embedded in the exoskeleton devices.

# CHAPTER 3 OBJECTIVES AND RESEARCH PROCESS

## 3.1 Problem

The critical review of literature allowed to identify the following elements:

- Section 2.2: The geometric and dynamic design constraints for upper limb assistive and wearable exoskeletons are stricter than rehabilitation or augmentation exoskeletons. Generally, the global size and weight of the system need to be lower to allow the exoskeleton to be worn and used for long periods of time.
- Section 2.2 and Section 2.5.2: The choice of power transmission systems is crucial in the development of an exoskeleton. The selection or combination of active systems or passive could be a valid solution, although the characteristics of both active and passive systems must be chosen carefully.
- Section 2.5.1: To identify the kinematic and dynamic impact of the exoskeleton on the human limb, optimizations need to vary trajectories and torques of the multibody system. An optimal control problem is a solution to this requirement.
- Section 2.5.2: There are few complete procedures for the geometric and dynamic design of 3D assistive and wearable upper limb exoskeletons for functional tasks.

## 3.2 General objective

The objective of this research project is to develop a geometric and dynamic synthesis procedure to design and personalize an assistive upper limb exoskeleton for a healthy subject while doing specific functional tasks.

To achieve this general objective, three specific objectives are required.

## 3.3 Specific objectives

**O1:** Model the human-exoskeleton multibody system

**O2:** Develop the exoskeleton geometric optimization to maximize the kinematic fit to the user and develop the exoskeleton dynamic optimization to minimize the effort required by the user;

**O3**: Develop the exoskeleton geometric and dynamic synthesis and apply it for 6 functional tasks.

The functional tasks, for the right upper limb, are:

- Eat with a spoon;
- Arm frontal reach: The arm starts relaxed on the side of the person and then reaches in front of the person, at head level;
- Arm reach right to left: The arm starts relaxed on the side of the person and then reaches to the right of the person at head level, then all the way to the front of the person still at head level.
- Open a door;
- Zip your own coat;
- Comb your hair.

The accomplishment of the objectives is shown in Chapter 4 through a scientific paper. For **O1**, Section 5.1 completes the methodology from Sections 4.3.1 and 4.3.2.

# CHAPTER 4 ARTICLE I: DEVELOPMENT OF A PROCEDURE TO OPTIMIZE THE GEOMETRIC AND DYNAMIC DESIGNS OF ASSISTIVE UPPER LIMB EXOSKELETONS

This article was submitted to the Multibody System Dynamics Journal on the 27th of January 2020.

## Development of a procedure to optimize the geometric and dynamic designs of assistive upper limb exoskeletons

Blanchet Laurent[1], Achiche Sofiane[1], Quentin Docquier[2], Paul Fisette[2], Raison Maxime[1]

[1]*Department of mechanical engineering, Polytechnique Montreal, Montreal, Canada*

[2]*Mechatronic, Electrical Energy, and Dynamic Systems (MEED), Institute of Mechanics, Materials and Civil Engineering (iMMC), Université catholique de Louvain, Louvain-la-Neuve, Belgium*

Email : laurent.blanchet@polymtl.ca, Phone : 450-931-0307

*Keywords: Multibody, exoskeleton, optimization, optimal control, biomechanics, design*

## 4.1 Abstract

The need for upper limb assistive and wearable exoskeletons is growing in various fields, e.g. either to support patients with neuromuscular disabilities or to reduce the effort strains on workers. These exoskeletons should reduce the efforts required by the user during functional tasks (dynamic consideration) and should fit the user's size (geometric consideration). This is a tedious task, due to the 3D human-exoskeleton interactions, and to the complex and interdependent selection of the power transmission characteristics, i.e. motors or passive elements. There are still few guidelines and few clear procedures to support geometric and dynamic syntheses of these exoskeletons.

The objective of this study is to develop a procedure for geometric and dynamic syntheses of assistive upper limb exoskeletons, to serve as a tool to optimize their design.

First, a geometric optimization of the exoskeleton dimensions enabled to maximize the kinematic loop closure and to avoid collisions with the body segments, while carrying out specific functional tasks. Secondly, through an optimal control problem, the dynamic characteristics of the exoskeleton were obtained by minimizing the user's joint torques for the functional tasks.

Closing the kinematic loops of the exoskeletons with optimized dimensions was achieved for all functional tasks, which was 10.8% more than with a visual identification of the dimensions. The resulting dynamic parameters could reduce the user's joint torque to less than 10.6% of the human-only simulations for nearly all joints and tasks.

These results showed that the geometric and dynamic synthesis procedures were successful. This is important, as it can enable the development of dedicated exoskeletons, such as lighter and smaller exoskeletons. The future

perspectives will be to build an optimization framework, where the geometric and dynamic parameters could be optimized together, and to minimize the user's muscle forces instead of joint torques for specific design purposes.

## 4.2 Introduction

Exoskeleton devices are proliferating in rehabilitation, human-augmentation, and assistance fields. In rehabilitation, devices are used either to recover or develop motor skills for different types of patients. In this field, most devices are non-wearable [1], [2], as they use strong and heavy motors to provide functions such as haptic feedback [3] and precise motion for patient evaluation [4]. On their part, human-augmentation exoskeletons generally aim to provide the user with more strength [5], [6] for tasks such as lifting heavy objects or transporting heavy loads for certain distances [7]. The use of human-augmentation exoskeletons is of high interest for military and industrial applications; however, they generally rely on strong motors and bulky frames. Finally, wearable assistive exoskeletons are increasingly prevalent in research and they aim to ease pain and fatigue for industrial workers [8] and to assist patients with neuromuscular troubles that cause a lack of muscle force [9]. However, it should be noted that this prevalence is mainly true for the exoskeletons of lower limbs [10]–[12], while for the upper limbs, assistive and wearable devices are at their infancy stage [13].

A major obstacle for the development of wearable assistive exoskeletons, compared to rehabilitation or augmentation devices, is the tight constraints on the system size. To be comfortable to wear for a long period of time, the constraints on the overall size, and therefore on the sizing of dynamic actuators and geometric parameters make the design task more challenging [1].

To achieve a functional and optimal upper limbs exoskeleton design, the dynamics must be properly considered, where a first important concern is the appropriate sizing in terms of geometric size and power of the actuators.

A second major concern is the choice of the power transmission system. Some studies [14], [15] tended to develop fully passive exoskeletons to reduce weight and enhance portability. However, these ones were not able to assist the upper limb in many different tasks, as the elastic power

transmission systems generally help the user for gravity affected movements only [16]. Therefore, for complex tasks such as opening a door, the user even tended to spend more effort with the exoskeleton [17], [18] than without it. To prevent such issues, some devices combined active and passive power transmissions [19], and one of the principal conclusions of these studies was that the passive mechanisms help lowering the size and power of the required motors [20].

To support the design of exoskeletons, different studies in multibody dynamics used models of kinematically constrained human limbs to an exoskeleton. These models were then optimized for various cost functions. For instance, the first optimized elements were often the geometric parameters, to find the optimal dimensions for the kinematic fit of the exoskeleton to the user [21] or to maximize force transmission from the exoskeleton to the user [22]. The second optimized elements were the dynamic parameters such as motor torques for active exoskeletons or passive elements characteristics such as springs for passive exoskeletons. In this case, the objective was to minimize the human effort such as joint torques [23] or powers [24], or muscle forces [25]. The dynamic optimizations can be formulated by non-linear problems using the computed generalized forces and torques from the inverse dynamics of the model for different tasks [25].

However, the inverse dynamics method does not consider the impact of the exoskeleton on the user's joint trajectories, as the generalized coordinates, velocities, and accelerations are not variables of the optimization. To overcome this challenge, one can use optimal control [26], where the optimization variables are the generalized positions, velocities and torques of the model, therefore the full interaction is considered. This approach was implemented in this study.

Despite the challenges of exoskeleton design related to the complex human-exoskeleton interaction and complex sizing and selection of power transmission systems, the literature has shown that there are very few guidelines and few clear procedures to support the geometric and dynamic syntheses of 3D wearable and assistive upper limb exoskeletons according to desired functional tasks.

Consequently, the objective of this study is to develop geometric and dynamic synthesis procedures, to serve as tools to design and personalize an upper limb exoskeleton for a given subject. This will be achieved through the execution of six specific functional tasks by one subject,

such as eating with a spoon or opening a door, which were recorded in a state-of-the-art motion capture environment. Specific objectives are, first, to size the exoskeleton to fit the user for all the functional tasks and, secondly, to select the characteristics of the motors and passive elements to reduce the user effort for each task.

### Highlights of this study

The main contribution of this research is the successful geometric and dynamic synthesis procedure for a 3D upper limb active and passive exoskeleton for 6 functional tasks. The specific highlights are that:

1. The developed geometric optimization framework enables the kinematic loop closure over all functional tasks, while avoiding collisions with the body segments.
2. The dynamic optimization framework reduces the torque required by the user's joints, while closely following the experimental trajectories of the functional tasks.
3. The dynamic optimization shows the importance of combining passive elements with motors, by enabling the size reduction of the required motors.

## 4.3 Methods

The global overview of the synthesis procedure of the upper limb exoskeleton is presented in Figure 4-1.

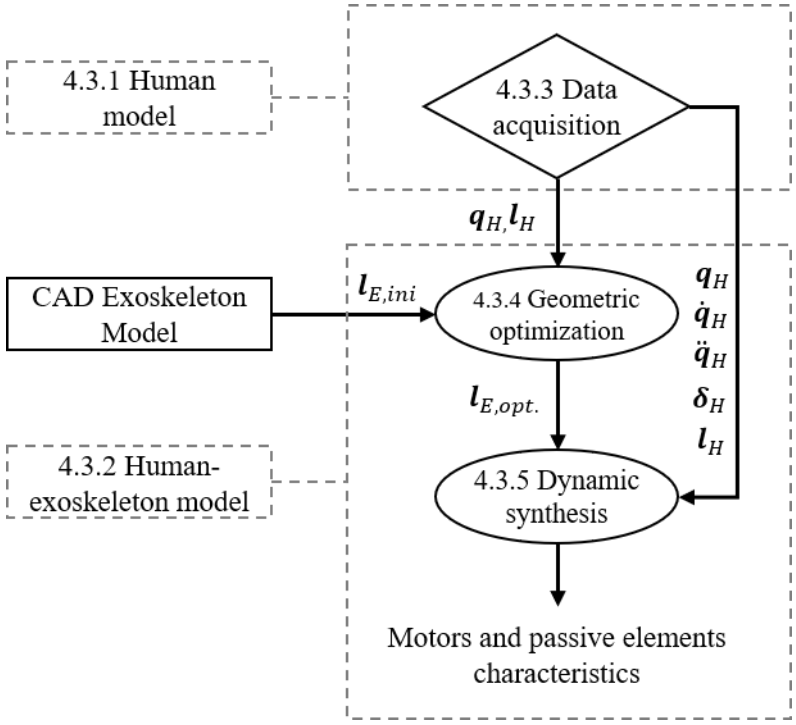


Figure 4-1. Synthesis procedure, including the functional tasks generalized positions, $\boldsymbol{q}_H$, velocities, $\dot{\boldsymbol{q}}_H$, and accelerations, $\ddot{\boldsymbol{q}}_H$, the subject body lengths $\boldsymbol{l}_H$ and the subject inertial parameters $\boldsymbol{\delta}_H$, the initial exoskeleton geometric parameters $\boldsymbol{l}_{E,ini}$ from the CAD exoskeleton model, the optimized exoskeleton geometric parameters $\boldsymbol{l}_{E,opt.}$

The first step of this procedure is the data acquisition (described in Section 4.3.3), which provides the functional tasks generalized positions, $\boldsymbol{q}_H$ [rad] or [m], velocities, $\dot{\boldsymbol{q}}_H$ $[\frac{\text{rad}}{\text{s}}]$ or $[\frac{\text{m}}{\text{s}}]$, and accelerations, $\ddot{\boldsymbol{q}}_H$ $[\frac{\text{rad}}{\text{s}^2}]$ or $[\frac{\text{m}}{\text{s}^2}]$, the subject body lengths $\boldsymbol{l}_H$ [m], and the body segment inertial parameters $\boldsymbol{\delta}_H$, i.e. mass [kg], center of mass [m], and moment of inertia [$\text{kgm}^2$]. The human model (Section 4.3.1), is used alone for this process. The geometric optimization and dynamic synthesis use the human-exoskeleton model (Section 4.3.2). The geometric optimization (Section 4.3.4) takes the $\boldsymbol{q}_H$, $\boldsymbol{l}_H$ provided by the data acquisition step, and the non-optimized exoskeleton geometric parameters $\boldsymbol{l}_{E,ini}$ [m] derived from its CAD model, to yield the optimized exoskeleton geometric parameters $\boldsymbol{l}_{E,opt.}$ [m] through a non-linear optimization. Finally, the dynamic synthesis (Section 4.3.5) takes the positions, $\boldsymbol{q}_H$, velocities, $\dot{\boldsymbol{q}}_H$, and accelerations, $\ddot{\boldsymbol{q}}_H$, the subject body

lengths $\boldsymbol{l}_H$ and inertial parameters $\boldsymbol{\delta}_H$ from the data acquisition step and the $\boldsymbol{l}_{E,opt.}$ from the geometric optimization to provide the motors and passive elements characteristics through an optimal control problem, solved as a non-linear problem.

### 4.3.1 Human model

The full upper limb model shown in Figure 4-2 is based on the kinematics chain proposed by Laitenberger et al. [27], composed of the thorax, clavicle, scapula, humerus, ulna, radius, and hand. The thorax is considered as the moving base of the system, as it can move freely in relation to the ground. However, in this study, the moving base was fixed to simplify the optimization processes. As can be seen in Figure 4-2, the sternoclavicular (SC), acromioclavicular (AC) and glenohumeral (GH) joints are defined with spherical joints ($q_{H,7-9}, q_{H,10-12}, q_{H,13-15}$, respectively). The flexion/extension of the elbow joint is defined with a single revolute joint $q_{H,16}$, followed by a pronation/supination (PS) closed loop ($q_{H,17-21}$). This loop contains the humeroulnar (HU), radioulnar (RU), a virtual center of rotation (CoR) and the humeroradial (HR) joint which consists in a ball cut, i.e. a cut of ball joint, to close the loop. Finally, the radiocarpal joint at the hand is modeled with a universal joint ($q_{H,22-23}$).

The positions of the CoR and axis of rotation (AoR) for all joints were calculated using the symmetrical CoR estimation (SCoRE) and symmetrical axis of rotation approach (SARA) functional methods [28]–[30] respectively. These positions are represented by the body lengths $\boldsymbol{l}_H$. The segment inertial parameters, $\boldsymbol{\delta}_H$, i.e., mass, center of mass, and inertia were calculated by using the Yeadon anthropometric model [31].

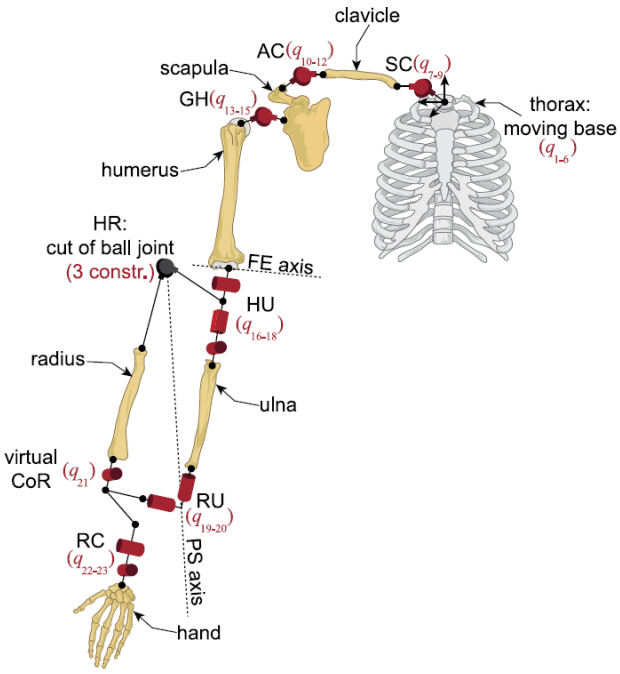


Figure 4-2. Kinematic chain of the human multibody model [27]. Sternoclavicular (SC) joint, $q_{H,7-9}$, acromioclavicular joint (AC), $q_{H,10-12}$, glenohumeral (GH) joint, $q_{H,13-15}$, humeroulnar (HU) joint, $q_{H,16-18}$, radioulnar (RU) joint, $q_{H,19-20}$, a virtual center of rotation (CoR), $q_{H,21}$, humeroradial (HR) joint, ball cut, and radiocarpal (RC) joint, $q_{H,22-23}$.

### 4.3.2 Human-Exoskeleton model

The exoskeleton model, based on [32] and shown in Figure 4-3, is a wearable and assistive exoskeleton, and its purpose is to help the user by compensating, in part or totally, the weight of his arm and in-hand objects in every day or work tasks.

The exoskeleton is designed to be attached to a wearable back brace. It is connected to the user's arm by braces at the upper arm and forearm, just before the wrist. These ones are described by the kinematics constraints of body cuts $h_{l,1-6}$ and $h_{l,7-12}$. The body cut constraints impose that the brace and arm possess a common point of attachment and that the orientation of the bodies must coincide at any time as described in [33].

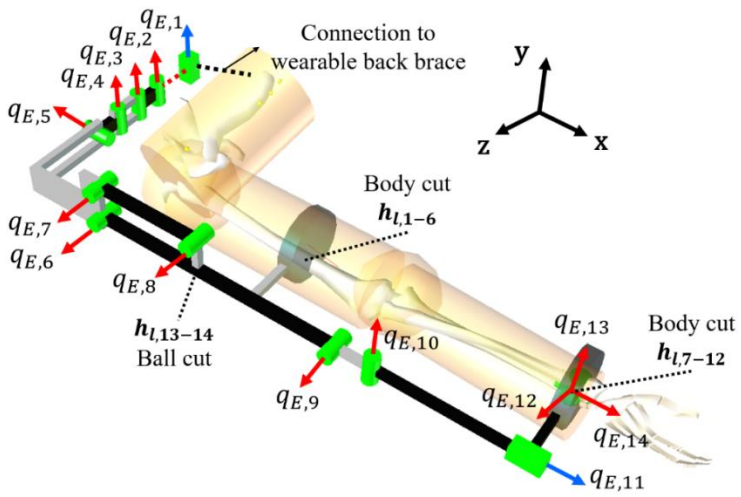


Figure 4-3. The exoskeleton model, with 14 generalized coordinates $\boldsymbol{q}_E$, 4 of which can be motorized and loaded with a torsion spring, $q_{E,5-6-9-14}$. The kinematic constraints by cutting the body represent the braces attached to the user's arm and the ball cut closes the four-bar loop mechanism.

In total, the exoskeleton is composed of four joints that could be motorized and eight additional passive joints. Additionally, each motorized joint can also be spring-loaded as a torsion spring can be inserted in the joint mechanism. To obtain a passive exoskeleton, the motorized joints can be compensated by the torsion springs only. The four-bar mechanism at the shoulder can be used to install a linear spring instead of a torsion spring in joint $q_{E,6}$, or to add an extra motor to assist the shoulder flexion extension movement.

In details, starting from the back fixation, there is one prismatic joint, $q_{E,1}$, and three redundant revolute joints, $q_{E,2-4}$ . These passive joints help the exoskeleton adjust to the shoulder movements. Then there is the first motorized joint, $q_{E,5}$, which assists the abduction and abduction at the shoulder (S. AA). The four-bar mechanism follows up with three revolute joints, $q_{E,6-8}$ and a ball cut, $h_{l,13-14}$. Joints $q_{E,6}$ can be motorized to assist the shoulder flexion/extension (S. FE). The elbow joint $q_{E,9}$ can also be motorized to compensate for the flexion extension of the user's elbow (E. FE). To reach the wrist joint, four passive joints, $q_{E,10-11-12-13}$, let the exoskeleton adjust to the complex forearm pronation supination (F. PS) movement. Finally, at the wrist, there is the last motorized joint, $q_{E,14}$, which helps the F. PS movement. The inertial parameters, $\boldsymbol{\delta}_E$, i.e. mass, centers of masses and inertial parameters of the exoskeleton were determined with a CAD software.

The differential algebraic equation (DAE) system describing the human-exoskeleton closed loop system is given by Eq. 4.1 to Eq. 4.4:

$$\boldsymbol{M}(\boldsymbol{q},\boldsymbol{\delta})\ddot{\boldsymbol{q}} + \boldsymbol{c}(\boldsymbol{q},\dot{\boldsymbol{q}}) = \boldsymbol{Q}(\boldsymbol{q},\dot{\boldsymbol{q}}) + \boldsymbol{J}^T\boldsymbol{\lambda} \tag{4.1}$$

$$\boldsymbol{h}_l(\boldsymbol{q}) = 0 \tag{4.2}$$

$$\dot{\boldsymbol{h}}_l = \boldsymbol{J}(\boldsymbol{q})\dot{\boldsymbol{q}} = 0 \tag{4.3}$$

$$\ddot{\boldsymbol{h}}_l = \boldsymbol{J}(\boldsymbol{q})\ddot{\boldsymbol{q}} + \dot{\boldsymbol{J}}\dot{\boldsymbol{q}}(\boldsymbol{q},\dot{\boldsymbol{q}}) = 0 \tag{4.4}$$

where $\boldsymbol{q} = [\boldsymbol{q}_H\ \boldsymbol{q}_E]$, $\dot{\boldsymbol{q}} = [\dot{\boldsymbol{q}}_H\ \dot{\boldsymbol{q}}_E]$, $\ddot{\boldsymbol{q}} = [\ddot{\boldsymbol{q}}_H\ \ddot{\boldsymbol{q}}_E]$ are the complete generalized positions, velocities and accelerations, respectively, $\boldsymbol{\delta} = [\boldsymbol{\delta}_H\ \boldsymbol{\delta}_E]$ corresponds to the dynamic parameters of the system (body masses, centers of mass, inertias), $\boldsymbol{M}$ is the generalized mass matrix, $\boldsymbol{c}$ is the non-linear vector containing the external, gravity, centrifugal and gyroscopic forces, $\boldsymbol{Q}$ [Nm] or [N] is the generalized forces or torques vector that can be separated as $\boldsymbol{Q}_H$ and $\boldsymbol{Q}_E$, respectively, in the human and exoskeleton joints, $\boldsymbol{h}_l$ are the loop closure geometrical constraints, $\boldsymbol{J}$ is the Jacobian matrix of the system, $\dot{\boldsymbol{J}}\dot{\boldsymbol{q}}$ is the quadratic term of the constraints at acceleration level and $\boldsymbol{\lambda}$ represents the Lagrange multipliers associated with the constraints. As mentioned in the previous sections, $\boldsymbol{q}$ ($\dot{\boldsymbol{q}}$ or $\ddot{\boldsymbol{q}}$) can be grouped in $\boldsymbol{q_H}$ the generalized coordinates of the human, which corresponds to $\boldsymbol{q}_u$ the independent generalized coordinates, $\boldsymbol{q}_{H,v}$ the dependent generalized coordinates of the human, $\boldsymbol{q_E}$ the exoskeleton generalized coordinates, and finally the global dependent generalized coordinates $\boldsymbol{q}_v = [\boldsymbol{q}_{H,v}\ \boldsymbol{q_E}]$. All models and all symbolic equations were generated using ROBOTRAN Multibody dynamics software [34] based on recursive formalisms for kinematics and dynamics [33].

### 4.3.3 Data acquisition

To develop and illustrate the development of geometric and dynamic synthesis procedures, data from one healthy subject (Age: 25, Mass: 90 kg, Height: 1.93 m) were acquired by using the set of reflective markers, as proposed in [27]. The study was approved by the institutional ethical committee, and the participant gave his informed consent. This set ensured at least 4 markers per body for redundancy and technical markers to minimize soft tissue artefacts. The 3D markers trajectories were measured at 100 Hz by a motion-capture system composed of 12 cameras (T40S,

Vicon-Oxford, UK). A total of 6 different functional tasks were executed and selected from the study by Rosen et al. [35]. The tasks, described in Table 4-1, were chosen to mimic activities of daily life and to ensure a broad range of amplitudes for each joint. The data for the SCoRE and SARA methods were also acquired to find the CoR and AoR of the subject. The user's relative coordinates $\boldsymbol{q}_H$ were computed by the kinematics identification process described in [36]. This process minimizes the difference between the experimental 3D marker coordinates and the marker coordinates obtained by the forward kinematics function of the multibody system.

Table 4-1. Recorded functional tasks and their abbreviations

| Functional tasks | Abbreviations |
|---|---|
| Eat with a spoon | ES |
| Arm frontal reach | AR |
| Arm reach right to left | RL |
| Open a door | OD |
| Zip your coat | ZC |
| Comb your hair | CH |

### 4.3.4 Geometric optimization

The goal of the geometric optimization is to maximize the *"exoskeleton fit"* to the user while doing functional tasks. This *"exoskeleton fit"* can be defined by the combination of three elements:

1. The loop constraints $\boldsymbol{h}_l(\boldsymbol{q}, \boldsymbol{l})$ between the arm and the exoskeleton must be satisfied, where $\boldsymbol{q}$ are the relative coordinates for the combined human-exoskeleton model and $\boldsymbol{l}$ are the combined human and exoskeleton dimensions;
2. There are no collisions between the arm and the exoskeleton during the execution of the functional tasks;
3. The exoskeleton is closely fit to the user to:

   - lower the size and weight of the exoskeleton, to increase the user's comfort;

   - reduce the lever arms across the exoskeleton bodies, although this was not studied in this research.

To combine all functional tasks in this study, each task was optimized one by one, and the results were used to provide a better initial guess for the second optimization, where all the functional

tasks were optimized simultaneously. This allowed for the exoskeleton to be sized to the user for all tasks.

#### 4.3.4.1 Loop closure

Generally, to solve the loop constraints $\boldsymbol{h}_l$ presented in Eq. 4.2, a Newton-Raphson algorithm is used [33]. However, if the constraints cannot be satisfied, i.e., the MBS cannot achieve loop closure, the result of the Newton-Raphson procedure is an inconsistent system, far from the loop closure [37]. In this study, and for exoskeletons in general, with the uncertainties coming from the user's skin movement, the precision of the exoskeleton dimensions or the 3D marker trajectories errors, constraints $\boldsymbol{h}_l$ may not always reach a solution. Instead, following the method proposed by [37], the loop constraints were minimized (Eq. 4.5), as this provides a solution even if the loop cannot be closed by the Newton-Raphson method. However, if the system can be closed, $\boldsymbol{h}_l$ will be equal to 0, as with Newton-Raphson.

$$\min_{\boldsymbol{l}_E, \boldsymbol{q}_v} L_C = \frac{1}{2} \boldsymbol{h}_l(\boldsymbol{q}, \boldsymbol{l})^T \boldsymbol{h}_l(\boldsymbol{q}, \boldsymbol{l}) \tag{4.5}$$

The independent relative coordinates $\boldsymbol{q}_u$ were not considered as optimization variables here as they describe the displacement of the user's arm in functional tasks. The optimization process makes vary the dependent relative coordinates $\boldsymbol{q}_v$**,** which are the exoskeleton joints $\boldsymbol{q}_E$, and the forearm loop dependent coordinates $\boldsymbol{q}_{H,v}$. The exoskeleton lengths, $\boldsymbol{l}_E$**,** are also variables of the optimization.

Figure 4-4 shows the optimized exoskeleton dimensions. Dimensions $l_{E,1-6,10}$ help to avoid collisions with the shoulder; dimension $l_{E,7-8}$ aim to help reach the arm brace; dimension $l_{E,11}$ aims to help reach the elbow joint and dimension $l_{E,9,12}$ aim to help reach the wrist brace. Finally, dimensions $l_{E,13-16}$ are used to size the four-bar mechanism, so that it does not interfere with the rest of the exoskeleton.

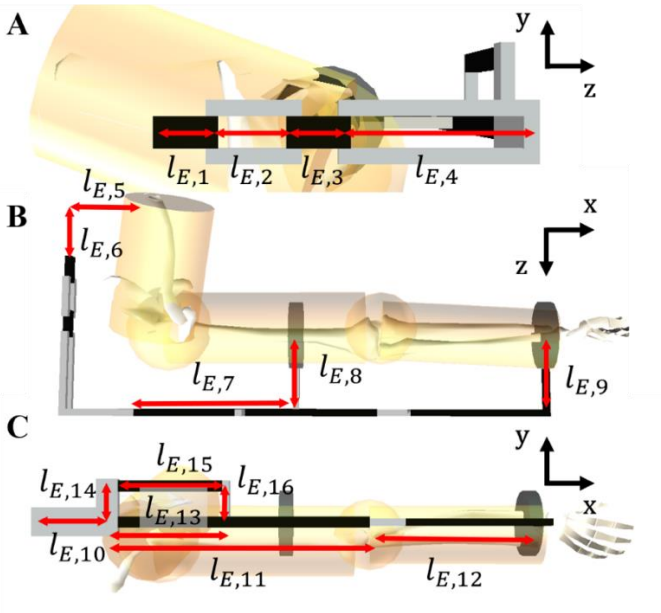


Figure 4-4. Exoskeleton optimized dimensions. A. Rear view of the human-exoskeleton model showing dimensions $l_{E,1-4}$. B. Top view of the human-exoskeleton model showing dimensions $l_{E,5-9}$. C. Side view of the human-exoskeleton model showing dimensions $l_{E,10-16}$.

#### 4.3.4.2 Collision avoidance

For the collision avoidance, the method was based on [38], where the human body is described as a succession of cylinders and spheres with dimensions according to the Yeadon anthropometric model [31], and describing each exoskeleton bodies as cylinders of radius $r_{body}$ [m] equal to the biggest dimension of the corresponding body. This ensures that the volume of the cylinder is bigger than the real body. Then the lowest distances $\boldsymbol{d}_c$ [m] between the human shapes and exoskeleton shapes were used as constraints, $\boldsymbol{d}_c > 0$.

#### 4.3.4.3 Minimization of the exoskeleton size

To reduce the exoskeleton size, the distances between the exoskeleton body points and the chosen human body points were minimized using Eq. 4.6. The set of minimized distance $\boldsymbol{d}$ [m] is exoskeleton dependent and should address the most important distances. In this case, the distance between the exoskeleton and the human body is mostly important around the shoulder and behind the user as the exoskeleton tends to be far from the shoulder joints to avoid collisions. Figure 4-5 shows the chosen points, SC, AC2, and AC. Moreover, according to the exoskeleton kinematic

chain and loop closure constraints, $d_7$ generally corresponds to the distance between the exoskeleton and the human arm, $l_{E,8}$ and $l_{E,9}$, for all bodies after joint $q_{E,6}$.

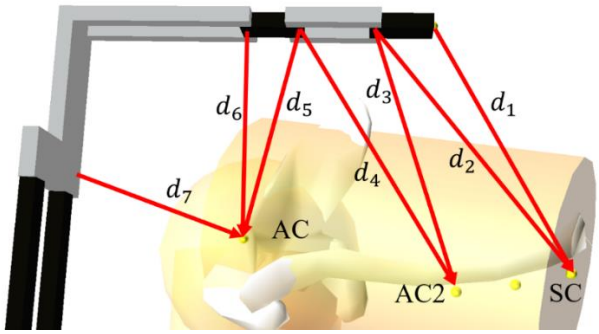


Figure 4-5. Close up of a top view of the human-exoskeleton model showing distances $d_{1-7}$

The minimization of these distances is then, as shown in Eq. 4.6:

$$\min_{\boldsymbol{l},\boldsymbol{q_v}} D = \sum_{i=1}^{n} d_i(\boldsymbol{q},\boldsymbol{l}) \tag{4.6}$$

where $d_i$ is the distance between each point $i$ , and $n$ is equal to the number of distances, here 7.

#### 4.3.4.4 Optimization framework

The optimization framework combining the three elements of the *exoskeleton fit* to the user is described by the cost function (Eq. 4.7) composed of weighted Eqs. 4.5, $L_C$, and 4.6, $D$, for all the recorded functional tasks $\boldsymbol{q}_{u,k}$ recorded for the functional tasks:

$$\min_{\boldsymbol{l}_E,\boldsymbol{q_v}} \sum_{\boldsymbol{q}_{u,1}}^{\boldsymbol{q}_{u,j}} \left[p_{loop}\, L_C + \, p_{dist}\, D\right] \tag{4.7}$$

where $p_{loop}$ and $p_{dist}$ are respectively weights for each part of the cost function. $j = 1\ to\ 6$ is the index of the functional task. As the loop closure is of the utmost most importance in this optimization process, $p_{loop}$ was chosen to be $1e^4$. This is a realistic choice, as Newton-Raphson loop closure is usually achieved at $1e^{-6}$ in this problem. $p_{dist}$ was chosen to be 1.

The constraints for this framework were the physical boundaries on the exoskeleton generalized coordinates, to ensure realistic mechanism movements. Furthermore, on top of the collision

avoidance constraints, more constraints were added to ensure the four-bar parallelism, and to keep the same distance between exoskeleton and the user's arm after the shoulder joint.

Initial values for the dimensions of the exoskeleton bodies $\boldsymbol{l}_{E,ini}$ were identified visually in the exoskeleton CAD model, and initial values for the $\boldsymbol{q}_v$ were obtained by the kinematics of the non-optimized exoskeleton while executing the functional tasks.

### 4.3.5 Dynamic synthesis

The global objective of the dynamic synthesis is to determine the required motors and passive elements characteristics to design the exoskeleton for the functional tasks and the user. An important part of this synthesis is the dynamic optimization problem described by Sections 4.3.5.1 to 4.3.5.3. Its objective is to find the adequate exoskeleton generalized joint torques $\boldsymbol{Q}_E$ to assist and minimize the user's generalized joint torques $\boldsymbol{Q}_H$. Finally, Section 4.3.5.4 presents the dynamic synthesis procedure.

#### 4.3.5.1 Exoskeleton generalized joint torques evaluation

The equivalent of torsion springs is used as passive elements as they are easy to model with the linear Hooke's Law. To evaluate the motors and springs characteristics, $\boldsymbol{Q}_E$ must be divided in two parts, $\boldsymbol{Q}_M$ for the torque produced by the motors and $\boldsymbol{Q}_S$ for spring induced torques. The latter can be written with Hooke's law for a torsion spring, as follows, Eq. 4.8:

$$Q_{S,i} = k_i(q_{E,i} - q_{0,i}) \tag{4.8}$$

where $k_i$ is the stiffness constant $[\frac{\mathrm{Nm}}{\mathrm{rad}}]$ of the spring $i$, and $q_{0,i}$ is its neutral position [rad]. These parameters will be variables of the optimization process. Then, the full joint torque can be computed as follows, Eq. 4.9:

$$Q_{E,i} = Q_{M,i} + Q_{S,i} \tag{4.9}$$

#### 4.3.5.2 Optimal control problem

The dynamic optimization taking the full human-exoskeleton interaction into account was formulated as DAE constrained optimal control problem (OCP) with cost functional $J$, and can be written as follows [39], [40]:

$$\min_{x(t),u(t)} J = \Phi(\boldsymbol{x}(t_0), t_0) + \int_{t_0}^{t_f} L(\boldsymbol{x}(t), \boldsymbol{u}(t), t)dt \tag{4.10}$$

where $\boldsymbol{x}(t)$ is the state vector, $\boldsymbol{u}(t)$ is the control vector, $t_0$ is the initial time, $t_f$ the final time, $\Phi$ is the scalar terminal weighting function, and $L$ the scalar function. Eq. 4.10 is subject to Eqs. 4.11 to 4.14:

$$\boldsymbol{x}_0 = \boldsymbol{x}(t_0) \tag{4.11}$$

$$F(\dot{\boldsymbol{x}}(t), \boldsymbol{x}(t), \boldsymbol{u}(t), t) = 0 \tag{4.12}$$

$$g(\boldsymbol{x}(t), \boldsymbol{u}(t), t) \geq 0 \tag{4.13}$$

$$\varphi\left(\boldsymbol{x}(t_f)\right) = 0 \tag{4.14}$$

where, $\boldsymbol{x}_0$ is the fixed initial state, $F$ are the dynamic equations of the system described by Eqs. 4.1 to 4.4, $g$ are the inequality constraints on the control and state variables, and $\varphi$ denotes the terminal state constraints. As a forward dynamic formulation of the dynamics was used, the state vector was defined as $\boldsymbol{x}(t) = [\dot{\boldsymbol{q}}_u \ \boldsymbol{q}_u]$, and the control vector as $\boldsymbol{u}(t) = [\boldsymbol{Q}_H \ \boldsymbol{Q}_M \ \boldsymbol{k} \ \boldsymbol{q_0}]$.

#### 4.3.5.3 Non-linear optimization process

To solve this OCP, a direct collocation approach was used, which allows simultaneous simulation and optimization [41]. The problem was built in CasADi symbolic framework [42]. In this method, the state vector $\boldsymbol{x}(t)$, and control vector $\boldsymbol{u}(t)$ were discretized on a fine grid of collocation points and then approximated by using Lagrange polynomials and piecewise constant function respectively. Time integration was approximated with quadrature formula for the same collocation points [43]. Continuity constraints ensure smoothness between the state intervals. We used a *Radau* time grid, as it provides a collocation point at the start and end of every state [44].

The first part of the cost function minimized the normalized user's joint torques, as follows, Eq. 4.15:

$$T = \min_{\boldsymbol{Q_H},\boldsymbol{Q_M},\boldsymbol{k},\boldsymbol{q_0},\dot{\boldsymbol{q}}_u\,\boldsymbol{q}_u} \sum_{j=1}^{N} \int_{t_j}^{t_{j+1}} \sum_{i=1}^{n} \frac{Q_{H,i,j} \cdot Q_{H,i,j}}{\max\left(Q_{H,i,exp.}\right)^2} dt \qquad (4.15)$$

where n was the number of independent actuated joints of the human, max ($Q_{H,i,exp.}$) was the maximum experimental torque for joint $i$, $t_j$ was the time of collocation interval $j$ and $N$ was the number of collocation intervals. As the goal of this process was the design of a user-centered exoskeleton device, the trajectory of the user's joints was important to produce feasible and intuitive movements. To do this, the error between the experimental data and the simulated generalized positions was minimized by using Eq. 4.16:

$$P = \min_{\boldsymbol{Q_H},\boldsymbol{Q_M},\boldsymbol{k},\boldsymbol{q_0},\dot{\boldsymbol{q}}_u\,\boldsymbol{q}_u} \sum_{j=1}^{N} \int_{t_j}^{t_{j+1}} \sum_{i=1}^{n} (\boldsymbol{q}_{u,j,exp.} - \boldsymbol{q}_{u,j})^2 dt \qquad (4.16)$$

The whole cost function was then Eq. 4.15 + Eq. 4.16, leading to the following minimization Eq. 4.17:

$$\min_{\boldsymbol{Q_H},\boldsymbol{Q_M},\boldsymbol{k},\boldsymbol{q_0},\dot{\boldsymbol{q}}_u\,\boldsymbol{q}_u} T + P \qquad (4.17)$$

The first set of constraints is described by the collocation continuity constraints between the state intervals as explained above. For the path constraints on the generalized positions, articular limits were considered for the user's joints [45], and kinematic limits in respect to the CAD model for the exoskeleton joints. No path constraints were used on the user's joint torques, as the minimization of the trajectory error ensured realistic torques and movements. However, these could easily be added as the maximum joint torques for each joint. For the exoskeleton dynamic passive elements, i.e. torsion springs, parameters $\boldsymbol{k}$ and $\boldsymbol{q_0}$, an equality constraint was used as they must be constant for the whole trajectory.

Eq. 4.9 describes the exoskeleton joint torques evaluation according to the use of either passive elements, or motors, or both. For the motor parameters, the torque and speed can be limited by their winding curve. Winding curves for several motors were approximated by a linear relationship between the motor maximum torque at quasi no velocity state, which is generally lower than the stall torque and the maximum continuous torque at the maximum continuous velocity of the motor. Continuous torques could not always be found therefore their value was safely put to 0 Nm. The motor parameters for three manufacturers, Herkulex (HKX), Dynamixel (DMX), and Maxon (MAX), each with several motors, are shown in Appendix A (Table 4-3) and were generally found on the datasheets listed on the Websites of the manufacturers. As an example, Figure 4-6 shows the intermediary result of the motor winding constraints on the shoulder joint. The motor used in this evaluation is the DMX XH540. Its limits are reached in the top right corner when used without a spring, but when used with a spring, the motor no longer reaches its torque limits.

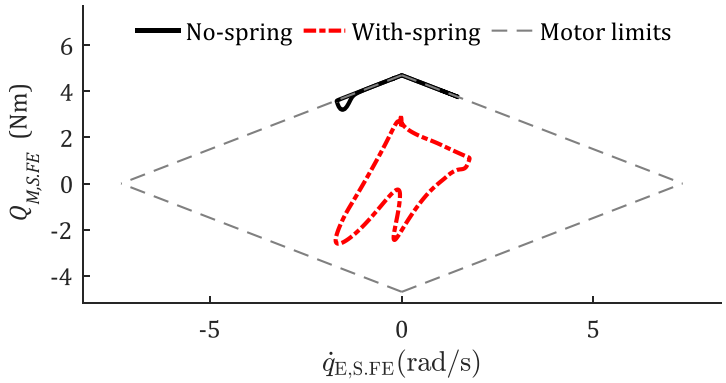


Figure 4-6. The exoskeleton motor (DMX XH540) torque at the shoulder joint compared with the motor speed. The no-spring optimization reaches the winding limits of the motor while the with-spring optimization is within the motor limits.

To help the solver, each experimental trajectory was divided by groups of collocation intervals which were then combined in a final optimization to obtain the full trajectory. This was done for all OCP evaluations. For each group of intervals, the experimental data kinematics and inverse dynamics results were used as initial guess for $\boldsymbol{Q_H}, \boldsymbol{\dot{q}_u}$ and $\boldsymbol{q_u}$. Additionally, $\boldsymbol{Q_M}, \boldsymbol{k}$ and $\boldsymbol{q_0}$ are set to zero. Results for human-only OCP trajectories and torques are shown in Appendix B.

#### 4.3.5.4 Dynamic synthesis procedure

To optimize the exoskeleton design for the six functional tasks, we follow the procedure presented in Figure 4-7, where $n_T$, $n_J$ and $n_M$ are respectively the current evaluated task, joint and motor, $N_T$, $N_J$ and $N_M$ are the quantity of tasks, joints and motors, here, 6, 4, and 9. $Q_{H,n_J}$ and $Q_{M,n_J}$ are, respectively, the user's joint torque and exoskeleton joint torque at the evaluated joint $n_J$. The joints $n_J$ are $q_{H,13,14,16\ and\ 19}$ from Figure 4-2 for the user's joints and $q_{E,5,6,9\ and\ 14}$ from Figure 4-3 for the exoskeleton. The 4 joints are for the S. AA, S. FE, E. FE and F. PS movements. $Q_{H,n_J.HO}$ is the user's joint torque for the human-only simulation.

As seen in Figure 4-7, the process starts with the first task and the most distal joint, F. PS, as the motor selection for $n_J$ affects $n_{J-1}, n_{J-2}$, etc. Therefore, this process can be seen as a backward recursive joint sizing. Then, the dynamic optimization is performed with $n_M = 1$ the smallest motor, here HKX 101. The most important element of the process is the final decision block, where 2 alternative conditions enable to accept the choice of motor for the joint and task:

- First condition: The ratio between the RMS value of user's joint torque while wearing the exoskeleton, and the RMS value of the user's joint torque without exoskeleton, is lower than the condition threshold $C$, where C is chosen between 0 and 1 by the exoskeleton designers. A 0 value means the user does not need to produce torque and a 1 value means the user needs to produce all the torque. Hereafter, threshold $C$ will be defined as the *user torque ratio.*
- Second condition: The motor torque, $Q_{M,n_J}$, is within the motor winding limits for the whole trajectory.

If either of those conditions are true, then, the motor and spring characteristics for task $n_T$ and joint $n_J$ are saved and the process moves on to the next joint. Then, if all joints have been optimized, the process goes to the next task until all tasks are done. If the condition on $C$ or $Q_{M,n_J}$ is false, then, the next motor characteristics will be used for the optimization until the conditions will be satisfied. If needed, stronger motors can be added manually to the list to satisfy the conditions. For this study, the condition $C$ is chosen to be 0, which means lowering the user's torque to a maximum, i.e. 0 Nm.

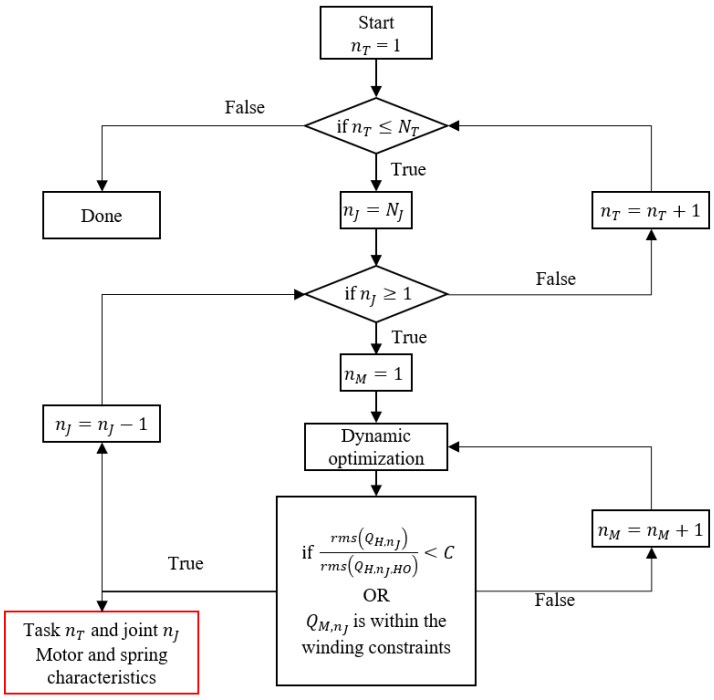


Figure 4-7. Dynamic synthesis procedure. $n_T$, $n_J$ and $n_M$ are respectively the current evaluated task, joint and motor. $N_T$, $N_J$ and $N_M$ are the quantity of task, joint and motor. $Q_{H,n_J}$ and $Q_{M,n_J}$ are, respectively, the user's joint torque and exoskeleton joint torque at the evaluated joint $n_J$. $Q_{H,n_J.HO}$ is the joint torque for the human-only (HO) simulation. $C$ is the condition to be satisfied.

The linear solver MUMPS from the IPOPT library was used with the three possible options of a threshold, a relative threshold, and a constraints violation threshold, which were all set at 1e-4 by default. The geometric optimizations took approximately 2 minutes for each functional task and 15 minutes for the combined optimization and the dynamic optimization took approximately 30 minutes (no-spring) to 2 hours (w-spring) on Windows 10, Intel® Core™ i7-7500U CPU @2.7 GHz.

## 4.4 Results

### 4.4.1 Geometrical optimization

Following the methodology presented in Section 4.3.4, we optimized the geometric dimensions $\boldsymbol{l}_E$ of the exoskeleton for the 6 functional tasks presented in Table 4-1. Figure 4-8A shows the norm of loop constraints $\boldsymbol{h}_l$. The red curves represent the non-optimized lengths that were approximately

chosen with the 3D CAD software, while the black curves are the optimized lengths. The average of the optimized values is $2.9 \times 10^{-5}$, compared with the non-optimized value, $4.2 \times 10^{-4}$.

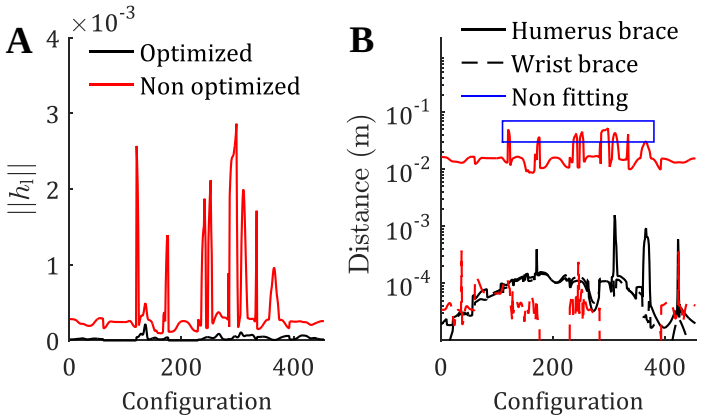


Figure 4-8. A. Norm of the loop constraints $\boldsymbol{h_{loop}}$ for the optimized and non-optimized lengths. B. Distance between the exoskeleton and the arm at the humerus brace point and wrist brace point for the optimized and non-optimized lengths.

Figure 4-8B presents the distance between the exoskeleton and the human arm at the humerus brace point and the wrist brace point. For the optimized lengths, the maximum distance is under 1 cm at both points. However, the humerus point distance for the non-optimized lengths is over 3 cm for 10.8% of the configurations, as shown in the blue box.

To evaluate the global distance between the exoskeleton and the arm around the shoulder, the summation part of Eq. 4.6 was used for all configurations for $d_{1-7}$. The non-optimized total sum was 0.89 m compared to 1.02 m with optimized values. The distance between the exoskeleton and the arm, $l_{E,8}$ and $l_{E,9}$, went from 8.0 cm for the non-optimized lengths, to 7.1 cm with the optimized lengths.

## 4.4.2 Dynamic Synthesis

### 4.4.2.1 Backward recursive joint sizing

The following results were obtained with the dynamic optimization from Sections 4.3.5.1 to 4.3.5.3. The most distal motorized articulation is the forearm joint. Evaluating the OCP with motor

HKX D101 reduced the user's joint torque to approximately zero, for the whole trajectory, as shown in Figure 4-9.

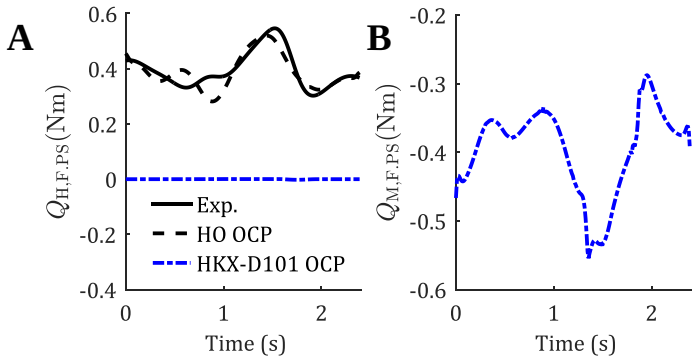


Figure 4-9. A. User's joint torque for the experimental data, HO OCP and with the HKX D101 motor. B. Exoskeleton joint torque for the PS movement.

At the elbow joint, Figure 4-10 presents the user's RMS joint torques in function of the exoskeleton RMS joint torque for each motor presented in Table 4-3 (Appendix A), with and without passive elements.

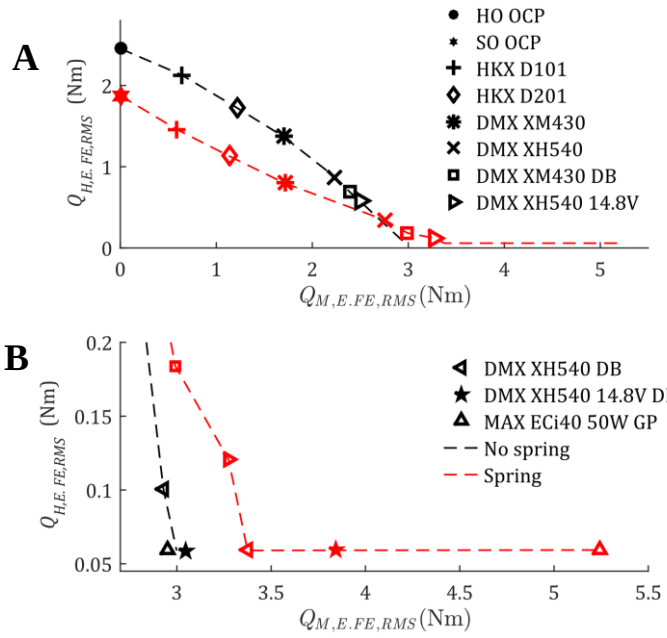


Figure 4-10. User's RMS elbow joint torques compared with exoskeleton RMS elbow joint torques for all the motors in tab X. A. Full graph. B. Close-up at the minimum user RMS torque. Lines are for visual aid, and are not related to additional data.

The result for the spring only (SO) OCP is also shown. For each result, one can see that adding passive elements lowers the RMS user's joint torque by an average of 0.56 Nm, 23% of the HO OCP, when discarding the motors that reduce the torque to a minimum without passive elements. For the DMX XH540 DB motor, we can also see that without the passive element, it cannot lower the user's torque to a minimum, although is able to with the passive element. This is also highlighted in Figure 4-11A, where one can see a small segment where this motor is not at the minimum torque, while the version with the passive element is at the minimum torque.

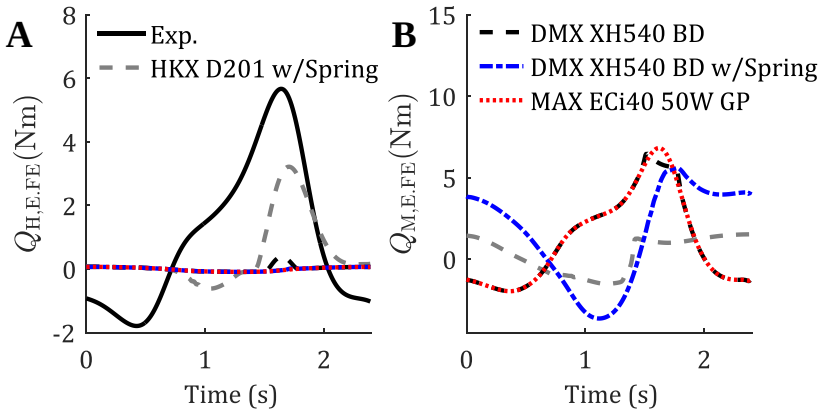


Figure 4-11. A. Human joint torque for the experimental data, HO OCP and several motors for the elbow flexion extension joint. B. Exoskeleton joint torques.

At the shoulder joint (Figure 4-12), adding passive elements lowers the RMS user's joint torque by an average of 3.31, 51% of the HO OCP, Nm for the *Eat with spoon* task and 3.06 Nm, 40% of the HO OCP, for the *Arm frontal reach* task. Both are evaluated with the DMX H540 DB at the elbow.

In Figure 4-12, to identify the impact on the shoulder joint of using a lighter or heavier motor at the elbow joint, a similar graph to the one of Figure 4-10 is presented for two functional tasks. *F*or the *Eat with a spoon* task, in the simulation without passive elements, the use of the lighter motor at the elbow either reduces the user's joint torque for smaller motors or reduces the motor torque for stronger motors by an average of 0.33 Nm. For the simulation with passive elements, the average torque difference between the two motors is negligible (0.02 Nm). The same observation can be made for the *Arm frontal reach* task presented in where the reduction is 0.45 Nm without passive elements and 0.05 Nm with passive elements.

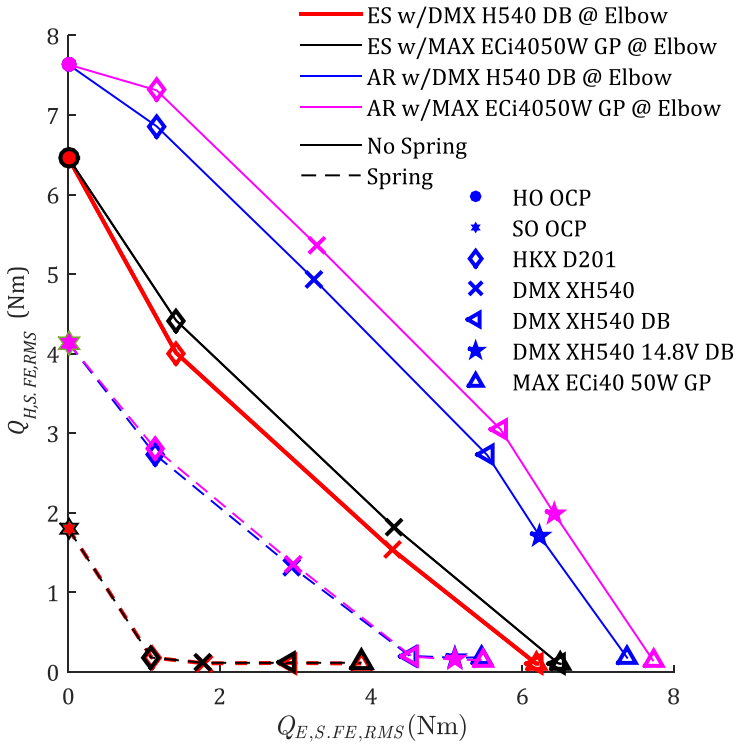


Figure 4-12. User RMS shoulder joint torques compared with the exoskeleton RMS shoulder joint torques for a selection of motors. Straight line are simulations without passive elements while dashed lines are with passive elements. Red and black lines are the *Eat with spoon* functional task with a lighter (DMX XH540 DB) and heavier motor (MAX ECi4050W GP) at the elbow joint respectively. Blue and purple lines are the *Arm frontal reach* functional task with a lighter (DMX XH540 DB) and heavier motor (MAX ECi4050W GP) at the elbow joint respectively. Lines are for visual aid and are not related to additional data.

#### 4.4.2.2 Dynamic synthesis procedure

The result presented in Table 4-2 were obtained by the task-specific dynamic synthesis procedure shown in Figure 4-7 in Section 4.3.5.4. The user's joints RMS torques were reduced to less than 11% of the human-only RMS torques, $Q_{H,HO}$, for all tasks and joints except the S. AA joint in task RL which is reduced to 27.2%. Therefore, the condition $C = 0$ was met for the F. PS joint and for all the other joints, the condition on the motor winding limit was met (see section 4.3.5.4).

Table 4-2. RMS user's joint torque $Q_H$, percentage of RMS user's joint torque without exoskeleton $Q_{H,HO}$, torsion spring stiffness $k$ and torsion spring neutral position $q_0$ for each joint and each task. The results come from the dynamic synthesis procedure.

| Joints | Value | Functional Task | | | | | |
|---|---|---|---|---|---|---|---|
| | | ES | AR | RL | OD | CH | ZC |
| S. AA | $Q_H$ [Nm] | 0.1 | 0.2 | 0.7 | 0.2 | 0.1 | 0.1 |
| | % of $Q_{H,HO}$ | 2.7 | 8.4 | 27.2 | 10.6 | 8.6 | 3.7 |
| | $k$ [Nm/rad] | 4.5 | 17.8 | 16.3 | 4.7 | 18.6 | 18.2 |
| | $q_0$ [rad] | 1.4 | 0.7 | 0.7 | 2.0 | 0.4 | 0.6 |
| | Motor | DMX XH540 | DMX XH540 | DMX XH540 DB | DMX XH540 DB | DMX XH540 | DMX XH540 |
| S. FE | $Q_H$ [Nm] | 0.1 | 0.2 | 0.2 | 0.1 | 0.1 | 0.1 |
| | % of $Q_{H,HO}$ | 0.7 | 1.8 | 2.2 | 1.1 | 1.8 | 0.9 |
| | $k$ [Nm/rad] | 6.6 | 3.3 | 3.8 | 2.8 | 2.8 | 3.9 |
| | $q_0$ [rad] | 0.1 | 1.5 | 0.9 | 0.8 | 1.1 | 0.1 |
| | Motor | DMX XH540 | DMX XH540 DB | DMX XH540 14.8V DB | DMX XH540 DB | DMX XH540 14.8V | DMX XH540 14.8V |
| E. FE | $Q_H$ [Nm] | 0.1 | 0.1 | 0.1 | 0.1 | 0.1 | 0.1 |
| | % of $Q_{H,HO}$ | 2.3 | 2.1 | 3.2 | 1.9 | 3.8 | 2.6 |
| | $k$ [Nm/rad] | 4.8 | 2.0 | 5.8 | 5.6 | 8.7 | 8.6 |
| | $q_0$ [rad] | 1.9 | 2.3 | 1.4 | 1.4 | 1.82 | 2.1 |
| | Motor | DMX XH540 14.8V | DMX XH540 DB | DMX XH540 DB | DMX XH540 DB | DMX XH540 DB | DMX XH540 14.8V |
| F. PS | $Q_H$ [Nm] | ~0.00 | ~0.00 | ~0.00 | ~0.00 | ~0.00 | ~0.00 |
| | % of $Q_{H,HO}$ | ~0.00 | ~0.00 | ~0.00 | ~0.00 | ~0.00 | ~0.00 |
| | Motor | HKX D101 | HKX D101 | HKX D101 | HKX D101 | HKX D101 | HKX D101 |

## 4.5 Discussion

The global objective of this study was to develop a procedure for geometric and dynamic synthesis of assistive upper limb exoskeletons, to serve as a tool to support their design. These exoskeletons should reduce the effort required by the user during functional tasks (dynamic consideration) and should fit the size of the user (geometric consideration). The results are discussed in descending order of importance: Section 4.5.1 discusses the complete dynamic synthesis procedure, then Section 4.5.2 discusses the dynamic optimization results, and Section 4.5.3 discusses the geometric optimization.

### 4.5.1 Dynamic synthesis procedure

The dynamic synthesis procedure and tools summarized in Figure 4-7 were developed for an assistive passive and active upper limb exoskeleton for six functional tasks. The main results of this procedure are reported in Table 4-2, which presents the selection of motors, the results for the passive element characteristics $k$ and $q_0$, the user's torque $Q_H$, in the assisted joint and the reduction percentage of the user's torque compared with the human-only simulations, % of $Q_{H,HO}$, for all joints during each functional task. This is a task-specific procedure to design the exoskeleton for one task and for one user. This type of design could be interesting in a work environment where a complex task is carried out repeatedly such as wall painting or in the assistive medical field for a specific task such as eating.

The results in Table 4-2 could be used in a more generalized approach. For instance, by selecting the largest motor for each joint across all the functional tasks, the exoskeleton would have the capacity to perform each task if the spring characteristics are switched between tasks. This could be done by the user with a clutch mechanism or simply by changing the spring directly. Additionally, optimizing the spring selection could limit the number of required springs. From a practical perspective, in a work environment where workers carry out multiple tasks in the manufacturing chain, such an exoskeleton could allow the employer to acquire one general exoskeleton instead of multiple task-specific exoskeletons.

To evaluate the dynamic performance of the developed procedure, the user's joint torques results presented in Table 4-2 were analyzed. For the F. PS joint, user's torque could be reduced to near 0 Nm and is the only joint where the condition $C = 0$ could be met. For the other joints, the condition on the motor winding was met (Section 4.3.5.4). The E. FE user's torque, $Q_H$, represents less than 5% of the human-only simulation torque, $Q_{H,HO}$, and 2% for the S. FE in all functional tasks. The last motorized joint torque, S. AA, could be reduced to less than 10.6% for five out of the six tasks. This still represents a significative reduction of effort for the user. For the *Arm frontal reach Left to Right* task, the resulting torque is still 27.2% of the human-only simulation.

For each motor that could not reach a *user torque ratio,* $C = 0$, it suggests that the motor axis is not correctly aligned with the user's joint rotation axis. These misalignments could cause parasitic torques in the user's joints that can eventually result in injuries. This is a well-known problem in exoskeleton design and has been discussed in many studies [21], [46]. Those parasitic torques and forces should be measured and minimized in the dynamic optimisation. A limitation of this work is that, as this problem is greatly linked to geometric parameters, a combination of both geometric and dynamic optimisations is required to reduce effectively the parasite torques. However, this was not implemented and could be investigated further in future works.

In this study, the *user torque ratio,* $C$ was chosen to be 0 for illustration. This implied that the user did not need to produce torque to use the exoskeleton. But a low user's joint torque is related to low muscle forces around this joint, which can be associated to muscular atrophy [47]. Studies should be pursued to evaluate the longer-term effect of wearing such exoskeletons where the user does not need to produce torque, and to determine a safe *user torque ratio* for the different purposes, such as workplace or medical assistance. Moreover, this study was limited to the evaluation of the user's joint torque, but a more biofidel evaluation of the user's effort are the muscle forces [36], [48], [49]. Then, a safe *user muscle force ratio* should also be evaluated through further studies.

### 4.5.2 Dynamic optimization

Figures 4-10 and 4-12 present a comparison between the user's RMS elbow joint torques and the exoskeleton RMS elbow joint torques. The reduction of the user's torque by adding passive elements is significative, with an average of 0.56 and 3.31 Nm for the *Eat with a spoon* task at the elbow and shoulder joints, respectively, while the average for the *Arm frontal reach* task at the shoulder joint is 3.06 Nm. This allowed the use of weaker motors in the three cases, enabling to globally reduce the torque required by the exoskeleton motors. This was true for all joints, except the F. PS. As shown in Figure 4-9 and Table 4-2, the HKX D101 motor could reduce the user's torques to 0 Nm without the use of passive elements. Springs are not relevant for this joint, as it is mostly in the horizontal plane and is, therefore, less affected by gravity.

Figure 4-12 also enables to compare the effects on the shoulder, between the use of a lighter or heavier motor at the elbow joint. For the *Eat with spoon* task and *Arm frontal reach* task the

difference of using lighter or heavier motor is 0.33 Nm and 0.45 Nm without passive elements and negligible values with passive elements, respectively 0.02 Nm and 0.05 Nm. This suggest that the passive elements can reduce the dependencies between joints. Indeed, the springs compensate the static effect, i.e. gravity effect of the heavier motor. The small differences, 0.02 Nm and 0.05 Nm are due to the increased inertia of the motors. This can be interesting if the exoskeleton is to be designed for low dynamic tasks, the passive elements could enable the use of bigger motors in distal joint such as the F. PS and E. FE without requiring bigger motors at the proximal joints S. FE and S. AA. In future studies, a sensitivity analysis on the level of dynamics and size of motors could be conducted to identify the limits of the previous statement. Moreover, adding bigger motors would globally add weight to the exoskeleton, and the effect on the back and lower limbs should be considered.

Figure 4-11A shows the impact of the spring for motor DMX H540 DB torque trajectory as the simulation with black dashed line, the no-spring simulation, cannot lower the torque to the minimum while the blue curve, the with-spring simulation, is at the minimum. This enabled to use this motor instead of the heavier MAX ECi40 50W GP. However, in Figure 4-11B, for the two motors (red and blue) that could reduce the user's joint torque to the minimum value, the torque curves differ largely because of the spring element. Therefore, the control strategy of the exoskeleton will require to take this in consideration.

### 4.5.3 Geometric optimization

The objective of the geometric optimization was to minimize the loop constraints $\boldsymbol{h}_l$ while avoiding collisions with the human. This was done for all functional tasks simultaneously resulting in a fully sized exoskeleton.

Figure 4-8A shows a reduction of the loop constraints norm $\|\boldsymbol{h}_l\|$ by an average factor of 14.6 when the lengths of the exoskeleton segments are optimized. This reduction yields, as seen in Figure 4-8B, a distance of less than 1 cm for all configurations in all functional tasks between the exoskeleton braces and the arm and forearm connection points. With the non-optimized lengths, 10.8% of the configuration had a difference of more than 3 cm at the arm connection point, as is presented by the blue box in Figure 4-8B. With the human arm skin movement that can vary greatly

[50] and the adjustments on the user, it can be assumed that distances of less than 3 cm could still fit the user. Therefore, the gain of this optimization compared with the non-optimized lengths is 11%. This is important to guarantee the fit of the exoskeleton to the user without collision with his body.

Another result is the sum of distance $d_{1-7}$, initially presented in Figure 4-5, which evaluates the distance between the exoskeleton and the shoulder complex. The total for the non-optimized lengths, 0.89 m, was lower than the total for the optimized lengths, 1.02 m. The distances between the exoskeleton and the user's arm, $l_{E,8}$ and $l_{E,9}$, initially presented in Figure 4-4, went from 8 cm to 7.1 cm, globally bringing the exoskeleton closer to the body, thus reducing the overall size of the system. However, the most interesting element of this geometric optimization is the automatization of the process to personalize exoskeletons faster than a visual identification or trial and error for different users.

## 4.6 Conclusion

This objective of the work presented in this study was to develop geometric and dynamic synthesis procedure to design and personalize a 3D assistive passive and active upper limb exoskeletons. This was applied to six specific functional tasks of one healthy subject. To do so, sub-objectives were, first, to find the exoskeleton size to fit the user for all functional tasks and, secondly, to find the motor selection and passive element characteristics to reduce the user effort to a minimum for each task.

Consequently, successful geometric and dynamic synthesis procedures were developed and applied to 6 functional tasks following a wide range of motion:

First, for the geometric optimization, a framework was built through a non-linear problem minimizing the loop closure constraints between the exoskeleton and the arm for all the functional tasks configurations. The output of this framework was the dimensions of the exoskeleton. The constraints were reduced by a factor 14.6, which resulted in a gain of 10.8% of closed configurations compared with a visual identification on the CAD model of the exoskeleton.

Secondly, for the dynamic optimization, a framework was built through an optimal control problem using the human position, velocities, and torques as well as exoskeleton torques and passive elements characteristics as variables. The goal was to reduce the user's joint torques to a minimum, while respecting the winding limits of the motors. The dynamic synthesis enabled to identify the characteristics of the motors and passive elements for all the functional tasks. Moreover, the user's joint torques could be lowered to 10.6% off of the human-only torques for all joints and tasks except for the S. AA joint in one task that stayed at 27.2%. These residual torques were caused by misalignment with the human joints, resulting in eventual parasitic torques that could harm the user. The dynamic optimization procedure also showed the importance of using passive elements in the E. FE, S. FE and S. AA joints as they could help the motors to reduce the user's joint torques. For instance, the spring reduced the S. FE joint torque by an average of 3.31 Nm for the *Eat with a spoon task*. This resulted in the selection of a smaller and lighter motor to compensate the user's effort at the shoulder.

Future works could be performed to further improve the developed procedures. Some possible avenues are as follows: First, the geometric and dynamic optimization could be combined to take care of the misalignment problem, as it is related to the geometric parameters. The parasitic torques could then be minimized. Secondly, the user muscle force could be minimized instead of the joint torque for a more anatomically and physiologically realistic reduction of the user effort by using the methods proposed in [49], [51]. Thirdly, one could find the safe *user muscle force ratio* that will not cause muscular atrophy when using the exoskeletons for long-term periods. Finally, a sensitive study could be carried out to characterize how the different geometric and dynamic parameters co-influence each other.

## 4.7 References


[1] R. A. R. C. Gopura, D. S. V. Bandara, K. Kiguchi, and G. K. I. Mann, "Developments in hardware systems of active upper-limb exoskeleton robots: A review," *Robotics and Autonomous Systems*, vol. 75, pp. 203–220, Jan. 2016, doi: 10.1016/j.robot.2015.10.001.

[2] D. Koo, P. H. Chang, M. K. Sohn, and J. Shin, "Shoulder mechanism design of an exoskeleton robot for stroke patient rehabilitation," in *2011 IEEE International Conference on Rehabilitation Robotics*, 2011, pp. 1–6, doi: 10.1109/ICORR.2011.5975505.

[3] A. Frisoli, F. Rocchi, S. Marcheschi, A. Dettori, F. Salsedo, and M. Bergamasco, "A new force-feedback arm exoskeleton for haptic interaction in virtual environments," in *First Joint Eurohaptics Conference and Symposium on Haptic Interfaces for Virtual Environment and Teleoperator Systems. World Haptics Conference*, 2005, pp. 195–201, doi: 10.1109/WHC.2005.15.

[4] M. Bartolo *et al.*, "Arm weight support training improves functional motor outcome and movement smoothness after stroke," *Functional Neuroly*, vol. 29, no. 1, pp. 15–21, Jul. 2014.

[5] S. Marcheschi, F. Salsedo, M. Fontana, and M. Bergamasco, "Body Extender: Whole body exoskeleton for human power augmentation," in *2011 IEEE International Conference on Robotics and Automation*, 2011, pp. 611–616, doi: 10.1109/ICRA.2011.5980132.

[6] Y. Bougrinat, S. Achiche, and M. Raison, "Design and development of a lightweight ankle exoskeleton for human walking augmentation," *Mechatronics*, vol. 64, p. 102-297, Dec. 2019, doi: 10.1016/j.mechatronics.2019.102297.

[7] A. Zoss and H. Kazerooni, "Design of an electrically actuated lower extremity exoskeleton," *Advanced Robotics*, vol. 20, no. 9, pp. 967–988, Jan. 2006, doi: 10.1163/156855306778394030.

[8] K. Huysamen, T. Bosch, M. de Looze, K. S. Stadler, E. Graf, and L. W. O'Sullivan, "Evaluation of a passive exoskeleton for static upper limb activities," *Applied Ergonomics*, vol. 70, pp. 148–155, Jul. 2018, doi: 10.1016/j.apergo.2018.02.009.

[9] M. Gunn, T. M. Shank, M. Eppes, J. Hossain, and T. Rahman, "User Evaluation of a Dynamic Arm Orthosis for People With Neuromuscular Disorders," *IEEE Transactions on Neural Systems and Rehabilitation Engineering*, vol. 24, no. 12, pp. 1277–1283, Dec. 2016, doi: 10.1109/TNSRE.2015.2492860.

[10] J. M. Font-Llagunes, U. Lugrís, D. Clos, F. J. Alonso, and J. Cuadrado, "Design, Control, and Pilot Study of a Lightweight and Modular Robotic Exoskeleton for Walking Assistance After Spinal Cord Injury," *Journal of Mechanisms and Robotics*, vol. 12, no. 3, Jun. 2020, doi: 10.1115/1.4045510.

[11] A. J. Young and D. P. Ferris, "State of the Art and Future Directions for Lower Limb Robotic Exoskeletons," *IEEE Transactions on Neural Systems and Rehabilitation Engineering*, vol. 25, no. 2, pp. 171–182, 2017, doi: 10.1109/TNSRE.2016.2521160.

[12] T. Yan, M. Cempini, C. M. Oddo, and N. Vitiello, "Review of assistive strategies in powered lower-limb orthoses and exoskeletons," *Robotics and Autonomous Systems*, vol. 64, pp. 120–136, Feb. 2015, doi: 10.1016/j.robot.2014.09.032.

[13] P. Maciejasz, J. Eschweiler, K. Gerlach-Hahn, A. Jansen-Troy, and S. Leonhardt, “A survey on robotic devices for upper limb rehabilitation,” *Journal of NeuroEngineering and Rehabilitation*, vol. 11, no. 1, p. 3, Jan. 2014, doi: 10.1186/1743-0003-11-3.

[14] T. Haumont *et al.*, “Wilmington Robotic Exoskeleton: A Novel Device to Maintain Arm Improvement in Muscular Disease,” *Journal of Pediatric Orthopaedics*, vol. 31, no. 5, p. e44, Aug. 2011, doi: 10.1097/BPO.0b013e31821f50b5.

[15] R. Altenburger, D. Scherly, and K. S. Stadler, “Design of a passive, iso-elastic upper limb exoskeleton for gravity compensation,” *Robomech Journal*, vol. 3, no. 1, p. 12, Apr. 2016, doi: 10.1186/s40648-016-0051-5.

[16] T. Shank, M. Eppes, J. Hossain, M. Gunn, and T. Rahman, “Outcome Measures with COPM of Children using a Wilmington Robotic Exoskeleton,” *The Open Journal of Occupational Therapy*, vol. 5, no. 1, Jan. 2017, doi: 10.15453/2168-6408.1262.

[17] G. Elliott, G. S. Sawicki, A. Marecki, and H. Herr, “The biomechanics and energetics of human running using an elastic knee exoskeleton,” in *2013 IEEE 13th International Conference on Rehabilitation Robotics (ICORR)*, 2013, pp. 1–6, doi: 10.1109/ICORR.2013.6650418.

[18] E. Perez Luque, "*Evaluation of the Use of Exoskeletons in the Range of Motion of Workers*." dissertation, University of Skövde, School of Engineering Science, 2019. [Online]. Availible: http://his.diva-portal.org/smash/get/diva2:1329519/FULLTEXT01.pdf

[19] R. P. Matthew, E. J. Mica, W. Meinhold, J. A. Loeza, M. Tomizuka, and R. Bajcsy, “Introduction and initial exploration of an Active/Passive Exoskeleton framework for portable assistance,” in *2015 IEEE/RSJ International Conference on Intelligent Robots and Systems (IROS)*, 2015, pp. 5351–5356, doi: 10.1109/IROS.2015.7354133.

[20] R. L. Smith, J. Lobo-Prat, H. van der Kooij, and A. H. A. Stienen, “Design of a perfect balance system for active upper-extremity exoskeletons,” in *2013 IEEE 13th International Conference on Rehabilitation Robotics (ICORR)*, 2013, pp. 1–6, doi: 10.1109/ICORR.2013.6650376.

[21] D. Galinski, J. Sapin, and B. Dehez, “Optimal design of an alignment-free two-DOF rehabilitation robot for the shoulder complex,” in *2013 IEEE 13th International Conference on Rehabilitation Robotics (ICORR)*, 2013, pp. 1–7, doi: 10.1109/ICORR.2013.6650502.

[22] M. Sarac, M. Solazzi, E. Sotgiu, M. Bergamasco, and A. Frisoli, “Design and kinematic optimization of a novel underactuated robotic hand exoskeleton,” *Meccanica*, vol. 52, no. 3, pp. 749–761, Feb. 2017, doi: 10.1007/s11012-016-0530-z.

[23] Y. Hayashi, R. Dubey, and K. Kiguchi, “Torque optimization for a 7DOF upper-limb power-assist exoskeleton robot,” in *2011 IEEE Workshop on Robotic Intelligence In Informationally Structured Space*, 2011, pp. 49–54, doi: 10.1109/RIISS.2011.5945786.

[24] Y. Aoustin and A. M. Formalskii, “Walking of biped with passive exoskeleton: evaluation of energy consumption,” *Multibody System Dynamics*, vol. 43, no. 1, pp. 71–96, May 2018, doi: 10.1007/s11044-017-9602-7.

[25] L. Zhou, Y. Li, and S. Bai, “A human-centered design optimization approach for robotic exoskeletons through biomechanical simulation,” *Robotics and Autonomous Systems*, vol. 91, pp. 337–347, May 2017, doi: 10.1016/j.robot.2016.12.012.

[26] P. Manns, M. Sreenivasa, M. Millard, and K. Mombaur, “Motion Optimization and Parameter Identification for a Human and Lower Back Exoskeleton Model,” *IEEE Robotics and Automation Letters*, vol. 2, no. 3, pp. 1564–1570, Jul. 2017, doi: 10.1109/LRA.2017.2676355.

[27] M. Laitenberger, M. Raison, D. Périé, and M. Begon, “Refinement of the upper limb joint kinematics and dynamics using a subject-specific closed-loop forearm model,” *Multibody System Dynamics*, vol. 33, no. 4, pp. 413–438, Apr. 2015, doi: 10.1007/s11044-014-9421-z.

[28] R. M. Ehrig, W. R. Taylor, G. N. Duda, and M. O. Heller, “A survey of formal methods for determining the centre of rotation of ball joints,” *Journal of Biomechanics*, vol. 39, no. 15, pp. 2798–2809, Jan. 2006, doi: 10.1016/j.jbiomech.2005.10.002.

[29] R. M. Ehrig, W. R. Taylor, G. N. Duda, and M. O. Heller, “A survey of formal methods for determining functional joint axes,” *Journal of Biomechanics*, vol. 40, no. 10, pp. 2150–2157, Jan. 2007, doi: 10.1016/j.jbiomech.2006.10.026.

[30] J. F. O’Brien, R. E. Bodenheimer, G. J. Brostow, and J. K. Hodgins, “Automatic Joint Parameter Estimation from Magnetic Motion Capture Data,” in *2000 Graphics Interface* , p. 8., 1999.

[31] M. R. Yeadon, “The simulation of aerial movement—II. A mathematical inertia model of the human body,” *Journal of Biomechanics*, vol. 23, no. 1, pp. 67–74, Jan. 1990, doi: 10.1016/0021-9290(90)90370-I.

[32] S. Lecours, “Développement d’un exosquelette portable motorisé des membres supérieurs pour les enfants atteints de troubles neuromusculaires,” masters, Mechanical Engineering, Polytechnique Montréal, Montréal, Québec, Canada, 2019.

[33] J.-C. Samin and P. Fisette, *Symbolic Modeling of Multibody Systems*. Springer Netherlands, 2003.

[34] N. Docquier, A. Poncelet, and P. Fisette, “ROBOTRAN: a powerful symbolic gnerator of multibody models,” *Mechanical Sciences*, vol. 4, no. 1, pp. 199–219, May 2013, doi: https://doi.org/10.5194/ms-4-199-2013.

[35] J. Rosen, J. C. Perry, N. Manning, S. Burns, and B. Hannaford, “The human arm kinematics and dynamics during daily activities - toward a 7 DOF upper limb powered exoskeleton,” in *ICAR ’05. Proceedings., 12th International Conference on Advanced Robotics, 2005.*, 2005, pp. 532–539, doi: 10.1109/ICAR.2005.1507460.

[36] M. Raison, “On the quantification of joint and muscle efforts in the human body during motion,” Ph.D. Thesis, Université Catholique de Louvain, Belgique, 2009.

[37] J.-F. Collard, “Geometrical and kinematic optimization of closed-loop multibody systems/Optimisation géométrique et cinématique de systèmes multicorps avec boucles cinématiques,” Ph.D. Thesis, Université Catholique de Louvain, Belgique, 2007.

[38] D. Galinski, “Conception et optimisation d’un robot de rééducation neuromotrice du membre supérieur avec compensation active de la gravité,” Ph.D. Thesis, Université Catholique de Louvain, Belgique, 2014.

[39] M. L. Bell and R. W. H. Sargent, “Optimal control of inequality constrained DAE systems,” *Computers & Chemical Engineering*, vol. 24, no. 11, pp. 2385–2404, Nov. 2000, doi: 10.1016/S0098-1354(00)00566-4.

[40] B. C. Fabien, “Numerical solution of constrained optimal control problems with parameters,” *Applied Mathematics and Computation*, vol. 80, no. 1, pp. 43–62, Nov. 1996, doi: 10.1016/0096-3003(95)00280-4.

[41] O. von Stryk, “Numerical Solution of Optimal Control Problems by Direct Collocation,” in *Optimal Control: Calculus of Variations, Optimal Control Theory and Numerical Methods*, R. Bulirsch, A. Miele, J. Stoer, and K. Well, Eds. Basel: Birkhäuser, 1993, pp. 129–143.

[42] J. A. E. Andersson and J. B. Rawlings, “Sensitivity Analysis for Nonlinear Programming in CasADi,” *IFAC-PapersOnLine*, vol. 51, no. 20, pp. 331–336, Jan. 2018, doi: 10.1016/j.ifacol.2018.11.055.

[43] M. Diehl and S. Gros, “Numerical Optimal Control,” 2017. [Online]. Available: https://www.syscop.de/files/2017ss/NOC/script/book-NOCSE.pdf

[44] S. Gros, “Numerical Optimal Control with DAEs Lecture 12: Optimal Control with DAEs.” [Online]. Available: https://www.syscop.de/files/2015ws/noc-dae/lecture%20slides/12-DAEOptimalControl.pdf.

[45] K. Petuskey, A. Bagley, E. Abdala, M. A. James, and G. Rab, “Upper extremity kinematics during functional activities: Three-dimensional studies in a normal pediatric population,” *Gait & Posture*, vol. 25, no. 4, pp. 573–579, Apr. 2007, doi: 10.1016/j.gaitpost.2006.06.006.

[46] M. B. Näf, K. Junius, M. Rossini, C. Rodriguez-Guerrero, B. Vanderborght, and D. Lefeber, “Misalignment Compensation for Full Human-Exoskeleton Kinematic Compatibility: State of the Art and Evaluation,” *Applied Mechanics Reviews*, vol. 70, no. 5, Sep. 2018, doi: 10.1115/1.4042523.

[47] C. K. Thomas, E. Y. Zaidner, B. Calancie, J. G. Broton, and B. R. Bigland-Ritchie, “Muscle Weakness, Paralysis, and Atrophy after Human Cervical Spinal Cord Injury,” *Experimental Neurology*, vol. 148, no. 2, pp. 414–423, Dec. 1997, doi: 10.1006/exnr.1997.6690.

[48] R. D. Crowninshield and R. A. Brand, “A physiologically based criterion of muscle force prediction in locomotion,” *Journal of Biomechanics*, vol. 14, no. 11, pp. 793–801, Jan. 1981, doi: 10.1016/0021-9290(81)90035-X.

[49] J. Wen, M. Raison, and S. Achiche, “Using a cost function based on kinematics and electromyographic data to quantify muscle forces,” *Journal of Biomechanics*, vol. 80, pp. 151–158, Oct. 2018, doi: 10.1016/j.jbiomech.2018.09.002.

[50] J. Mahmud, C. A. Holt, and S. L. Evans, “An innovative application of a small-scale motion analysis technique to quantify human skin deformation in vivo,” *Journal of Biomechanics*, vol. 43, no. 5, pp. 1002–1006, Mar. 2010, doi: 10.1016/j.jbiomech.2009.11.009.

[51] M. Raison, C. Detrembleur, P. Fisette, and J.-C. Samin, “Assessment of Antagonistic Muscle Forces During Forearm Flexion/Extension,” in *Multibody Dynamics: Computational*

*Methods and Applications*, K. Arczewski, W. Blajer, J. Fraczek, and M. Wojtyra, Eds. Dordrecht: Springer Netherlands, 2011, pp. 215–238.

## 4.8 Appendix A: Motor parameters

Table 4-3. Motor parameters

| Motors (Abbreviation) | Voltage (V) | Max torque (Nm) | Cont. torque (Nm) | Cont. speed (rad/s) | Mass (kg) |
|---|---|---|---|---|---|
| Herkulex DRS-101 (HKX D101) | 12 | 0.8 | 0.17 | 6.3 | 0.05 |
| Herkulex DRS-201 (HKX D201) | 12 | 1.6 | 0.22 | 7.1 | 0.06 |
| Dynamixel XM430 210W (DMX XM430) | 12 | 2.4 | 0.00 | 9.9 | 0.08 |
| Dynamixel XM430 210W x2 (DMX 430 DB) | 12 | 4.8 | 0.00 | 9.9 | 0.16 |
| Dynamixel XM540 150W (DMX XH540/ DMX XH540 14.8V) | 12 | 4.7 | 0.00 | 7.3 | 0.17 |
| | 14.8 | 5.6 | 0.00 | 8.9 | 0.17 |
| Dynamixel XM540 150W x2 (DMX XH540 DB/ DMX XH540 14.8V DB) | 12 | 9.4 | 0.00 | 7.3 | 0.33 |
| | 14.8 | 11.2 | 0.00 | 8.9 | 0.33 |
| Maxon ECi40 50W w/ Maxon Gearhead GP42 15Nm (MAX ECi4050W GP) | 24 | 9.4 | 1.01 | 187 | 0.54 |

## 4.9 Appendix B: Optimal control problem evaluation

Unless otherwise indicated, the following results were obtained with the *Eat with spoon* functional task to illustrate the process for one movement. The first step was to valid the kinematics and dynamics obtained with a human-only OCP following the method proposed in sections 4.3.5.1 to 4.3.5.3. These results are presented in Figure 4-13: sub-Figures 4-13A-D shows that the kinematics of the movement was respected, while sub-Figures 4-13E-F show a reduction of the RMS human joint torque by 3% for the elbow joint and 5% for the shoulder joint.

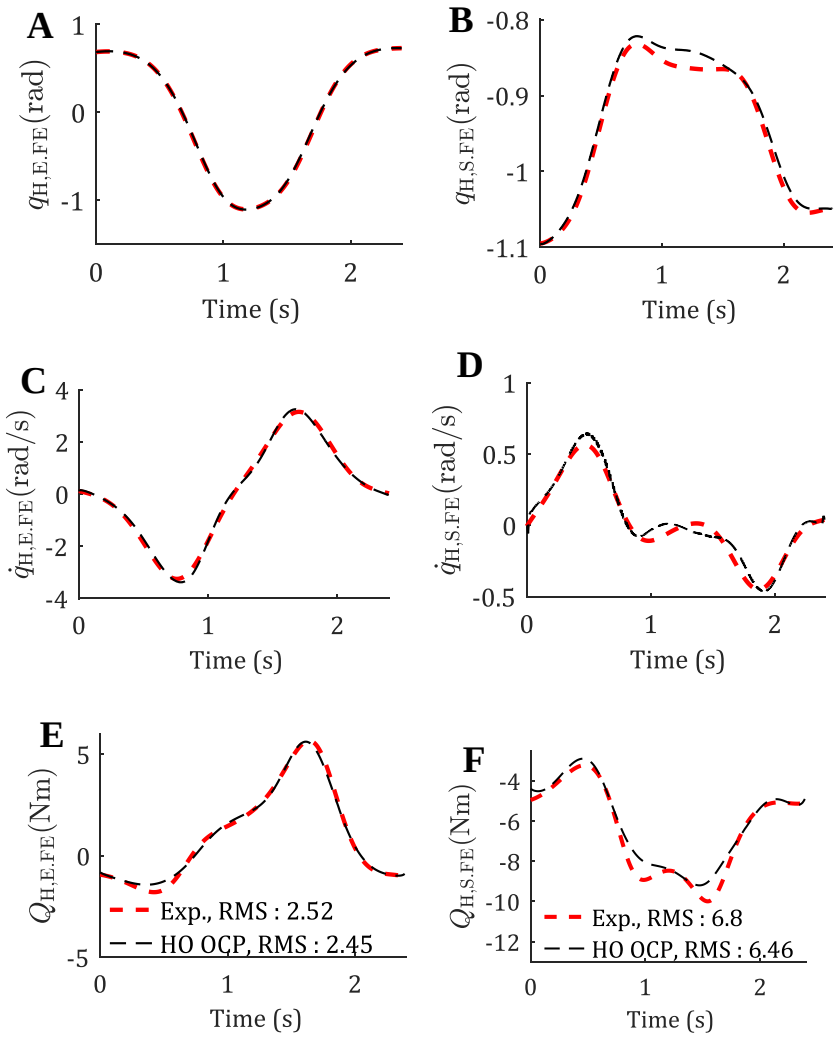


Figure 4-13. Experimental data and human only (HO) optimal control problem (OCP), A and B, position, C and D, velocities, E and F, joint torques and RMS torques.

Figure 4-13 enables to validate the kinematics and dynamics obtained with the OCP. In Figures 4-13A-D the kinematics were respected thus keeping a valid human trajectory. This is important,

especially for a task such as eating, where the orientation of the hand is crucial. The small differences in kinematics are reflected in the dynamics by Figures 4-13E-F, where there is a slight reduction of the human joint torque with the OCP suggesting the solver changed the trajectory to minimize the joint torques. This fits the cost function described by Eq. 4.17.

# CHAPTER 5 COMPLEMENTARY METHODS AND RESULTS

This chapter presents the complementary methods and results that were not included in the article. First, the methods to build the exoskeleton multibody model in the ROBOTRAN software is shown. Then, the fitting results between the simulated and experimental cartesian 3D trajectories are presented for the *Eat with spoon* functional task. Finally, the motor winding curves are depicted for the *Arm front reach right to left* functional task.

## 5.1 Methods: Exoskeleton multibody representation

The methods to achieve specific objective O1 were not fully covered in the research article. This section completes Sections 4.3.1 and 4.3.2 from the research article on the Human model and Exoskeleton Model respectively.

To develop kinematic chains, the ROBOTRAN software provides a graphic user interface [92]. Figure 5-1 shows the implementation of the assistive exoskeleton form Lecours et al. [28] in the interface with generalized coordinates $\boldsymbol{q}_{1-15}$. When comparing Figure 5-1 and Figure 4-3, one difference is that the exoskeleton generalized coordinates $\boldsymbol{q}_E$ only span from 1 to 14. This is due to the fixed coordinate $q_9$ used to turn the arm brace in the right orientation to fit the kinematic constraints of the body cut $\boldsymbol{h}_{l,1-6}$ shown in Figure 4-3.

As presented in Section 2.4.3, the body cut, in 3D, creates 6 constraints to block all DOF between two connected bodies such as the limb and the braces in this case. Therefore, to obtain a non-singular Jacobian matrix $\boldsymbol{J}$ from Equation 2.26, the model requires 6 dependent variables for each body cut. To connect the arm brace to the arm and the wrist brace to the forearm, 12 dependent joints are required. Adding the planar ball cut in the exoskeleton four-bar mechanism, 2 more dependent joints are required. In total, 14 dependant joints are necessary to obtain a successful partitioning of the system. In Figure 5-1, joints $\boldsymbol{q}_{1-8}$ and $\boldsymbol{q}_{10-15}$ are all dependent as $\boldsymbol{q}_9$ is fixed.

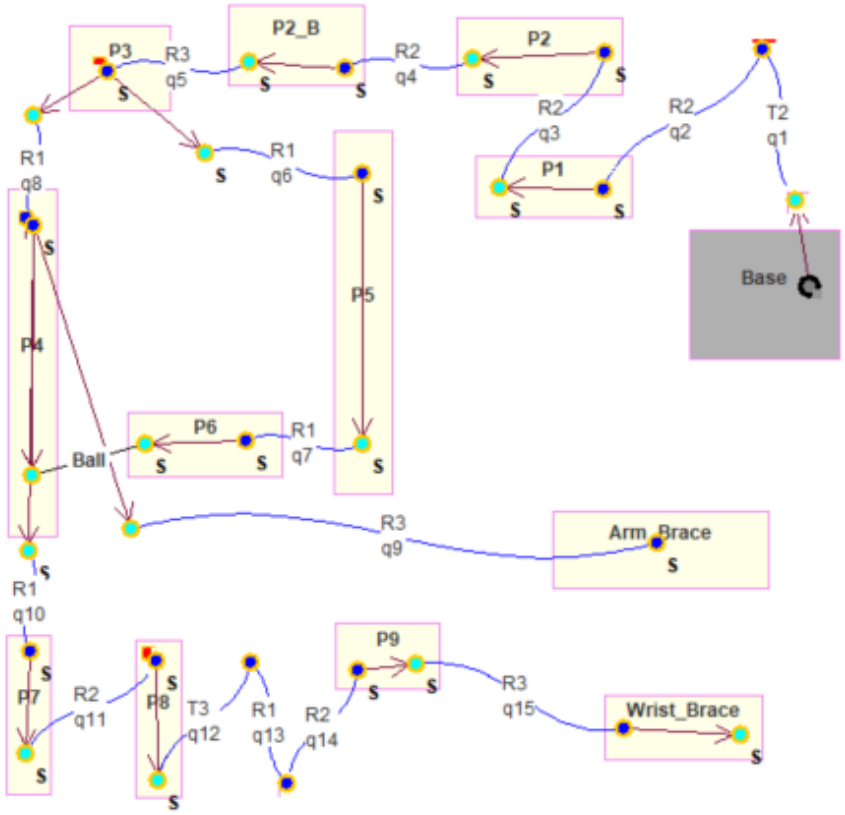


Figure 5-1. The implementation of the assistive exoskeleton in the ROBOTRAN graphic interface with generalized coordinates $\boldsymbol{q}_{1-15}$.

The full human-exoskeleton model graphic representation is shown in Appendix B, Figure 7-1. From this model, the symbolic equations of the loop constraints, the direct kinematics, direct dynamics and inverse dynamics were generated by ROBOTRAN symbolic generator based on a recursive formalism [91].

To help with the visualization of the Human-Exoskeleton model, Figure 5-2 shows the model during the *Eat with a spoon* task.

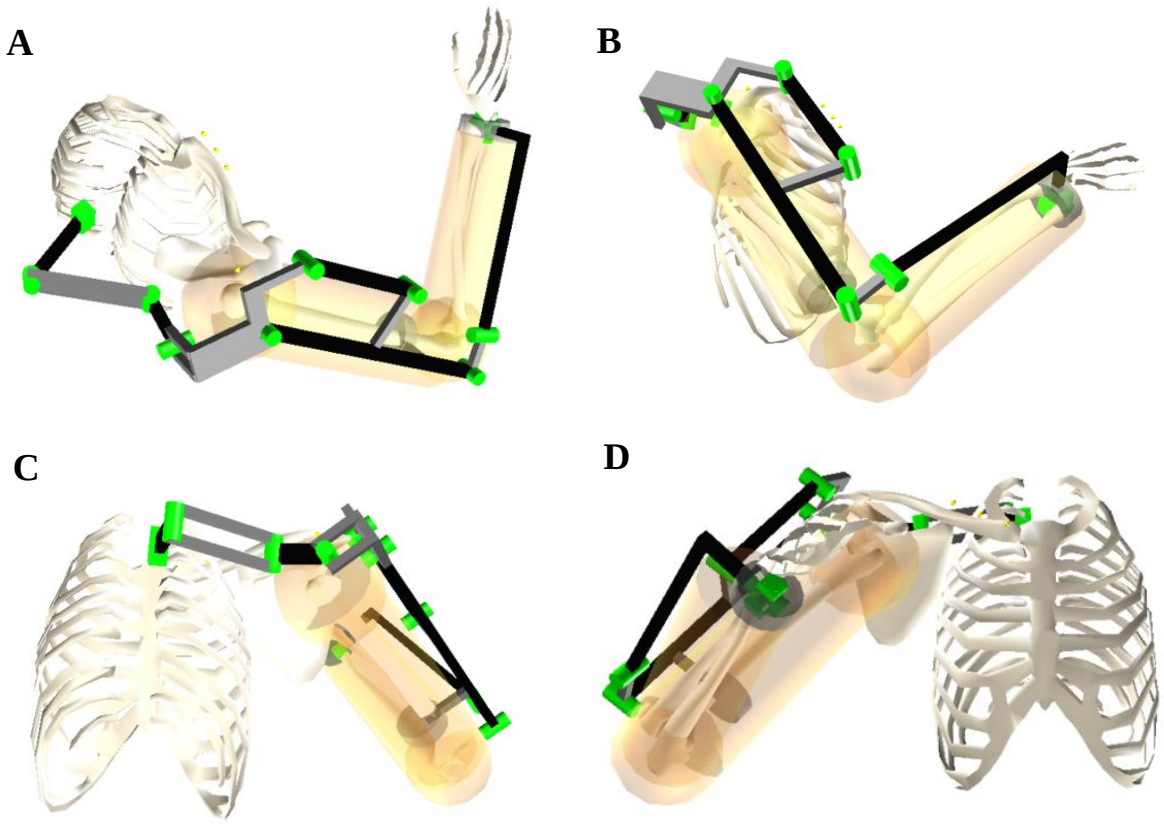


Figure 5-2. Human-Exoskeleton model during the Eat with a spoon task. A. Isometric view. B. Side view. C. Rear view. D. Front view.

## 5.2 Methods: Exoskeleton generalized joint torques design

To complete section 4.3.5.1 on the exoskeleton generalized joint torques evaluation, the following section presents the exoskeleton joint torque design that could be implemented in a prototype. The design needs to combine the motors and the torsion springs in a same joint as shown in Figure 5-3.

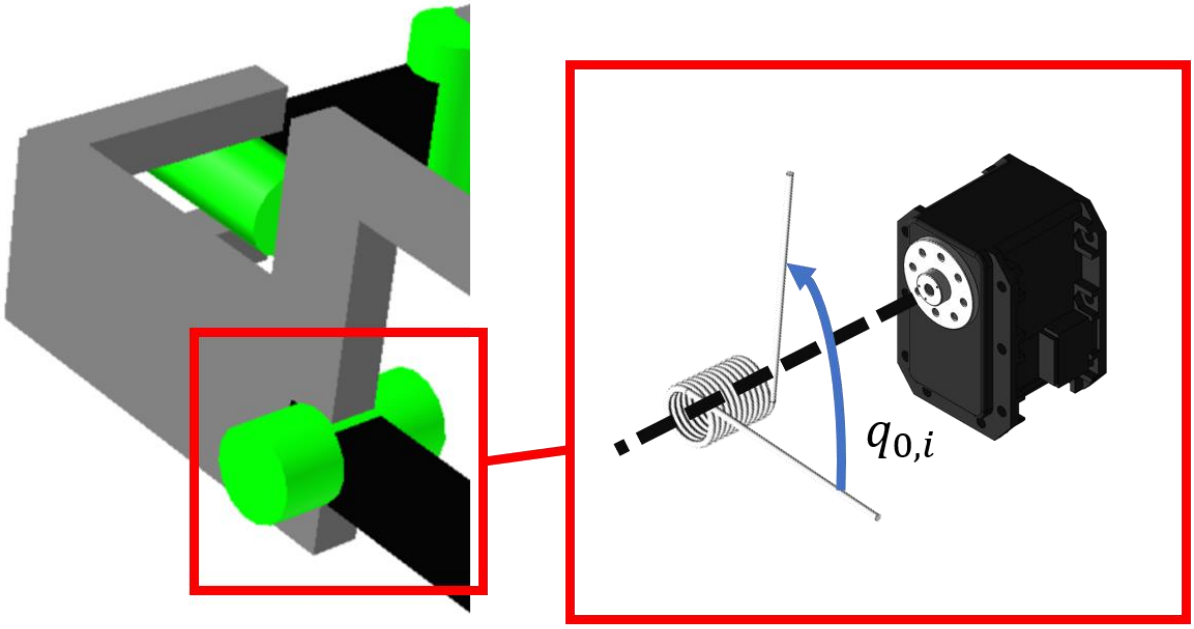


Figure 5-3. Design to combine the motors and torsion spring. The spring and the motors are aligned with the exoskeleton joint and the spring $q_{0,i}$ is ajusted according to the dynamic synthesis results.

The reference position of the exoskeleton is shown in Figure 4-3. The neutral angle of the torsion springs $q_{0,i}$, which are obtained from the dynamic optimization process, are relative to that reference position.

## 5.3 Results: 3D Trajectories

The cost function presented by Eq. 4.17 minimizes the user joint torque as well as the difference between the experimental trajectory $\boldsymbol{q}_{u,exp.}$ and the simulated trajectory $\boldsymbol{q}_u$. Partial results are shown in Section 4.9 where the experimental elbow and shoulder joint positions, velocities, and torques data are compared to the human-only OCP simulation.

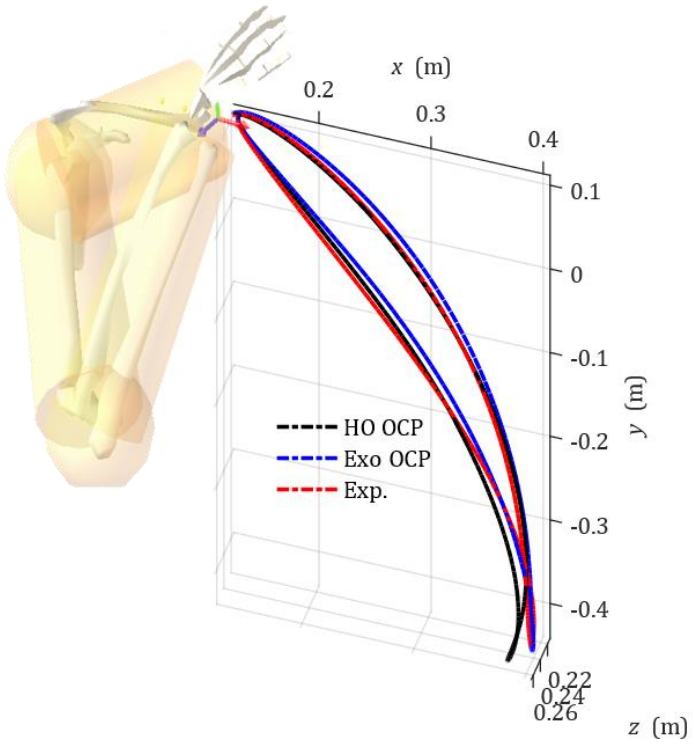


Figure 5-4. Cartesian 3D trajectory of the hand for the *Eat with spoon* functional task. The arm is at the *Eating* segment of the trajectory.

To complete these results, Figure 5-4 presents the cartesian 3D trajectory of the hand for the *Eat with spoon* task. The black, blue and red curves are the human-only OCP, exoskeleton OCP and experimental data trajectories respectively. The RMS value of the norm of the difference between the experimental, human-only OCP and exoskeleton OCP trajectories are shown in Table 5-1. Similar results were found for all trajectories.

Table 5-1. RMS value of the norm of the difference between the experimental, human-only OCP and exoskeleton OCP trajectories.

| Trajectories | $RMS(\|\|Traj_1 - Traj_2\|\|)$ [m] |
|---|---|
| Exp. to HO OCP | 0.019 |
| Exp. to Exo OCP | 0.009 |
| HO OCP to Exo OCP | 0.017 |

## 5.4 Results: Motor winding

In section 4.4.2.2, the results of the dynamic synthesis procedure are presented for each functional task. The main constraints for the dynamic optimization were the motor winding limits. The result for each motorized joint for the *Arm frontal reach right to left* (RL) task are presented in Figure 5-5.

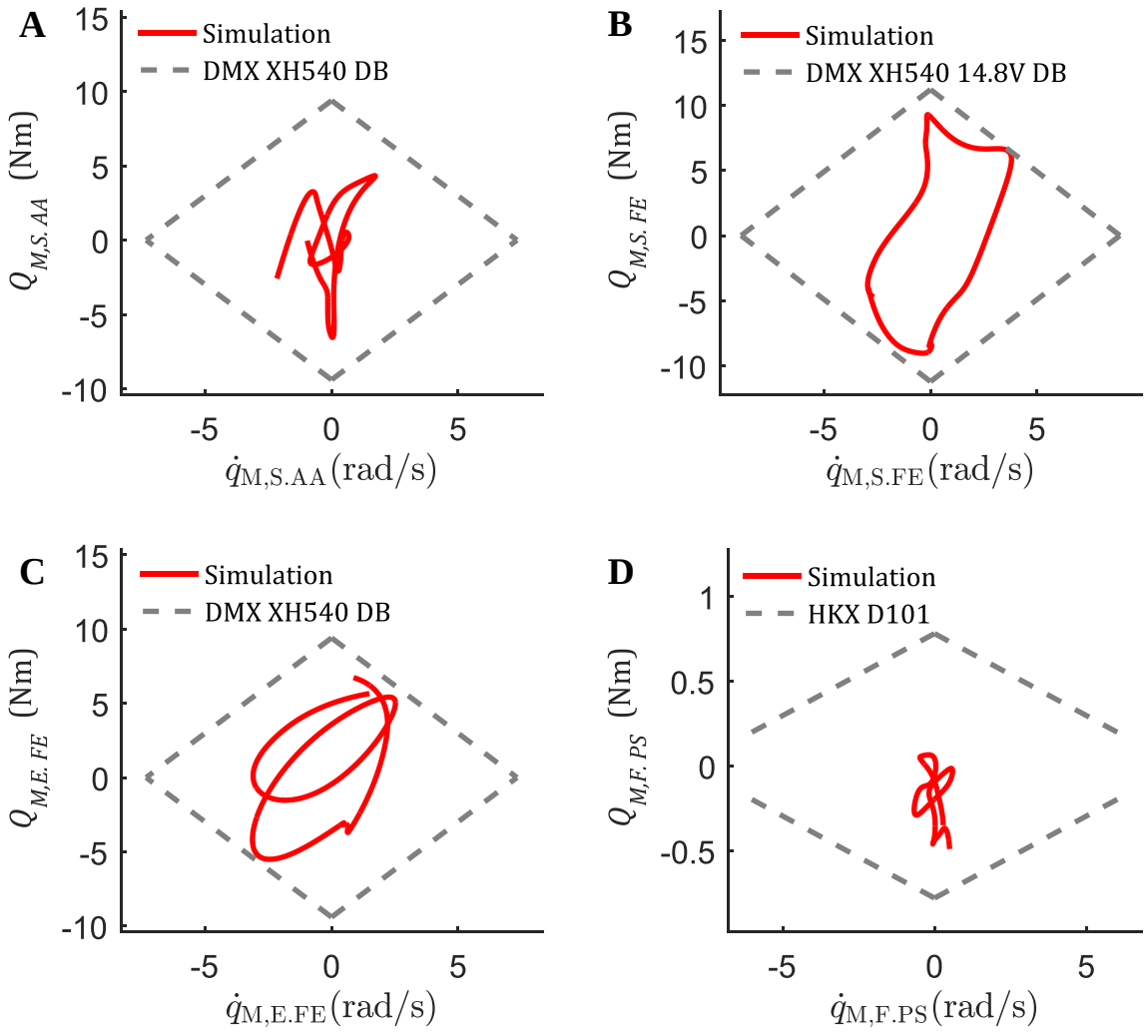


Figure 5-5. Motor winding limits (grey lines) and the simulation motor torque $Q_{M,joint}$ compared to motor velocity $\dot{q}_{M,joint}$ (red lines). **A**. S. AA joint and DMX XH540 DB limits. **B**. S. FE joint and DMX XH540 14.8V DB limits. **C**. E. FE joint and DMX XH540 DB limits. **D**. F. PS joint and HKX D101 limits.

# CHAPTER 6 GENERAL DISCUSSION

The objective of this study, which was the development of a geometric and dynamic synthesis procedure to design and personalize an assistive upper limb exoskeleton for a subject while doing specific functional tasks, was achieved. This chapter presents a brief synthesis of the article followed by the complementary discussion on the additional results of Chapter 5 and is concluded by the limits of the project, the future work, and recommendations.

## 6.1 Research article synthesis

In short, the success of specific objective **O1** is presented in Sections 4.3.1, 4.3.2 and 5.1. The success of objective **O2** is presented and discussed in Sections 4.3.4, 4.3.5.1 to 4.3.5.3, 4.4.1, 4.4.2.1, 4.5.2, 4.5.3. Finally, the success of **O3** is presented and discussed in Sections 4.3, 4.3.5.4, 4.4.2.2 and 4.5.1.

The results and discussion from the research article presented in Sections 4.4 and 4.5 showed that the whole geometric and dynamic procedure could be done for a healthy subject and for 6 functional tasks. These results include the final dimensions of the exoskeleton and the selection of motors and spring characteristics to best reduce the human joint torque. By using an OCP constrained by the DAE system formed by the equations of motion (Eqs. 2.26-2.30), the complete human-exoskeleton interaction could be considered.

The article also shows the importance of using passive elements in the model and the optimization process. Figure 4-6 showed that adding the spring element enabled the motor to use a broader range of its capabilities and could then reduce the human joint torque to a minimum. This is important because otherwise, a bigger motor would have been required in order to obtain the same results. This conclusion was validated for the 6 functional tasks on the gravity affected joints, S. AA, S. FE, and E. FE, globally reducing the weight and size of the exoskeleton.

In general, the proposed procedure is centered around an upper limb assistive and wearable exoskeleton. However, the methods are transferable to other types of exoskeletons or even other robotic devices in dynamic interaction with the human body. The constraints, i.e., collision avoidance and motor winding, as well as cost functions are applicable for these devices. In Figure 4-1, which shows the global synthesis procedure, the human and exoskeleton model are used by the data acquisition, geometric optimization, and dynamic synthesis. To apply the procedure to

another device such as a lower limb exoskeleton, these two models need to be modified and adapted. If required, other parameters can be added. As an example, in the case of a lower limb exoskeleton, the ground force contact would need to be added to the synthesis during the data acquisition process and would be fed to the dynamic synthesis.

## 6.2 Complementary results discussion

### 6.2.1 3D Trajectories

Figure 5-4 shows the 3D cartesian trajectories of the *Eat with spoon* functional task for the experimental data, the human-only OCP and the exoskeleton OCP. The three curves are visually similar, and this is confirmed by Table 5-1 where the RMS value of the norm of the distance between each curve is presented. With less than 2 cm RMS difference for the whole trajectories, the difference is negligible in most daily living context. However, Table 5-1 still shows that the trajectory with the exoskeleton is closer to the experimental trajectory than the human-only simulation which suggests the motorization is important to conserve a better fit.

One of the main obstacles of exoskeleton use is the comfort and feel of the device for the user. Hence, if the exoskeleton cannot reproduce the normal trajectory because of a lack of power or wrong geometric parameters, there is a risk that users will not use it. In the case of this study, the closeness of the curves suggests a good fit, increasing the likelihood that the exoskeleton will be worn by the users. Of course, this research does not consider real-time control of the exoskeleton and the embedded control system which will play a big part in the comfort and feel of the device. This research is limited to choosing the geometric and dynamic elements that can produce the right trajectories.

### 6.2.2 Motor winding

In the article, Table 4-2 shows the reduction percentage of human torque compared with the human-only simulations, % of $Q_{H,HO}$. For RL functional task, S. AA still has an RMS value of the human torque of 27.2%, while the other joints are much lower: S. FE, 2.2%, E. FE, 3.2%, and F. PS, 0%. However, as presented in Figure 5-5, the motors associated with each joint are all within their winding curve limits. This suggests that the motor rotation axes are not aligned with the human

joint axes. Indeed, the motor cannot compensate for the misaligned component of the user's joint torque. This can cause parasitic torques in the human joints which can lead to injuries or pain [44].

## 6.3 Limits of the work, future work, and recommendations

Even if the general objective of this study was successfully achieved, the commercial or medical use of the procedure is not yet possible. These limitations offer the possibility of new research studies to increase the robustness and anatomical accuracy of the procedure as well as adding new features to complete the exoskeleton designs. Limits are presented along with their respective future work and recommendations.

**The procedure was only conducted on one subject:**

To evaluate the need of refinement of the exoskeleton to fit different users, the procedure should be tested for different populations with different characteristics. A first evaluation should take a group of healthy subjects of similar size and test if an average size solution could fit all subjects, and if not, if it is possible to only optimize parts of the exoskeletons to each user. This has a high commercial value as it would reduce the number of hyper-personalized parts.

Another evaluation should be done with patients affected by neuromuscular disabilities. As they cannot produce high joint torques, it would be important to see if the dynamic synthesis can lower the required user's joint torque to their capabilities. Moreover, some subjects in those populations also suffer from articular stiffness, resulting in stricter joint limits [128] that could, potentially, prevent the user to be able to reproduce normal human trajectories. The dynamic procedure should then be modified to allow more difference to normal trajectories to compensate for those constraints.

**Geometric and dynamic parameters were optimized separately:**

The synthesis procedure was divided into two main components, the geometric optimization which variates the dimensions of the exoskeleton and the dynamic optimization which variates the motor torques and springs characteristics. However, the geometry affects the dynamic of the system by changing the lever arms and angles of the motor and spring induced torques. Moreover, the geometric parameters also allow aligning the exoskeleton joints with the human joints, reducing

the possibility or amount of parasitic torques affecting the user. Hence, a combined geometric and dynamic optimization could help to maximize the transmission of the motors and springs torques to the user and to minimize the parasitic torques. The latter could be directly added in the optimization cost function.

**The procedure does not consider topologic optimization:**

In this research, a single kinematic chain, or topology, was considered for the exoskeleton model. In some studies [44], [129], the topologies are optimized, especially for the parasitic forces problem. These studies generally try to create passive mechanisms to automatically align the motorized joint to the human joint, reducing the level of misaligned torque. Such topologic optimization could be implemented in the design procedure. This would also affect the loop closure constraints and should be combined with the geometric optimization.

**User joint torque was used as the main element of the dynamic cost function:**

To minimize the user's effort, the joint torques were minimized. However, these joint torques are generated by groups of muscles that pull on the bones to move the arm. To increase the anatomical realism of the dynamic optimization, instead of minimizing the joint torques, muscle force could be minimized. This has been done in literature with [118] and without [95] exoskeleton and is not a simple problem. The work Wen et al. [130] propose a novel and electromyography free method to evaluate muscle forces and could be combined with the dynamic synthesis to minimize the muscle forces.

Moreover, as discussed in Section 4.5.1, the *user torque ratio* or *user muscle force ratio* need to be investigated. These ratios need to have a clinical meaning as the ratio will vary from one person to another and clinical professionals will make recommendations for each user. With this in mind, a *user muscle force ratio* is clinically easier to understand as it linked to a human body function. This adds to the interest of using the muscle forces in the synthesis procedure.

**Functional tasks were optimized one by one in the dynamic synthesis:**

In the proposed procedure, the functional tasks were optimized one by one for the dynamic synthesis limiting the synthesis of the exoskeleton to a specific task instead of a general synthesis that could perform all functional tasks. As explained in the methods of the article, each functional

task was already divided by groups of intervals and then combined for a full functional task to help the linear solver as it was near its convergence limits.

Other optimization methods such as Sequential Quadratic Programming (SQP) or genetic algorithms, could allow combining the functional tasks. However, each method has its own limitations. For SQP, the solution will be a local minimum near the initial values while the genetic algorithms can be slow and will propose a range of solutions, requiring the engineer to make design choices.

Combining the functional tasks could also allow to obtain a global solution of spring characteristics, thus completely designing the exoskeleton through one optimization.

**The procedure was not tested with additional weights in the user's hands:**

The general use of the exoskeleton will require picking and placing objects, like eating, writing or using tools in the workplace. To consider this in the procedure, weight could be added in the hand rigid body, however, this was not tested. To create a more complete procedure, a weight parameter could be added, such as a maximum weight to be picked up by the user or the weight of the specific tool for a task. An interesting hypothesis could be that the motor selection remains the same, but the spring element characteristics will change. The user could only need to change the springs for different tasks instead of changing the whole system.

# CHAPTER 7 CONCLUSION

The goal of the research was to propose and develop a geometric and dynamic synthesis procedure for an upper limb assistive and wearable exoskeleton. Specifically, the human-exoskeleton model had, first, to be modeled and evaluated. Then, the geometric synthesis was to be developed to consider the subject size, to avoid collisions with his body and to reduce the size of the exoskeleton. Finally, the dynamic synthesis aimed at finding the best motors and spring element characteristics to reduce the user's effort in specific functional tasks. One main constraint of the project was to be able to consider the full interaction between the exoskeleton and the human limb. To do so, joint torques, positions, and velocities needed to be variables in the optimization process. Moreover, to reduce the size of the motors, spring elements were added to the model, thus augmenting the size of the problem. The solution was the use of a DEA constrained OCP formulated through direct collocation and solved by a linear solver. Solving this OCP for the complex upper limb system and for complex tasks like opening a door is a novelty on its own in the multibody dynamics field.

Globally, this research allowed to design and personalize the geometric and dynamic parameters to a specific subject and for specific tasks, bringing the model closer to a complete mechatronic design. Of course, such a design requires many other parameters like cost, reliability, sustainability, comfort, and more.

However, other limits need to be tackled before moving on to these parameters. First, joints alignment and parasitic forces should be added to the synthesis procedure, requiring a combined geometric and dynamic optimization. Eventually, a topologic optimization could also be integrated to create self-aligning mechanism to reduce the parasitic torques to a maximum. The study should also be pursued on a full-body model, to observe the impact of the exoskeleton on the whole human body.

For medical or industrial use of this procedure and the exoskeleton devices that it could design, a more thorough study should be conducted, comparing the need of refinement of the optimization between subjects. This could lead to parts of the design to be fully optimized to one subject and other parts could be a "small, medium, large" system. The procedure should also be tested for tasks considering picking and placing objects to identify the impact on the exoskeleton and the human

limb and need of additional motorization or bigger spring element to compensate for the added weight.

This procedure has the potential to accelerate the design of exoskeletons and their commercialization in the near future. As the exoskeletons are used to restore or give autonomy to patients, the clinical staff could be relieved of follow-ups and treatments, thus reducing the health cost for the government. The exoskeleton could also provide a certain relief to the families who take care of their relatives. On the other hand, the exoskeletons targeted at worker populations have the potential to reduce fatigue, and, therefore, long term injuries. This could also be a relief to the government and the Comission des normes, de l'équité, de la santé et de la sécurité au Travail (CNESST) knowing that work-related injuries cost were around 2.2 billion dollars in Quebec in 2018 [131].

# BIBLIOGRAPHY


[1] M. Gunn, T. M. Shank, M. Eppes, J. Hossain, and T. Rahman, “User Evaluation of a Dynamic Arm Orthosis for People With Neuromuscular Disorders,” *IEEE Transactions on Neural Systems and Rehabilitation Engineering*, vol. 24, no. 12, pp. 1277–1283, Dec. 2016, doi: 10.1109/TNSRE.2015.2492860.

[2] E. Perez Luque, "Evaluation of the Use of Exoskeletons in the Range of Motion of Workers." dissertation, University of Skövde, School of Engineering Science, 2019. [Online]. Availible: http://his.diva-portal.org/smash/get/diva2:1329519/FULLTEXT01.pdf

[3] C. Bousquet-Jette, S. Achiche, D. Beaini, Y. S. Law-Kam Cio, C. Leblond-Ménard, and M. Raison, “Fast scene analysis using vision and artificial intelligence for object prehension by an assistive robot,” *Engineering Applications of Artificial Intelligence*, vol. 63, pp. 33–44, Aug. 2017, doi: 10.1016/j.engappai.2017.04.015.

[4] E. Guglielmelli *et al.*, “Self-feeding apparatus,” US20090104004A1, 23-Apr-2009.

[5] R. A. R. C. Gopura, D. S. V. Bandara, K. Kiguchi, and G. K. I. Mann, “Developments in hardware systems of active upper-limb exoskeleton robots: A review,” *Robotics and Autonomous Systems*, vol. 75, pp. 203–220, Jan. 2016, doi: 10.1016/j.robot.2015.10.001.

[6] “Wilmington Robotic Exoskeleton (WREX) Dynamic Arm Support.” [Online]. Available: https://at-aust.org/items/11185. [Accessed: 18-Jan-2020].

[7] M. C. Doyle, “Adaptive arm support systems and methods for use,” US9737374B2, 22-Aug-2017.

[8] S. Kim, M. A. Nussbaum, M. I. Mokhlespour Esfahani, M. M. Alemi, S. Alabdulkarim, and E. Rashedi, “Assessing the influence of a passive, upper extremity exoskeletal vest for tasks requiring arm elevation: Part I – ‘Expected’ effects on discomfort, shoulder muscle activity, and work task performance,” *Applied Ergonomics*, vol. 70, pp. 315–322, Jul. 2018, doi: 10.1016/j.apergo.2018.02.025.

[9] I. A. Kapandji, *Anatomie fonctionnelle*. 6th ed. Paris, France: Maloine, 2005.

[10] M. Laitenberger, M. Raison, D. Périé, and M. Begon, “Refinement of the upper limb joint kinematics and dynamics using a subject-specific closed-loop forearm model,” *Multibody Syste, Dynamics*, vol. 33, no. 4, pp. 413–438, Apr. 2015, doi: 10.1007/s11044-014-9421-z.

[11] S. J. Hall, *Basic biomechanics*, 6th ed. New York, NY: McGraw-Hill, 2012.

[12] M. Jackson, B. Michaud, P. Tétreault, and M. Begon, “Improvements in measuring shoulder joint kinematics,” *Journal of Biomechanics*, vol. 45, no. 12, pp. 2180–2183, Aug. 2012, doi: 10.1016/j.jbiomech.2012.05.042.

[13] M. Fung *et al.*, “Scapular and clavicular kinematics during humeral elevation: A study with cadavers,” *Journal of Shoulder and Elbow Surgery*, vol. 10, no. 3, pp. 278–285, May 2001, doi: 10.1067/mse.2001.114496.

[14] Z. Dvir and N. Berme, “The shoulder complex in elevation of the arm: a mechanism approach,” *Journal of Biomechanics*, vol. 11, no. 5, pp. 219–225, 1978, doi: 10.1016/0021-9290(78)90047-7.

[15] B. Delaney, « Muscles That Move the Arm », ACE Fitness. [Online]. Available: https://www.acefitness.org/blog/3535/muscles-that-move-the-arm. [Accessed: 23-juin-2016].

[16] H. E. J. Veeger and B. Yu, "Orientation of axes in the elbow and forearm for biomechanical modelling," in *Proceedings of the 1996 Fifteenth Southern Biomedical Engineering Conference*, 1996, pp. 377–380, doi: 10.1109/SBEC.1996.493254.

[17] A. Kecskeméthy and A. Weinberg, "An Improved Elasto-Kinematic Model of the Human Forearm for Biofidelic Medical Diagnosis," *Multibody System Dynamics*, vol. 14, no. 1, pp. 1–21, Aug. 2005, doi: 10.1007/s11044-005-1756-z.

[18] R. Altenburger, D. Scherly, and K. S. Stadler, "Design of a passive, iso-elastic upper limb exoskeleton for gravity compensation," *Robomech Journal*, vol. 3, no. 1, p. 12, Apr. 2016, doi: 10.1186/s40648-016-0051-5.

[19] M. Gilliaux *et al.*, "Using the Robotic Device Reaplan as a Valid, Reliable, and Sensitive Tool to Quantify Upper Limb Impairments in Stroke Patients," Feb-2014. [Online]. Available: https://www.ingentaconnect.com/content/mjl/sreh/2014/00000046/00000002/art00003. [Accessed: 26-Jan-2020].

[20] Y. Yang, L. Wang, J. Tong, and L. Zhang, "Arm Rehabilitation Robot Impedance Control and Experimentation," in *2006 IEEE International Conference on Robotics and Biomimetics*, 2006, pp. 914–918, doi: 10.1109/ROBIO.2006.340342.

[21] "EksoZeroG - Heavy Chipping & Drilling Tools Feel Weightless," *Ekso Bionics*. [Online]. Available: https://eksobionics.com/eksoworks/eksozerog/. [Accessed: 26-Jan-2020].

[22] P. Maciejasz, J. Eschweiler, K. Gerlach-Hahn, A. Jansen-Troy, and S. Leonhardt, "A survey on robotic devices for upper limb rehabilitation," *Journal of NeuroEngineering and Rehabilitation*, vol. 11, no. 1, p. 3, Jan. 2014, doi: 10.1186/1743-0003-11-3.

[23] H. S. Lo and S. Q. Xie, "Exoskeleton robots for upper-limb rehabilitation: State of the art and future prospects," *Medical Engineering & Physics*, vol. 34, no. 3, pp. 261–268, Apr. 2012, doi: 10.1016/j.medengphy.2011.10.004.

[24] S. Marcheschi, F. Salsedo, M. Fontana, and M. Bergamasco, "Body Extender: Whole body exoskeleton for human power augmentation," in *2011 IEEE International Conference on Robotics and Automation*, 2011, pp. 611–616, doi: 10.1109/ICRA.2011.5980132.

[25] "Armeo®Spring," *Hocoma*. [Online]. Available: https://www.hocoma.com/solutions/armeo-spring/. [Accessed: 18-Jan-2020].

[26] T. Haumont *et al.*, "Wilmington Robotic Exoskeleton: A Novel Device to Maintain Arm Improvement in Muscular Disease," *Journal of Pediatric Orthopaedics*, vol. 31, no. 5, p. e44, Aug. 2011, doi: 10.1097/BPO.0b013e31821f50b5.

[27] K. Huysamen, T. Bosch, M. de Looze, K. S. Stadler, E. Graf, and L. W. O'Sullivan, "Evaluation of a passive exoskeleton for static upper limb activities," *Applied Ergonomics*, vol. 70, pp. 148–155, Jul. 2018, doi: 10.1016/j.apergo.2018.02.009.

[28] S. Lecours, "Développement d'un exosquelette portable motorisé des membres supérieurs pour les enfants atteints de troubles neuromusculaires," masters, Mechanical Engineering, Polytechnique Montréal, Montréal, Québec, Canada, 2019.

[29] H.-S. Park, Yupeng Ren, and Li-Qun Zhang, "IntelliArm: An exoskeleton for diagnosis and treatment of patients with neurological impairments," in *2008 2nd IEEE RAS EMBS International Conference on Biomedical Robotics and Biomechatronics*, 2008, pp. 109–114, doi: 10.1109/BIOROB.2008.4762876.

[30] J. C. Perry, J. Rosen, and S. Burns, "Upper-Limb Powered Exoskeleton Design," *IEEE/ASME Transactions in Mechatronics*, vol. 12, no. 4, pp. 408–417, Aug. 2007, doi: 10.1109/TMECH.2007.901934.

[31] M. H. Rahman, M. Saad, J. P. Kenné, and P. S. Archambault, "Exoskeleton robot for rehabilitation of elbow and forearm movements," in *18th Mediterranean Conference on Control and Automation, MED'10*, 2010, pp. 1567–1572, doi: 10.1109/MED.2010.5547826.

[32] T. Nef, M. Guidali, and R. Riener, "ARMin III – Arm Therapy Exoskeleton with an Ergonomic Shoulder Actuation," *Applied Bionics and Biomechanics*, 6. [Online]. Available: https://www.hindawi.com/journals/abb/2009/962956/. [Accessed: 26-Jan-2020].

[33] S. J. Ball, I. E. Brown, and S. H. Scott, "MEDARM: a rehabilitation robot with 5DOF at the shoulder complex," in *2007 IEEE/ASME international conference on advanced intelligent mechatronics*, 2007, pp. 1–6, doi: 10.1109/AIM.2007.4412446.

[34] C. Carignan, J. Tang, and S. Roderick, "Development of an exoskeleton haptic interface for virtual task training," in *2009 IEEE/RSJ International Conference on Intelligent Robots and Systems*, 2009, pp. 3697–3702, doi: 10.1109/IROS.2009.5354834.

[35] N. Sylla, V. Bonnet, F. Colledani, and P. Fraisse, "Ergonomic contribution of ABLE exoskeleton in automotive industry," *International Journal of Industrial Ergonomics*, vol. 44, no. 4, pp. 475–481, Jul. 2014, doi: 10.1016/j.ergon.2014.03.008.

[36] M. Solazzi, M. Abbrescia, R. Vertechy, C. Loconsole, V. Bevilacqua, and A. Frisoli, "An interaction torque control improving human force estimation of the rehab-exos exoskeleton," in *2014 IEEE Haptics Symposium (HAPTICS)*, 2014, pp. 187–193, doi: 10.1109/HAPTICS.2014.6775453.

[37] E. Rocon, J. M. Belda-Lois, A. F. Ruiz, M. Manto, J. C. Moreno, and J. L. Pons, "Design and Validation of a Rehabilitation Robotic Exoskeleton for Tremor Assessment and Suppression," *IEEE Transactions on Neural Systems and Rehabilitation Engineering*, vol. 15, no. 3, pp. 367–378, Sep. 2007, doi: 10.1109/TNSRE.2007.903917.

[38] S. Balasubramanian *et al.*, "RUPERT: An exoskeleton robot for assisting rehabilitation of arm functions," in *2008 Virtual Rehabilitation*, 2008, pp. 163–167, doi: 10.1109/ICVR.2008.4625154.

[39] F. Aggogeri, T. Mikolajczyk, and J. O'Kane, "Robotics for rehabilitation of hand movement in stroke survivors," *Advances in Mechanical Engineering*, vol. 11, no. 4, p. 1687814019841921, Apr. 2019, doi: 10.1177/1687814019841921.

[40] M.-H. Milot *et al.*, "A crossover pilot study evaluating the functional outcomes of two different types of robotic movement training in chronic stroke survivors using the arm exoskeleton BONES," *Journal of NeuroEngineering Rehabilitation*, vol. 10, no. 1, p. 112, Dec. 2013, doi: 10.1186/1743-0003-10-112.

[41] M. A. Ergin and V. Patoglu, "ASSISTON-SE: A self-aligning shoulder-elbow exoskeleton," in *2012 IEEE International Conference on Robotics and Automation*, 2012, pp. 2479–2485, doi: 10.1109/ICRA.2012.6225117.

[42] Y. Mao and S. K. Agrawal, "Design of a Cable-Driven Arm Exoskeleton (CAREX) for Neural Rehabilitation," *IEEE Transactions on Robotics*, vol. 28, no. 4, pp. 922–931, Aug. 2012, doi: 10.1109/TRO.2012.2189496.

[43] P. Letier *et al.*, "SAM : A 7-DOF portable arm exoskeleton with local joint control," in *2008 IEEE/RSJ International Conference on Intelligent Robots and Systems*, 2008, pp. 3501–3506, doi: 10.1109/IROS.2008.4650889.

[44] D. Galinski, J. Sapin, and B. Dehez, "Optimal design of an alignment-free two-DOF rehabilitation robot for the shoulder complex," in *2013 IEEE 13th International Conference on Rehabilitation Robotics (ICORR)*, 2013, pp. 1–7, doi: 10.1109/ICORR.2013.6650502.

[45] "Myomo - Medical Robotics Solutions for Stroke, BPI, Upper Limb Paralysis," *Myomo*. [Online]. Available: https://myomo.com/. [Accessed: 26-Jan-2020].

[46] W. T. Latt, T. P. Luu, C. Kuah, and A. W. Tech, "Towards an Upper-limb Exoskeleton System for Assistance in Activities of Daily Living (ADLs)," in *Proceedings of the international Convention on Rehabilitation Engineering & Assistive Technology*, ITE College East, Singapore, 2014, pp. 1–4.

[47] "EXOSKELETON MATE." [Online]. Available: https://www.comau.com/fr/our-competences/integratedrobotics/exoskeleton. [Accessed: 26-Jan-2020].

[48] "Paexo Shoulder - Das Exoskelett für die Schultern," *Ottobock Industrials*. [Online]. Available: https://paexo.com/paexo-shoulder/?lang=fr. [Accessed: 26-Jan-2020].

[49] "ShoulderX | suitX." [Online]. Available: https://www.suitx.com/shoulderx. [Accessed: 26-Jan-2020].

[50] "Home," *Skelex*. [Online]. Available: https://www.skelex.com/. [Accessed: 26-Jan-2020].

[51] "Sarcos Guardian XO Full-body Powered Exoskeleton," *Sarcos Robotics*. [Online]. Available: https://www.sarcos.com/products/guardian-xo-powered-exoskeleton. [Accessed: 26-Jan-2020].

[52] "x-Ar exoskeletal arm support." [Online]. Available: http://www.equipoisllc.com/products/xAr/. [Accessed: 26-Jan-2020].

[53] "Hyundai Motor Group develops wearable vest exoskeleton to alleviate burden in overhead work: VEX," *Green Car Congress*. [Online]. Available: https://www.greencarcongress.com/2019/09/20190904-vex.html. [Accessed: 26-Jan-2020].

[54] M. Gerdts, *Optimal Control of ODEs and DAEs*. Berlin, Boston: De Gruyter, 2012.

[55] D. L. Ma, D. K. Tafti, and R. D. Braatz, "Optimal control and simulation of multidimensional crystallization processes," *Computers & Chemical Engineering*, vol. 26, no. 7, pp. 1103–1116, Aug. 2002, doi: 10.1016/S0098-1354(02)00033-9.

[56] M. I. Kamien and N. L. Schwartz, *Dynamic Optimization: The Calculus of Variations and Optimal Control in Economics and Management*. Courier Corporation, 2012.

[57] Q. Docquier, O. Brüls, and P. Fisette, “Comparison and Analysis of Multibody Dynamics Formalisms for Solving Optimal Control Problem,” in *IUTAM Symposium on Intelligent Multibody Systems – Dynamics, Control, Simulation*, Cham, 2019, pp. 55–77, doi: 10.1007/978-3-030-00527-6_3.

[58] B. C. Fabien, “Numerical solution of constrained optimal control problems with parameters,” *Applied Mathematics and Computation*, vol. 80, no. 1, pp. 43–62, Nov. 1996, doi: 10.1016/0096-3003(95)00280-4.

[59] M. Diehl, “Numerical Optimal Control Overview,” 2016. [Online]. Available: https://www.syscop.de/files/2015ws/noc-dae/lecture%20slides/04a-OptimalControl.pdf.

[60] F. Biral, E. Bertolazzi, and P. Bosetti, “Notes on Numerical Methods for Solving Optimal Control Problems,” *IEEJ Journal IA*, vol. 5, no. 2, pp. 154–166, 2016, doi: 10.1541/ieejjia.5.154.

[61] J. T. Betts, *Practical Methods for Optimal Control and Estimation Using Nonlinear Programming*. Society for Industrial and Applied Mathematics, 2010.

[62] R. Bellman, “Dynamic Programming,” *Science*, vol. 153, no. 3731, pp. 34–37, Jul. 1966, doi: 10.1126/science.153.3731.34.

[63] W. H. Fleming, “Generalized Solutions of Hamilton-Jacobi Equations (P.-L. Lions),” *SIAM Review*, vol. 27, no. 2, p. 2, 1985, doi: http://dx.doi.org/10.1137/1027078.

[64] J. Andersson, J. Åkesson, and M. Diehl, “Dynamic optimization with CasADi,” in *2012 IEEE 51st IEEE Conference on Decision and Control (CDC)*, 2012, pp. 681–686, doi: 10.1109/CDC.2012.6426534.

[65] L. S. Pontryagin, *Mathematical Theory of Optimal Processes*. CRC Press, 1987.

[66] M. Diehl, H. G. Bock, H. Diedam, and P.-B. Wieber, “Fast Direct Multiple Shooting Algorithms for Optimal Robot Control,” in *Fast Motions in Biomechanics and Robotics: Optimization and Feedback Control*, M. Diehl and K. Mombaur, Eds. Berlin, Heidelberg: Springer, 2006, pp. 65–93.

[67] A. Waechter and C. Laird, “Ipopt: Documentation.” [Online]. Available: https://coin-or.github.io/Ipopt/. [Accessed: 24-Jan-2020].

[68] D. Kraft, “On Converting Optimal Control Problems into Nonlinear Programming Problems,” in *Computational Mathematical Programming*, Berlin, Heidelberg, 1985, pp. 261–280, doi: 10.1007/978-3-642-82450-0_9.

[69] H. G. Bock and K. J. Plitt, “A Multiple Shooting Algorithm for Direct Solution of Optimal Control Problems*,” *IFAC Proceedings Volumes*, vol. 17, no. 2, pp. 1603–1608, Jul. 1984, doi: 10.1016/S1474-6670(17)61205-9.

[70] L. T. Biegler, “Solution of dynamic optimization problems by successive quadratic programming and orthogonal collocation,” *Computers & Chemical Engineering*, vol. 8, no. 3, pp. 243–247, Jan. 1984, doi: 10.1016/0098-1354(84)87012-X.

[71] N. Feng, J. Yong, and Z. Zhan, “A direct multiple shooting method to improve vehicle handling and stability for four hub-wheel-drive electric vehicle during regenerative braking,” *Proceedings of the Institution of Mechanical Engineers, Part D: Journal of Automobile Engineering*, p. 0954407019867510, Aug. 2019, doi: 10.1177/0954407019867510.

[72] R. Bulirsch, F. Montrone, and H. J. Pesch, “Abort landing in the presence of windshear as a minimax optimal control problem, part 2: Multiple shooting and homotopy,” *Journal of Optimization Theory and Applications*, vol. 70, no. 2, pp. 223–254, Aug. 1991, doi: 10.1007/BF00940625.

[73] S. Gros, “Numerical Optimal Control with DAEs Lecture 12: Optimal Control with DAEs.” [Online]. Available: https://www.syscop.de/files/2015ws/noc-dae/lecture%20slides/12-DAEOptimalControl.pdf.

[74] O. von Stryk, “Numerical Solution of Optimal Control Problems by Direct Collocation,” in *Optimal Control: Calculus of Variations, Optimal Control Theory and Numerical Methods*, R. Bulirsch, A. Miele, J. Stoer, and K. Well, Eds. Basel: Birkhäuser, 1993, pp. 129–143.

[75] S. Kameswaran and L. T. Biegler, “Convergence rates for direct transcription of optimal control problems using collocation at Radau points,” *Comput Optim Appl*, vol. 41, no. 1, pp. 81–126, Sep. 2008, doi: 10.1007/s10589-007-9098-9.

[76] M. Diehl and S. Gros, “Numerical Optimal Control,” 2017. [Online]. Available: https://www.syscop.de/files/2017ss/NOC/script/book-NOCSE.pdf.

[77] R. Quirynen, S. Gros, B. Houska, and M. Diehl, “Lifted collocation integrators for direct optimal control in ACADO toolkit,” *Mathematical Programming Computation*, pp. 527–571, Nov. 2017, doi: 10.1007/mpc.v0i0.204.

[78] B. C. Fabien, “Piecewise Polynomial Control Parameterization in the Direct Solution of Optimal Control Problems,” *Journal of Dynamic Systems, Measurement, and Control*, vol. 135, no. 3, May 2013, doi: 10.1115/1.4023401.

[79] C. Chang and J. J. P. Tsai, "Ergonomic Designs Based on Musculoskeletal Models," 2011 IEEE 11th International Conference on Bioinformatics and Bioengineering, Taichung, 2011, pp. 112-116.

[80] B. A. Slavens and G. F. Harris, “The biomechanics of upper extremity kinematic and kinetic modeling: applications to rehabilitation engineering,” *Critical Review in Biomedical Engineering*, vol. 36, no. 2–3, pp. 93–125, 2008, doi: 10.1615/critrevbiomedeng.v36.i2-3.20.

[81] F. Leboeuf, G. Bessonnet, P. Seguin, and P. Lacouture, “Energetic versus sthenic optimality criteria for gymnastic movement synthesis,” *Multibody System Dynamics*, vol. 16, no. 3, pp. 213–236, Oct. 2006, doi: 10.1007/s11044-006-9024-4.

[82] C.-E. Aubin, “Scoliosis study using finite element models,” *Studies in Health Technology and Informatics*, vol. 91, pp. 309–313, 2002.

[83] D. Benoit, X. Wang, D. G. Crandall, and C.-É. Aubin, “Biomechanical analysis of sagittal correction parameters for surgical instrumentation with pedicle subtraction osteotomy in adult spinal deformity,” *Clinical Biomechanics*, vol. 71, pp. 45–52, Jan. 2020, doi: 10.1016/j.clinbiomech.2019.10.014.

[84] A.A. Shabana, "Flexible Multibody Dynamics: Review of Past and Recent Developments," *Multibody System Dynamics*, pp. 189–222, Jun. 1997, doi: 10.1023/A:1009773505418

[85] B. Gervais, A. Vadean, M. Brochu *et al.* “Influence of the load modelling during gait on the stress distribution in a femoral implant,” *Multibody System Dynamics*, pp. 93-105, Sep.

2018 [Online]. Available: https://link.springer.com/article/10.1007/s11044-018-9621-z. [Accessed: 22-Jan-2020].

[86] "Adams - The Multibody Dynamics Simulation Solution." [Online]. Available: http://www.mscsoftware.com/product/adams. [Accessed: 22-Jan-2020].

[87] M. Damsgaard, J. Rasmussen, S. T. Christensen, E. Surma, and M. de Zee, "Analysis of musculoskeletal systems in the AnyBody Modeling System," *Simulation Modelling Practice and Theory*, vol. 14, no. 8, pp. 1100–1111, Nov. 2006, doi: 10.1016/j.simpat.2006.09.001.

[88] S. L. Delp *et al.*, "OpenSim: Open-Source Software to Create and Analyze Dynamic Simulations of Movement," *IEEE Transactions on Biomedical Engineering*, vol. 54, no. 11, pp. 1940–1950, Nov. 2007, doi: 10.1109/TBME.2007.901024.

[89] "Simpack - Simulation Software - Dassault Systèmes®." [Online]. Available: https://www.3ds.com/products-services/simulia/products/simpack/. [Accessed: 22-Jan-2020].

[90] M. Tändl, T. Stark, and A. Kecskeméthy, "Application of MOBILE for accurate bone motion reconstruction using motion-measurements and MRI measurements," in *Progress in industrial mathematics at ECMI 2008. Proceedings of the 15th European conference on mathematics for industry, London, UK, June 30 - July 4, 2008.*, Berlin: Springer, 2010, pp. 571–576.

[91] J.-C. Samin and P. Fisette, *Symbolic Modeling of Multibody Systems*. Springer Netherlands, 2003.

[92] N. Docquier, A. Poncelet, and P. Fisette, "ROBOTRAN: a powerful symbolic gnerator of multibody models," *Mechanical Sciences*, vol. 4, no. 1, pp. 199–219, May 2013, doi: https://doi.org/10.5194/ms-4-199-2013.

[93] T. Kurz, P. Eberhard, C. Henninger, and W. Schiehlen, "From Neweul to Neweul-M2: symbolical equations of motion for multibody system analysis and synthesis," *Multibody System Dynamics*, vol. 24, no. 1, pp. 25–41, Jun. 2010, doi: 10.1007/s11044-010-9187-x.

[94] St. Staicu and D. C. Carp-Ciocardia, "Dynamic analysis of Clavel's Delta parallel robot," in *2003 IEEE International Conference on Robotics and Automation*, 2003, vol. 3, pp. 4116–4121 vol.3, doi: 10.1109/ROBOT.2003.1242230.

[95] M. Raison, "On the quantification of joint and muscle efforts in the human body during motion," Ph.D. Thesis, Université Catholique de Louvain, Belgique, 2009.

[96] B. Michaud, S. Duprey, and M. Begon, "Scapular kinematic reconstruction – segmental optimization, multibody optimization with open-loop or closed-loop chains: which one should be preferred?," *International Biomechanics*, vol. 4, no. 2, pp. 86–94, Nov. 2017, doi: 10.1080/23335432.2017.1405741.

[97] A. El Habachi, S. Duprey, L. Cheze, and R. Dumas, "A parallel mechanism of the shoulder—application to multi-body optimisation," *Multibody System Dynamics*, vol. 33, no. 4, pp. 439–451, Apr. 2015, doi: 10.1007/s11044-014-9418-7.

[98] M. Raison, C. Detrembleur, P. Fisette, and J.-C. Samin, "Assessment of Antagonistic Muscle Forces During Forearm Flexion/Extension," in *Multibody Dynamics: Computational Methods and Applications*, K. Arczewski, W. Blajer, J. Fraczek, and M. Wojtyra, Eds. Dordrecht: Springer Netherlands, 2011, pp. 215–238.

[99] R. A. Wehage and E. J. Haug, “Generalized Coordinate Partitioning for Dimension Reduction in Analysis of Constrained Dynamic Systems,” *Journal of Mechanical Design*, vol. 104, no. 1, pp. 247–255, Jan. 1982, doi: 10.1115/1.3256318.

[100] “EduExo: The First Robotic Exoskeleton Kit for STEM Education,” *Kickstarter*. [Online]. Available: https://www.kickstarter.com/projects/1485976654/eduexo-the-first-robotic-exoskeleton-kit-for-stem. [Accessed: 26-Jan-2020].

[101] F. Ferrati, R. Bortoletto, and E. Pagello, “Virtual Modelling of a Real Exoskeleton Constrained to a Human Musculoskeletal Model,” in *Biomimetic and Biohybrid Systems*, Berlin, Heidelberg, 2013, pp. 96–107, doi: 10.1007/978-3-642-39802-5_9.

[102] J.-F. Collard, “Geometrical and kinematic optimization of closed-loop multibody systems/Optimisation géométrique et cinématique de systèmes multicorps avec boucles cinématiques,” Ph.D. Thesis, Université Catholique de Louvain, Belgique, 2007.

[103] D. Galinski, “Conception et optimisation d’un robot de rééducation neuromotrice du membre supérieur avec compensation active de la gravité,” Ph.D. Thesis, Université Catholique de Louvain, Belgique, 2014.

[104] P. Fisette and Q. Docquier, “Modeling Multibody Systems with ROBOTRAN,” 2019, [Online]. Available: http://robotran-doc.gitpage.immc.ucl.ac.be/RobotranBasic/Robotran_basics.pdf. [Accessed: 26-Jan-2020]

[105] M. Millard, M. Sreenivasa, and K. Mombaur, “Predicting the Motions and Forces of Wearable Robotic Systems Using Optimal Control,” *Frontiers in Robotics and AI*, vol. 4, 2017, doi: 10.3389/frobt.2017.00041.

[106] M. H. Rahman, M. Saad, C. Ochoa-Luna, J. P. Kenné, and P. S. Archambault, “Cartesian trajectory tracking of an upper limb exoskeleton robot,” in *IECON 2012 - 38th Annual Conference on IEEE Industrial Electronics Society*, 2012, pp. 2668–2673, doi: 10.1109/IECON.2012.6389155.

[107] A. H. A. Stienen, E. E. G. Hekman, F. C. T. van der Helm, and H. van der Kooij, “Self-Aligning Exoskeleton Axes Through Decoupling of Joint Rotations and Translations,” *IEEE Transactions on Robotics*, vol. 25, no. 3, pp. 628–633, Jun. 2009, doi: 10.1109/TRO.2009.2019147.

[108] D. Zanotto, Y. Akiyama, P. Stegall, and S. K. Agrawal, “Knee Joint Misalignment in Exoskeletons for the Lower Extremities: Effects on User’s Gait,” *IEEE Transactions on Robotics*, vol. 31, no. 4, pp. 978–987, Aug. 2015, doi: 10.1109/TRO.2015.2450414.

[109] M. Malosio, N. Pedrocchi, F. Vicentini, and L. M. Tosatti, “Analysis of elbow-joints misalignment in upper-limb exoskeleton,” in *2011 IEEE International Conference on Rehabilitation Robotics*, 2011, pp. 1–6, doi: 10.1109/ICORR.2011.5975393.

[110] S. Crea, M. Cempini, S. Mazzoleni, M. C. Carrozza, F. Posteraro, and N. Vitiello, “Phase-II Clinical Validation of a Powered Exoskeleton for the Treatment of Elbow Spasticity,” *Frontiers in Neuroscience*, vol. 11, May 2017, doi: 10.3389/fnins.2017.00261.

[111] M. A. Rahman and A. Al-Jumaily, “Design and Development of a Hand Exoskeleton for Rehabilitation Following Stroke,” *Procedia Engineering*, vol. 41, pp. 1028–1034, Jan. 2012, doi: 10.1016/j.proeng.2012.07.279.

[112] M. Sarac, M. Solazzi, E. Sotgiu, M. Bergamasco, and A. Frisoli, “Design and kinematic optimization of a novel underactuated robotic hand exoskeleton,” *Meccanica*, vol. 52, no. 3, pp. 749–761, Feb. 2017, doi: 10.1007/s11012-016-0530-z.

[113] R. P. Matthew, E. J. Mica, W. Meinhold, J. A. Loeza, M. Tomizuka, and R. Bajcsy, “Introduction and initial exploration of an Active/Passive Exoskeleton framework for portable assistance,” in *2015 IEEE/RSJ International Conference on Intelligent Robots and Systems (IROS)*, 2015, pp. 5351–5356, doi: 10.1109/IROS.2015.7354133.

[114] H.-C. Hsieh, L. Chien, and C.-C. Lan, “Mechanical design of a gravity-balancing wearable exoskeleton for the motion enhancement of human upper limb,” in *2015 IEEE International Conference on Robotics and Automation (ICRA)*, 2015, pp. 4992–4997, doi: 10.1109/ICRA.2015.7139893.

[115] C. J. Walsh, K. Endo, And H. Herr, “A quasi-passive leg exoskeleton for load-carrying augmentation,” *International Journal of Humanoid Robotics*, Nov. 2011, doi: 10.1142/S0219843607001126.

[116] Y. Hayashi, R. Dubey, and K. Kiguchi, “Torque optimization for a 7DOF upper-limb power-assist exoskeleton robot,” in *2011 IEEE Workshop on Robotic Intelligence In Informationally Structured Space*, 2011, pp. 49–54, doi: 10.1109/RIISS.2011.5945786.

[117] Y. Aoustin and A. M. Formalskii, “Walking of biped with passive exoskeleton: evaluation of energy consumption,” *Multibody System Dynamics*, vol. 43, no. 1, pp. 71–96, May 2018, doi: 10.1007/s11044-017-9602-7.

[118] L. Zhou, Y. Li, and S. Bai, “A human-centered design optimization approach for robotic exoskeletons through biomechanical simulation,” *Robotics and Autonomous Systems*, vol. 91, pp. 337–347, May 2017, doi: 10.1016/j.robot.2016.12.012.

[119] Y. Bougrinat, S. Achiche, and M. Raison, “Design and development of a lightweight ankle exoskeleton for human walking augmentation,” *Mechatronics*, vol. 64, p. 102297, Dec. 2019, doi: 10.1016/j.mechatronics.2019.102297.

[120] X. Zhou and X. Chen, “Design and Evaluation of Torque Compensation Controllers for a Lower Extremity Exoskeleton,” *ArXiv*, 2019, [Online]. Available: https://arxiv.org/abs/1907.02200

[121] L. Zhou, S. Bai, M. S. Andersen, and J. Rasmussen, “Design and Optimization of a Spring-loaded Cable-driven Robotic Exoskeleton,” in *Proceedings of the 25th Nordic Seminar on Computational Mechanics*, 2012, pp. 205–208.

[122] M. G. Carmichael and D. K. Liu, "Human biomechanical model based optimal design of assistive shoulder exoskeleton," in *Field and Service Robotics*, L. Mejias, P. Corke, J. Roberts, edit., Cham, Switzerland: Springer, 2015.

[123] J. Iqbal, N. G. Tsagarakis, and D. G. Caldwell, “A human hand compatible optimised exoskeleton system,” in *2010 IEEE International Conference on Robotics and Biomimetics*, 2010, pp. 685–690, doi: 10.1109/ROBIO.2010.5723409.

[124] P. Manns, M. Sreenivasa, M. Millard, and K. Mombaur, “Motion Optimization and Parameter Identification for a Human and Lower Back Exoskeleton Model,” *IEEE Robotics*

*and Automation Letters*, vol. 2, no. 3, pp. 1564–1570, Jul. 2017, doi: 10.1109/LRA.2017.2676355.

[125] H. Koch and K. Mombaur, "ExoOpt - A framework for patient centered design optimization of lower limb exoskeletons," in *2015 IEEE International Conference on Rehabilitation Robotics (ICORR)*, 2015, pp. 113–118, doi: 10.1109/ICORR.2015.7281185.

[126] D. Kaneishi, R. P. Matthew, and M. Tomizuka, "Optimal Control Parameterization for ActivelPassive EXoskeleton with Variable Impedance Actuator," in *2018 7th IEEE International Conference on Biomedical Robotics and Biomechatronics (Biorob)*, 2018, pp. 713–719, doi: 10.1109/BIOROB.2018.8487719.

[127] T. Matsubara, T. Noda, S.-H. Hyon, and J. Morimoto, "An optimal control approach for hybrid actuator system," in *2011 11th IEEE-RAS International Conference on Humanoid Robots*, 2011, pp. 300–305, doi: 10.1109/Humanoids.2011.6100825.

[128] B. Kowalczyk and J. Feluś, "Arthrogryposis: an update on clinical aspects, etiology, and treatment strategies," *Archive of Medical Science*, vol. 12, no. 1, pp. 10–24, Feb. 2016, doi: 10.5114/aoms.2016.57578.

[129] M. B. Näf, K. Junius, M. Rossini, C. Rodriguez-Guerrero, B. Vanderborght, and D. Lefeber, "Misalignment Compensation for Full Human-Exoskeleton Kinematic Compatibility: State of the Art and Evaluation," *Applied Mechanics Reviews*, vol. 70, no. 5, Sep. 2018, doi: 10.1115/1.4042523.

[130] J. Wen, M. Raison, and S. Achiche, "Using a cost function based on kinematics and electromyographic data to quantify muscle forces," *Journal of Biomechanics*, vol. 80, pp. 151–158, Oct. 2018, doi: 10.1016/j.jbiomech.2018.09.002.

[131] D. Lamarche and J. Aubin, "Statistiques annuelles 2018,", *Comission des normes, de l'équité, de la santé et de la sécurité du travail*, 2018. [Online]. Available: https://www.cnesst.gouv.qc.ca/Publications/200/Documents/DC200-1046web.pdf.

# APPENDIX A – COMPLETE REPRESENTATION OF THE HUMAN-EXOSKELETON MULTIBODY MODEL IN ROBOTRAN

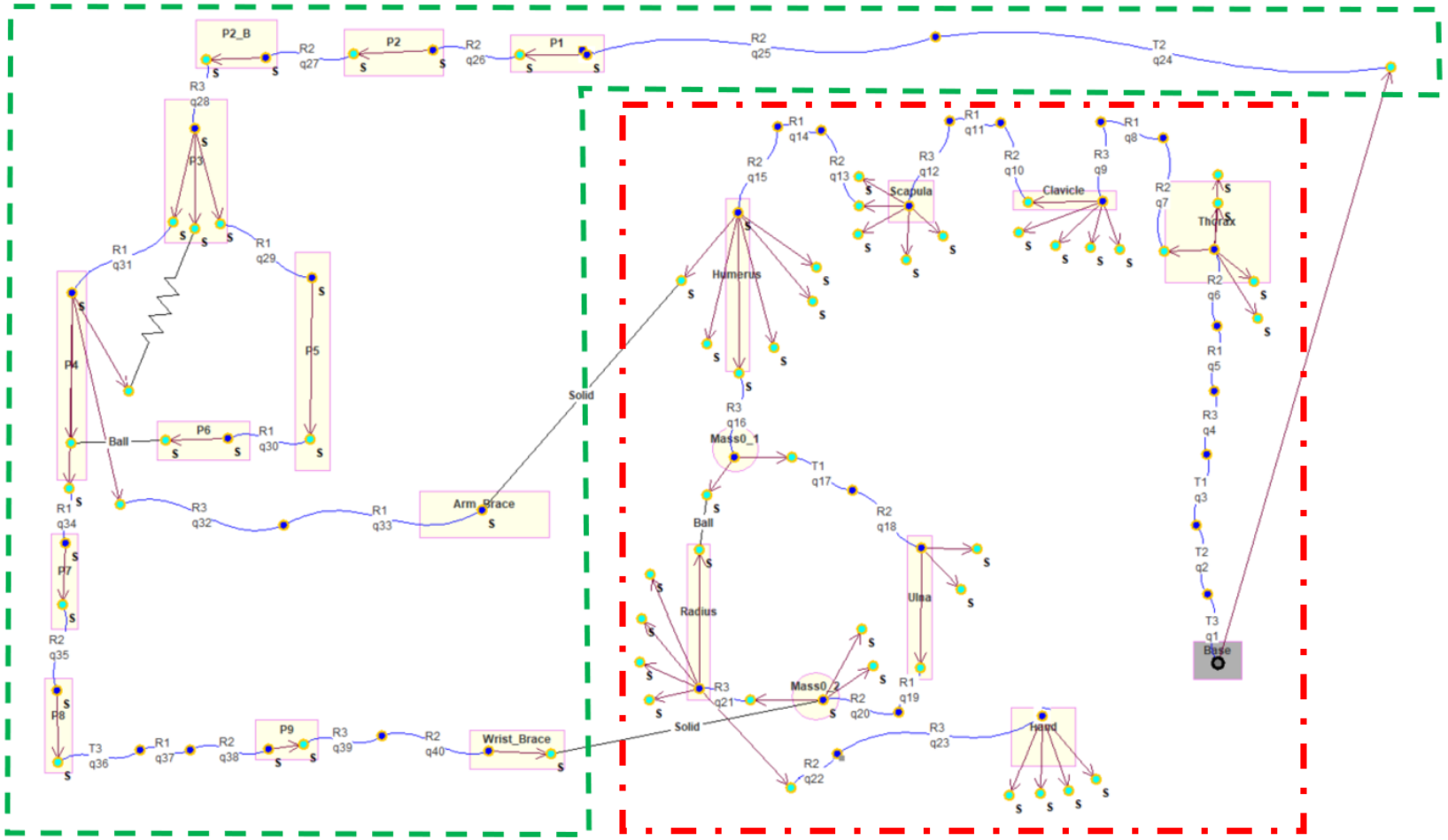


Figure 7-1. Complete representation of the human-exoskeleton multibody model in ROBOTRAN graphic pad. The red square includes the human model and the green square includes the exoskeleton model.